Journal of NUCLEAR SCIENCE and TECHNOLOGY, Supplement 5, p. 594–597 (June 2008)

A Predictive Model for a Radioactive Contamination in an Urban Environment and Its Performance Capability to the EMRAS Project

Won Tae HWANG*, Moon Hee HAN, Hyo Joon JEONG, and Eun Han KIM

Nuclear Environmental Safety Research Center, Korea Atomic Energy Research Institute, Daedeokdaero 1045, Yuseong, Daejeon, KOREA 305-353.

A model, called METRO-K, has been developed for a radiological dose assessment due to a radioactive contamination for the Korean urban environment. The model has been taking part in the Urban Remediation Working Group within the IAEA's EMRAS project to provide an opportunity to compare the modeling approaches and the predictive results of models that describe the behavior of radionuclide in an urban environment. The modeling approaches of METRO-K and the predictive results that have been carried out as a part of the Working Group's activities are presented and discussed. Contribution of contaminated surfaces to absorbed dose rates revealed a distinct difference for the locations of a receptor.

KEYWORDS: Korean urban environment, METRO-K, EMRAS project, radiological dose assessment

I. Introduction

Following the Chernobyl accident, the interest on radionuclide behavior in an urban environment, where most people actually live, has increased[1,2]. In the meantime, a variety of efforts for describing a radionuclide behavior have mainly concentrated on agricultural ecosystems which represent a typical rural environment. Characteristics of the typical surfaces in a rural environment are different from those in an urban environment. Consequently, the radionuclide behavior including a deposition onto surfaces and subsequent exposure dose to humans may be different between the two environments.

We developed a model, called METRO-K (Model for Evaluating the Transient Behavior of RadiOactive Materials in the Korean Urban Environment), for a radiological dose assessment due to a radioactive contamination in the Korean urban environment[3,4]. The modeling approaches of METRO-K are similar to those of the Canadian model CHERURB-95[5], but we tried to describe the Korean urban environment, as accurately as possible. Characteristics of METRO-K are as follows ; (1) mathematical structures are simple (*i.e.* less input parameter) and easy to understand due to being based on analytic approaches, (2) a geometrically complex urban environment can be constructed easily by using just 5 types of surfaces and (3) various remediation actions can be applied to different surfaces by evaluating the exposure doses resulting from each contaminated surface. Since 2004, METRO-K has been taking part in the Urban Remediation Working Group within the IAEA's (International Atomic Energy Agency) EMRAS (Environmental Modeling for RAdiation Safety) project[6]. The project is to provide an opportunity to compare modeling approaches and predictive results of models that describe a radionuclide behavior in an urban environment. Major emphases include (1) prediction of the variations in radionuclide concentrations or dose rates as a function of the location and time, (2) identification of the most important pathways for a human exposure, and (3) prediction of a reduction in the radionuclide concentrations, dose rates, or doses resulting from various remediation efforts. The Working Group's activities will be completed by the end of 2007, and a final report will be published as one of the IAEA's TECDOC.

The modeling approaches of METRO-K and its predictive results that have been carried out as a part of the Working Group's activities are presented and discussed in this paper.

II. Material and Methods

1. Radionuclide Behavior on Urban Surfaces

Radioactive materials released into the environment will be deposited onto surfaces due to not only atmospheric turbulence and gravitation, but also washout by a precipitation. The former is called dry deposition, and the latter is called wet deposition. Surface contamination by dry and wet processes can be predicted from a radionuclide concentration in air by a well defined terminology, so-called deposition velocity and washout ratio, respectively. Dry deposited radionuclide is assumed to be either mobile or fixed to surfaces. If it is mobile radionuclides, it can be removed from surfaces by rain, but if it is fixed ones, it can not be easily removed. If there is no precipitation during a contamination of air, dry deposition will consist of a mobile fraction and a fixed one. A certain fraction of the mobile radionuclide accumulated from the previous day will be fixed due to moisture for the night of that day. A fixed fraction will increase day by day with a certain fraction. If a daily precipitation is below a critical amount of precipitation (CAP), both dry and wet depositions will occur and all of the radionuclides will be fixed. All of the mobile radionuclides that were deposited by dry processes until the previous days will be fixed. If a daily precipitation exceeds a CAP, all of

*Corresponding Author, Tel No: +82-42-868-2344, Fax No: +82-42-868-2370, E-mail: wthwang@kaeri.re.kr

the radionuclides will be deposited by wet processes and run-off will occur. A certain fraction of the radionuclides in the run-off water will be still retained on the surfaces. After a deposition is completed, radionuclide concentration on the surfaces will be affected by weathering processes including wind, pedestrians and traffic, and a migration into soil. A variation of radionuclide concentrations is described by two exponential terms together with radioactive decay ; one is short-term weathering half-lives and another is long-term weathering half-lives. Weathering half-lives are strongly dependent on a type of radionuclide and surface. Mathematical formula and parameter values for describing a radionuclide behavior on surfaces are described elsewhere in detail[3].

As shown from the Chernobyl accident, radioactive materials may be released for several days. The initial input data to METRO-K is a daily air concentration (Bq m^{-3}) and precipitation (mm). And the outputs are radionuclide concentrations on different surfaces and subsequent exposure doses as a function of the location of a receptor. **Fig. 1** shows a schematic diagram of METRO-K.

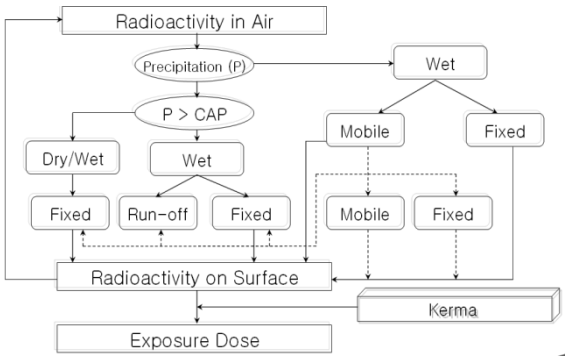

Fig. 1. Schematic diagram of METRO-K. CAP represents a critical amount of precipitation. Dotted lines represent the behavior of the radionuclides deposited from previous days

2. Exposure Dose in an Urban Environment

To predict exposure doses in an urban environment may be a difficult task because of the complexity and variety of surrounding structures. For a simplicity, METRO-K uses a method that a surrounding environment is composed of a combination of 5 types of basic surfaces (roofs, paved ground, outer walls, lawn/soil, trees) and the exposure dose from contaminated surfaces is calculated from predetermined kerma (dose rate per unit deposition). The model calculates the exposure doses contributing from all of the surfaces affecting a specified location.

$$H_i(t) = 8.64 \times 10^{-14}\, DCF_i \sum_k y_k \sum_j \omega_j\, C_j(t)\, K_{ijk}$$

i : location of a receptor
j : contaminated surface
k : energy
$H_i(t)$: exposure dose rate (Sv d^{-1})
DCF_i : γ -ray dose conversion factor (Sv Gy^{-1})
ω_j : dose reduction by surface roughness
y_k : γ -ray yield (γ sec^{-1} Bq^{-1})
$C_j(t)$: radionuclide concentration on surface (Bq m^{-2})
K_{ijk} : kerma (pGy per γ mm^{-2})

Mechbach et. al. calculated kerma as a function of the location of a receptor, contaminated surface and gamma energy for 4 types of representative European buildings by using the Monte Calro method[7]. Although environmental characteristics are different region by region, these are being widely used to predict exposure doses in the existing models such as PARATI[8] and CHERURB-95. METRO-K considers 7 types of representative Korean buildings ;

(1) prefabricated 1 storey house,
(2) 1 storey semi-detached house with flat concrete roof,
(3) 2 storey semi-detached house with flat concrete roof,
(4) 2 storey semi-detached house with tile roof
(5) 3 storey terrace house with tile roof
(6) 5 storey large commercial building
(7) 10 storey apartment.

Mechbach's kerma values were rearranged to apply them to the Korean urban environment. **Fig. 2** shows an example for a rearrangement between two different buildings. The figures of the left-hand side and the right-hand side represent the simplified European building and Korean one, respectively. For the contamination of the roofs, it is assumed that kerma for the top floor of a 10 storey apartment is the same as that for the top floor of a 5 storey building, and kerma for the 5th floor of a 10 storey apartment is the same as that for the 1st floor of a 5 storey building. The kerma from the contaminated roofs for the other floors is obtained by an interpolation logarithmically. For the contamination of the trees, it is assumed that the kerma for the 5th floor of a 10 storey apartment building is the same that for the top floor of a 5 storey building. A predetermined data library for 7 types of buildings is made in a similar way described above. METRO-K calculates not only the exposure doses contributing from a contaminated building where a receptor resides, but also those contributing from the contamination of surrounding surfaces such as neighboring buildings and a large park. The parameter values to predict exposure doses from radionuclide concentrations including the kerma are described elsewhere in detail[4].

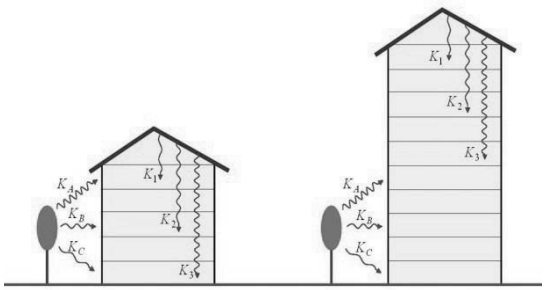

Fig. 2. An example for a rearrangement of Mechbach's kerma to apply it to the environment to be described in METRO-K. Figures of the left-hand side and the right-hand side present a simplified European building and a Korean one

III. Results and Discussion

METRO-K has been taking part in the Urban Remediation Working Group within the IAEA's EMRAS project for a model testing of Pripyat scenarios. The town of Pripyat is located 3 km northwest of the Chernobyl Nuclear Power Plant in the Ukraine. Participants were asked to submit predictive results for external dose rates at specified locations from all relevant surfaces and radionuclides, the contribution to dose rates from important surfaces and radionuclides, contamination densities at outdoor locations, and annual and accumulative (up to 20 years) external doses for specified reference individuals. Predictive results were requested for with and without remediation actions. Predictive results for various endpoints were submitted, and were compared and discussed at the Working Group meetings. In addition, predictive results were also compared with available measurements for dose rates at or near the test locations. Starting point given from the Working Group was 7 types of radionuclide concentrations (^{137}Cs, ^{134}Cs, ^{103}Ru, ^{106}Ru, ^{144}Ce, ^{95}Nb, ^{95}Zr) in soil on September 26th 1986.

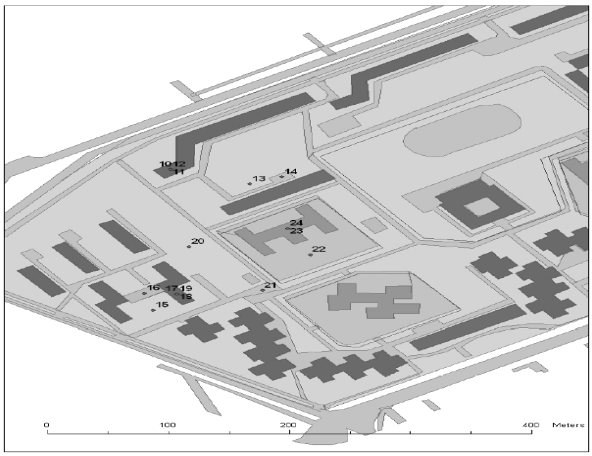

Fig. 3. Locations for the model calculations in District #4 of Pripyat. Location 21 is outdoor on paved ground, and location 24 is indoor on the 2nd floor of a 2 storey kindergarten building

Fig. 3 shows the locations for the model calculations in District #4 of Pripyat. The environment to be described in METRO-K may be different from what be described in the Pripyat scenarios due to the width of the roads and the area of the buildings. In this case, it is assumed that the kerma is proportional to the contaminated area and inversely squarely proportional to the distance from a receptor. **Fig. 4** shows the absorbed dose rates predicted at location 21 (outdoor on paved ground) using METRO-K. Soil or lawn was the highest contributor for several years following the Chernobyl accident. In addition, trees and paved ground played an important role in the absorbed dose rate.

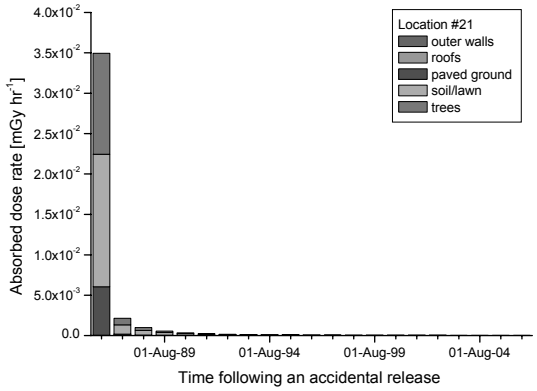

Fig. 4. Absorbed dose rates predicted from METRO-K at a location 21 in District #4 of Pripyat

Fig. 5 shows the absorbed dose rates at location 24 (2nd floor of a 2 storey kindergarten building). Roofs were the highest contributor for several years. Paved roads and soil also played an important role in the absorbed dose rates. Absorbed indoor dose rates were lower than those outdoor because of the shielding effects of the buildings. Contribution of contaminated surfaces to absorbed dose rates showed a distinct difference for the time following the accident as well as the location of a receptor.

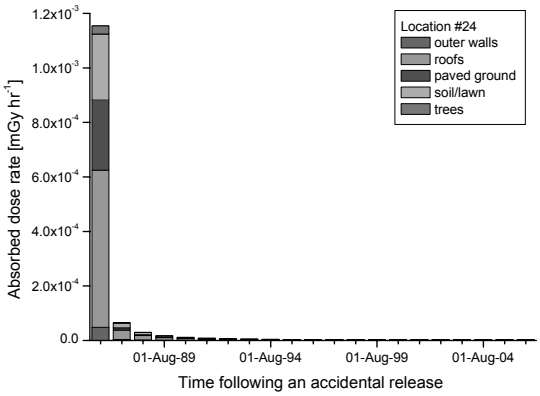

Fig. 5. Absorbed dose rate predicted from METRO-K at location 24 in Distirct #4 of Pripyat

Fig. 6 shows the contribution of the radionuclide in the absorbed dose rates at location 21. The contribution of ^{95}Nb was the highest in the first year of the Chernobyl accident, while the contribution of ^{137}Cs increased rapidly with time due to its long half-life.

Fig. 7 shows the contribution of the radionuclide to the absorbed dose rates at location 24. The contribution of the radionuclide showed a similarity for different locations of the same district.

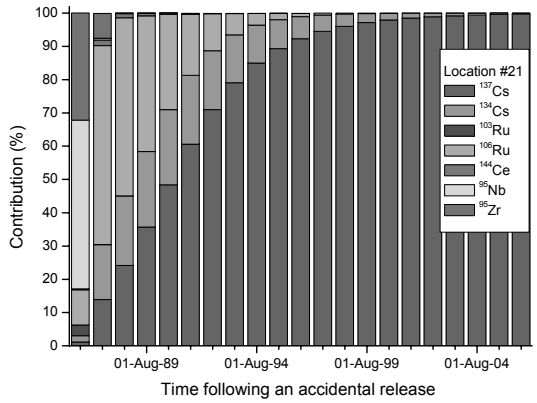

Fig. 6. Contribution of radionuclides at location 21 in District #4 of Pripyat

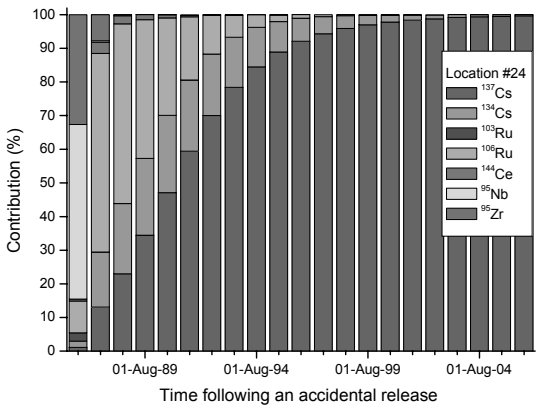

Fig. 7. Contribution of radionuclides at location 24 in District #4 of Pripyat

IV. Conclusions

For contamination scenarios of Pripyat District #4, predictive results using METRO-K were carried out as a part of the IAEA's EMRAS project. A comparative study with the predictive results of other models and measurements was not dealt in this paper because it is in progress within the project. Also the effectiveness on a variety of remediation actions was not dealt with. Even if the predictive results using METRO-K, which were requested from the Working Group, are not fully dealt with in this paper, it was possible to confirm that METRO-K is a good tool to predict exposure doses in an urban environment. The comprehensive results and discussions carried out in the Working Group will be published as one of IAEA's TECDOC by the end of 2007.

References

1) Workshop on Accidental Accidental Urban Contamination, Riso National Laboratory, Denmark (1987).
2) Conference on Radioactive Contamination in Urban Areas, Riso National Laboratory, Denmark (2003)
3) W. T. Hwang, E. H. Kim, H. J. Jeong, K. S. Suh and M. H. Han, "A Model for Evaluating the Radioactive Contamination in the Urban Environment", Journal of Radiation Protection, 30[3], 99 (2005).
4) W. T. Hwang, E. H. Kim, H. J. Jeong, K. S. Suh and M. H. Han, "A Model for Radiological Dose Assessment in an Urban Environment", Journal of Radiation Protection, 32[1], 1 (2007).
5) S-R. Peterson, S. Chouhan, B. Heinmiller and J. Koch, "CHERURB-95 : Urban Contamination and Dose Model", A research report prepared for the Atomic Energy Control Board (1995).
6) http://www.ns-iaea.org/projects/emras
7) R. Meckbach, P. Jocob and H. G. Parezke, "Gamma Exposures to Radionuclides Deposited in Urban Environments – Part I : Kerma Rates from Contaminated Surfaces", Radiation Protection Dosimetry, 21[3], 167 (1988).
8) E. R. Rochedo, L. F. Conti and H. G. Parezke, "PARATI : A Dynamic Model for Radiological Assessments in Urban Areas – Part I : Modelling of Urban Areas Their Contamination and Radiation Fields", Radiat. Environ. Biophys. 35, 243 (1996).

Journal of NUCLEAR SCIENCE and TECHNOLOGY, Supplement 5, p. 598–601 (June 2008)

Study on the Worldwide Estimation of Probabilistic Effective Dose from Intake of Marine Products

Masanao NAKANO*

Japan Atomic Energy Agency, 4-33 Muramatsu, Tokai-mura, Naka-gun, Ibaraki,319-1194, Japan

The public generally requires worldwide environmental protection. A long-term environmental assessment from nuclear fuel cycle facilities to the aquatic environment also becomes more important to utilize nuclear energy globally. Evaluation of long-term risk carried out not only in Japan but also in neighbouring countries is considered to be necessary in order to develop nuclear power industry. In advance of a multinational assessment of nuclear fuel cycle facilities, a worldwide estimation of effective dose due to the atmospheric nuclear tests was carried out by the deterministic and probabilistic methods as a case study. The deterministic calculation made it clear that ^{14}C contributes the most to the averaged effective dose from the intake of marine products due to the atmospheric nuclear tests. The averaged dose for Japanese was very small but it is about 7 times higher than the world average.

Although it depended on the deviation of each parameter, the 95th percentile of the effective dose by probabilistic method was calculated as 1/3 to 2/3 of that by the deterministic method in proforma calculation.

KEYWORDS: dose assessment, deterministic method, probabilistic method, ICRP, marine products, public, environment, atmospheric nuclear test

I. Introduction

The public generally requires worldwide environmental protection. A long-term environmental assessment from nuclear fuel cycle facilities to the aquatic environment also becomes more important to utilize nuclear energy globally. Evaluation of long-term risk including not only in Japan but also in neighboring countries is considered to be necessary in order to develop nuclear power industry.

The author has successfully simulated the distribution of radionuclides in seawater and seabed sediment produced by the atmospheric nuclear tests using LAMER (Long-term Assessment ModEl for Radioactivity in the oceans). A part of the LAMER calculated the advection- diffusion-scavenging processes for radionuclides in the oceans in cooperate with Oceanic General Circulation Model (OGCM) and was validated[1,2].

Recently, International Committee of Radiation Protection (ICRP) published new recommendation[3]. It implies probabilistic assessment as well as traditional deterministic assessment (averaged and 95th percentile) for dose evaluation (**Table 1**). It might be economic to assess the probabilistic risk from nuclear fuel cycle facilities.

In this paper, the effective dose from the radionuclides in several marine products, which were originated from the atmospheric nuclear tests, were carried out by the deterministic and the probabilistic methods as a case study. The deterministic method includes both averaged and 95th percentile assessment. Then, the results are discussed as preparatory investigations to apply the assessment of nuclear fuel cycle facilities.

Table 1 Summary of methods used for determining dose to the representative person[3]

	CALCULATION METHOD	
	Probabilistic	**Deterministic**
Environmental concentration data	Distribution of estimated or measured concentration	Single values for parameters
Habit data	Range or fixed values for habit data	Average value for the more highly exposed group or 95th percentile of appropriate national or regional data
Dose coefficient	Fixed value based on age	Fixed value based on age
Dose to the representative person	Method selected by operator or regulator. Representative personis identified such that the probability is less than about 5% that a person drawn at random from the population will receive a greater dose	Product of above values

II. Model

1. Outline

The dose to the representative person (S) is simply calculated by multiplying radionuclides concentration in seawater (Cw), concentration factor (CF), intake amount of marine product ($Intake$), and dose coefficient (DC) expressed as:

$$S = \sum_i \sum_k \sum_j (DC)_i (Intake)_{j,k} (CF)_{i,k} (Cw)_{i,j} \quad (1)$$

where, i, j and k express nuclide, sea area, and species of marine product, respectively.

In order to calculate the effective dose by the probabilistic methods from intake of marine products, Cw and $Intake$ have their distributions, not fixed values. As shown in **Table 1**, DC does not have distribution as well as CF. The monte-carlo calculation repeated 1,000 times to obtain dose distribution.

*Corresponding Author, E-mail: nakano.masanao@jaea.go.jp

The OGCM, advection-diffusion model and scavenging model were applied to determine *Cw*, with the fallout input from the atmospheric nuclear tests.

2. Oceanic General Circulation Model

In this study, a modified version of the robust diagnostic OGCM described by Fujio et al.[4] has been applied. The model covers the world ocean with real topography and divides it horizontally into 2º × 2º grids and vertically into 15 levels. It covers the area from 79ºS to 75ºN, with the exception of the Arctic Ocean, which is not included in the model. The model consists of equations of motion, continuity, state, advection and diffusion. Based on the annual average hydrographic data and the wind stress data, the annually averaged velocity fields were determined diagnostically. The further description is found elsewhere[1].

3. Advection-Diffusion Model

The procedure of tracking particles was the same as that described by Fujio et al.[4] Let $\mathbf{x}(t)$ be the position vector of a particle at time t, and $\mathbf{u}(\mathbf{x})$ be the three-dimensional velocity vector at position $\mathbf{x}(t)$ calculated by the above robust diagnostic OGCM. The tracking is expressed as the initial value problem by the equations (2) and (3).

$$\frac{d\mathbf{x}(t)}{dt} = \mathbf{u}(\mathbf{x}) \tag{2}$$

$$\mathbf{x}(0) = \mathbf{x}_0(0) \tag{3}$$

The random walk method was applied for the description of the diffusion of radionuclides in water. The distance (dL) of the movement caused by diffusion can be expressed by the equation (4).

$$dL = R\sqrt{24Kdt} \tag{4}$$

K is the horizontal or vertical turbulence coefficient, using the values of 1.3×10^4 m^2 s^{-1} and 3×10^{-5} m^2 s^{-1} for the horizontal and vertical diffusion coefficients, respectively. R is one of uniform random numbers (-0.5 ~ 0.5). The time step (dt) of the calculation was 10 days.

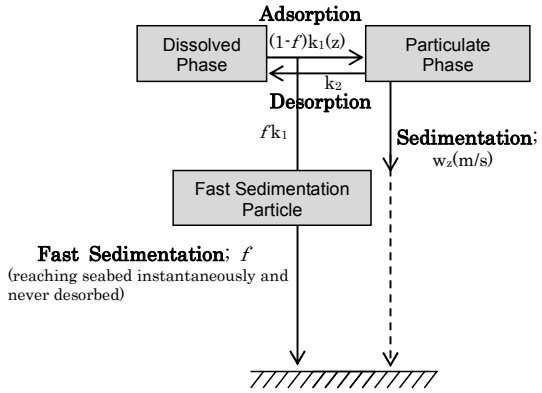

Fig.1 A simplified scavenging model in this study.

4. Scavenging Model

As shown in **Fig.1**, the one-dimensional, two-phase Pu model, which was applied for the Tahiti region (southeast Pacific Ocean), developed by Perianez[5], has been adopted in the present advection-diffusion model. Transfer between the dissolved phase and the particulate phase is subject to the kinetic transfer coefficients, $k_1(z)$ (adsorption) and k_2 (desorption). The particulate phase sinks at sedimentation velocity Wz. The further description is found elsewhere[2].

5. Fallout Input onto Sea Surface

The annual and latitudinal deposition of ^{3}H, ^{14}C, ^{90}Sr, ^{137}Cs and $^{239,240}Pu$ from global and local fallout was estimated and input on the basis on UNSCEAR 2000 report[6]. Annual deposition amounts of the radionuclides are shown in **Fig. 2**. The methods to determine the deposition amounts of these nuclides are as follows.

(1) ^{90}Sr, ^{137}Cs and $^{239,240}Pu$

The global and local fallouts from past atmospheric nuclear fission tests were used. Atmospheric nuclear tests of 543 (155 Mt of TNT equivalent) carried out between 1945 and 1980 contributed significantly to radionuclide contamination of the world ocean. The fallout from most nuclear tests has been distributed globally, and the fallout from Bikini and Enewetak comprised a substantial amount as well.

(2) ^{3}H and ^{14}C

Tritium (^{3}H) and ^{14}C were mainly originated not only from 251 Mt of fusion tests but also from the interaction of nitrogen and oxygen with cosmic ray. These nuclides in seawater are easily exchangeable with atmosphere, biosphere and geosphere. The material recycling models of hydrogen and carbon are essential to consider the net fallout amount of ^{3}H and ^{14}C, respectively.

In this study, ^{3}H and ^{14}C originated from only the fusion tests were considered to calculate the effective dose to human beings.

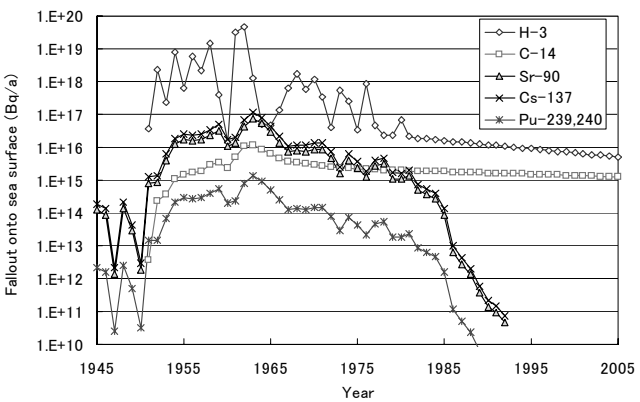

Fig.2 Total amounts of radionuclides fallen onto the sea surface

6. Intake Amount of Marine Products

The world and Japanese total marine production from 1950 to 2003 were compiled from FAO's (United Nations Food and Agriculture Organization) database[7]. The total production includes non-edible parts such as shell, bone, and lever. And it includes animal feeding stuff. Thus the intake amount was not the same with the production amount.

As shown in **Table 2**, the Japanese intake ratio, which was defined by (intake) / (production), was calculated with Japanese total production by FAO and intake in Japan by the national nutrition survey of Ministry of Health, Labor and Welfare (MHLW)[8]. The world intake ratio was assumed to be same with the Japanese intake ratio. The Japanese and world intakes of marine product can be calculated by the Japanese and world production multiplied with the estimated intake ratio.

Table 2 Estimated intake ratio for each marine product.

species	Production in Japan*1 (kt/a)	Intake in Japan *2 per capita (g/d)	Intake in Japan *2 Total (kt/a)	Estimated intake ratio (%)
Fish	4,787	77.8	3,582	75
Crustaceans, cephalopod	902	15.4	709	79
Shellfishery	855	5.0	230	27
seaweed	683	5.2	239	35

*1 Total marine production in 1997 by FAO[7]

*2 Intake of marine products in 1997 by MHLW[8]

As for intake amount of marine products, very few references described the distribution form of intake amount. According to Byrom et al.[9], established database suggested that 95th percentile of consumption rates for many staple foods tended to exceed the mean value of the distribution by approximately a factor of 3. Based on this description, the logarithm distribution, that 3 times of average was equal to 95th percentile, was assumed and applied for the probabilistic risk assessment.

7. Concentration Factor and Other Parameters

The concentration factors (*CF*) of marine products and the dose coefficients (*DC*) of radionuclides were quoted as **Table 3** from IAEA Technical report series No.422.[10] and ICRP publication 72[11], respectively.

Table 3 Concentration factor and dose coefficient for each nuclide.

		^{3}H	^{14}C	^{90}Sr	^{137}Cs	^{239}Pu
CF[10]	Fish (Surface fish)	1	20,000	3	100	100
	Crustaceans	1	20,000	5	50	200
	Shellfishery (Molluscs)	1	20,000	10	60	3,000
	cephalopod	(1)*	(20,000)*	2	9	50
	Seaweed (Macroalgae)	1	10,000	10	50	4,000
DC	(Sv/Bq)[11]	4.2e-11	5.8e-10	2.8e-8	1.3e-8	2.5e-7

* No description in IAEA Technical report No.422

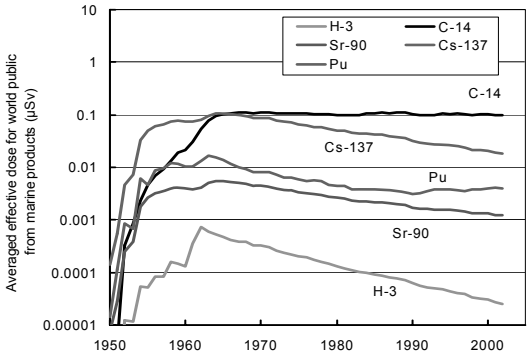

Fig. 3 Average effective dose for world public from marine products.

III. Result and Discussion

1. Deterministic Dose (averaged)

World averaged dose from the intake of marine products due to the atmospheric nuclear weapon tests is shown in **Fig.3**. After 1965, ^{14}C was the most contributing nuclide, and cumulative dose of ^{14}C from 1950 to 2003 occupied about half of all nuclides, and ^{137}Cs was the second one. The averaged dose had a maximum (0.23 μSv/a) in 1966, then gradually decreased to 0.12 μSv/a in 2003.

Japanese averaged dose is shown in **Fig.4**. It was 1.6 μSv/a in 1963, and 0.36 μSv/a in 2003. Japanese averaged dose was larger than world averaged dose throughout the calculation period.

The reason is considered that the radioactive concentration in surface seawater in the northwestern of Pacific Ocean has relatively high, and that Japanese generally has a lot of marine products by dietary habit.

But the diffusion of radionuclides, and downslide of intake of marine products by westernization of dietary habit made the dose ratio between Japan and world to be about 3 times in 2003, though it was about 7 times in 1963. The cumulative dose for 54 years from 1950 to 2003 was 7.6 μSv for world average and 55 μSv for Japanese average. The effective dose from intake of marine products was confirmed to be sufficiently less than the dose limit defined by ICRP.

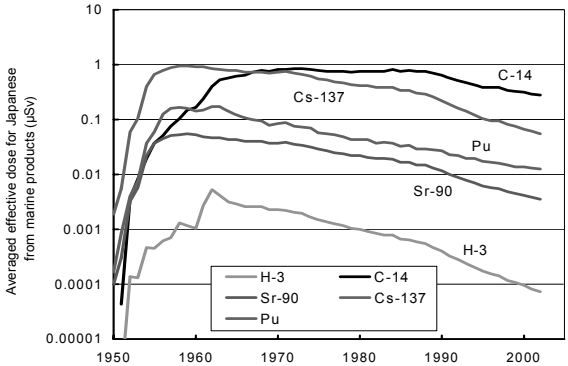

Fig.4 Average effective dose for Japanese from marine products.

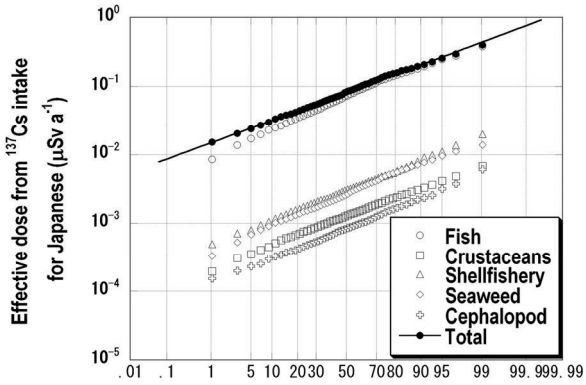

Fig.5 The distribution of Japanese effective dose for ^{137}Cs by the intake of several kinds of marine products.

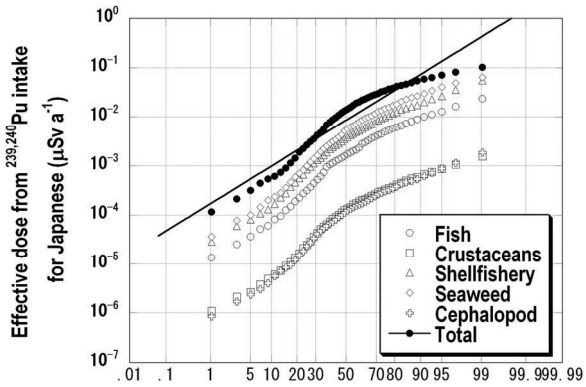

Fig.6 The distribution of Japanese effective dose for ^{239,240}Pu by the intake of several kinds of marine products.

2. Probabilistic Dose

The distribution of Japanese effective dose for ^{137}Cs and for ^{239,240}Pu by the intake of several kinds of marine products caught in the northwestern Pacific Ocean in 1997 is shown in **Figs .5 and 6**.

As for ^{137}Cs, the distribution looked like log-normal, and the total dose of each marine product was 0.024 μSv/a, 0.083 μSv/a, 0.25 μSv/a for 5th, 50th, 95th percentile, respectively.

As for ^{239,240}Pu, the distribution did not look like log-normal. Plutonium, which is insoluble element to seawater, is considered to be easily transported downward by scavenging process. The variation of ^{239,240}Pu concentration in the same area was larger than that of ^{137}Cs. The total dose of each marine product for ^{239,240}Pu was 0.00031 μSv/a, 0.013 μSv/a, 0.070 μSv/a for 5th, 50th, 95th percentile, respectively.

3. Comparison of Deterministic (averaged and 95th percentile) and Probabilistic Assessment

The result of the deterministic assessment in the section 'III 1.' showed the averaged figure using the averaged parameters. To compare the result of probabilistic assessment, the deterministic assessment for Japanese from northwest Pacific in 1997 was performed using the 95th percentile of the parameters. As shown in **Table 4**, the 95th percentiles of the deterministic assessment were confirmed to be about 1.5 to 3 times of the 95th percentiles of the probabilistic assessment.

Table 4 Comparison of the effective dose for Japanese from northwest Pacific in 1997

Method	Deterministic (Averaged)	Probabilistic (95th percentile)	Deterministic (95th percentile)
^{137}Cs	0.085 μSv	0.25 μSv	0.41 μSv
^{239,240}Pu	0.020 μSv	0.070 μSv	0.20 μSv

VI. Conclusions

The deterministic calculation made it clear that ^{14}C contributes at the most to the effective dose from the intake of marine products due to the atmospheric nuclear tests. Then, ^{137}Cs, ^{239,240}Pu, ^{90}Sr and ^{3}H contribute to the effective dose in order.

The averaged dose for Japanese was very small but about 7 times higher than the world average.

Although it depended on the deviation of each parameter, the 95th percentile of the effective dose by probabilistic method was calculated as 1 third to 2 thirds of the 95th percentile of the effective dose by deterministic method in proforma calculation.

This method can show the deterministic and probabilistic worldwide dose due to the past atmospheric nuclear tests. Also, the practical procedure and control factor of the probabilistic assessment were confirmed in this study. In near future, the deterministic and probabilistic assessment from nuclear fuel cycle facilities will be carried out using the technique developed in this study.

References

1) M. Nakano and P.P.Povinec, "Oceanic general circulation model for the assessment of the distribution of 137Cs in the world ocean", Deep Sea Res. Part II, 50, 2803-2816 (2003).
2) M. Nakano and P.P.Povinec, "Modeling the distribution of plutonium in the Pacific Ocean", J. Env. Radioact., 69, 85-106 (2003).
3) ICRP, "Publ.101: "Assessing Dose of the Representative Person for the Purpose of Radiation Protection of the Public", (2007).
4) S.Fujio and N.Imasato, "Diagnostic Calculation for Circulation and Water Mass Movement in the Deep Pacific", J. Geophys. Res. 96, 759-774 (1991).
5) R.Perianez, "Modeling the Distribution of Radionuclides in Deep Ocean Water Columns. Application to 3H, 137Cs and 239,240Pu", J. Environ. Radioactivity. 38, 173-194 (1998).
6) UNSCEAR, 2000 report (2000).
7) Food and Agriculture Organization of the United Nations (FAO); "Total production 1950-2003", ftp://ftp.fao.org/fi/stat/windows/fishplus/fstat.zip (2005).
8) Ministry of Health, Labor and Welfare (MHLW), "National nutrition survey in 1997", p.78, Daiichi shuppan, Tokyo (1999).(in Japanese)
9) Byrom, J., C. Robinson, J.R.Simmonds, B.Walters, and R.R. Taylor, "Food Consumption Rates for Use in Generalised Radiological Dose Assessments", J. Radiol. Prot. 15(4) 335-341 (1995).
10) IAEA, Technical Report Series No.422, (2006).
11) ICRP, "Age-dependent Doses to the Members of the Public from Intake of Radionuclides Part 5, Compilation of Ingestion and Inhalation Coefficients", Publication 72 (1995).

Journal of NUCLEAR SCIENCE and TECHNOLOGY, Supplement 5, p. 602–605 (June 2008)

First Report of Environmental Gamma Radiation Levels in Twenty Four Towns and Cities of Khorasan Region-Iran

BAHREYNI TOOSSI Mohammad Taghi[1*], BAYANI Shahram[1], ABDOLRAHIMI Mohammad Reza[2] and SAZGARNIA Ameneh[1]

[1]*Medical Physics Research Center, Environmental Dosimetry Laboratory, Mashad University of Medical Sciences, Mashad-Iran*
[2]*Medical Physics Department, Faculty of Medicine, Mashad University of Medical Sciences, Mashad-Iran*

Although many researchers have focused their attention to man made sources, but natural sources constitute more than 85% of human exposure to ionizing radiation. Due to the significance of natural sources, comprehensive studies have been carried out in developed countries. In Iran like many other developing countries, this subject has not been considered as a research priority. Until 1990 only Ramsar located in the south coast of Caspian sea had attracted attention of some researchers. In 1996 preparation of out-door natural radiation map of Iran was defined as a long term goal in my center. Since then environmental gamma radiation dose rate of residential area of 10 counties have been estimated. In this article only annual dose rates of Khorasan are reported.

In every one city five stations were selected. A survey meter model RDS-110 was placed one meter above the ground level.

Dose rates were measured for one hour in three successive days. Although average dose rates of every one of the stations were numerically different, but their differences are not significant. Out-door gamma dose rates acquired for 24 towns are within the range of 56 to 144 nGy/h.

Minimum and maximum dose rates are respectively attributed to Dargaz, in the north and Gonabad in the south.

KEYWORDS: natural radiation, dose rate, out-door gamma

I. Introduction

In fact we have all grown up on a planet which has, in some places quite a high level of background radiation and life on earth has evolved to cope with this.

Background radiation levels on earth have decreased by a factor of about 10 since life evolved on earth, although since the evolution of human it's reduction has been negligible[1,2].

Natural background radiation is originated from a few sources. Contribution of individual sources to the total activity depends on several factors. It varies around the globe by at least two order of magnitude[3].

Radiation dose from natural sources are originating from external sources (cosmic rays and terrestrial radiation) and internal sources, due to radon inhalation and ingestion of ^{210}Pb. In Europe average total natural background radiation varies from 1.5 mSv/y in UK to 7.5 mSv/y in Finland[4]. From the end of 19th century man made sources have also contributed to background activity. In the United States 82% of radiation exposure to man is emerging from natural sources e.g. Radon gas, cosmic rays, terrestrial and internal sources[5]. In our time human beings are exposed to a range of man made sources too. In most countries medical x-ray is the largest source of artificial exposure[5].

Although the biological effect of ionizing radiation does not depend on the nature of it's source (i.e. natural or artificial), but in early decades of the 20th century health consequence of man-made sources were more scrutinized. In the second half of the last century in many developed countries comprehensive studies were carried out and the map of natural background radiation and its components i.e. cosmic rays, radon in air and so on were prepared.

Lesser priority has been given to this subject in developing countries, although some sporadic work have been reported[6,7,8,9,10,11], mostly for specific sites with high natural background radiation[12].

In Iran before 1996 a few hot spots in Ramsar had been identified[3,13,14,15], yet no systematic study of normal area had been carried out. In 1996 preparation of out-door environmental gamma radiation map of residential area of towns and cities of Iran was defined as a long term goal in our center. Till now annual dose rates have been accomplished for: Khorasan (north), Khorasan (south), Khorasan (Razavi), Mazandaran, Azarbijan (West), Azarbijan (East), Kurdestan, Kerman, Sistan-Baluchestan and Hormozgan provinces, covering over 33% of the whole country[16,17,18,19,20,21]. In this article annual dose rates for twenty four towns and cities of big Khorasan province are reported. The results are compared with the corresponding dose rates of other counties as well as with the data reported by researchers from other countries.

II. Material and Method

1. Selection of Measuring Locations

As a practical method and based on the results of a pilot study and in order to attribute the final results to the whole residential area of a town five stations were selected for every town.

*Corresponding Author, Tel No : +98 511 882 8576, Fax No : +98 511 800 2320, E-mail: bahreynimt@mums.ac.ir

By the aid of a city map, first station was selected at a suitable place (as is described later) in the city center. The other four stations at the border line of every town residential area. The location of individual station was studied closely to comply with the recommended conditions in the literature i.e. to be on an area covered by grass (if available), untacked soil, at least 15 meters away from any natural or man made structure[22].

2. Choice of Proper Detector

In order to estimate the dose rate arising from environmental gamma radiation many researchers have employed a GM detector[7,8,22]. In this work three types of gas filled ionization chamber, Geiger Muller type, were examined.

(1) Intelligent RD-02

Intelligent RD-02 detector is made by RADOS-OY company in Finland. RD-02 is the heart of a very elaborate system Area Monitoring (AAM-90), it include two halogen quenched energy compensated Geiger Muller tube, one for low doses and the other for high doses. It measures the dose rate from normal background to catastrophically high levels. The probe it self is fully independent in it's operation, the dose rate measured by the probe is saved in it's internal memory and transfers the saved data to the system computer. The system is run and controlled by specially compiled software AAM 90/45, the brain of the system. The AAM-90 system is normally used as a country wide network. Although it can be used as a single station to monitor a building or a room. It is best to be employed for a vast area with several remote controlled probes. Measurement range for RD-02 is 0.01 μGy/h to 10 mGy/h[23].

(2) Environmental Radiation Meter 6-80

Environmental radiation meter 6-80 made by Mini Instrument Inc. is mainly consisted of a Geiger Muller tube MC-71 model, a display unit, a connecting cable and a tripod to hold the tube above the ground level. It is designed for environmental gamma monitoring. It has two independent displaying systems:

a) Digital display (scalar), equipped with a predefined auto-set measuring time. The scalar provides environmental activity in terms of count per second, which can be converted to dose rate in μGy/h.
b) Analogue display (Rate meter), displays environmental gamma dose rate in μGy/h. Measurement range for this system is 0.05 μGy/h to 75 μGy/h.

E.R.M. is a reasonably small, light weight, portable, DC operating system. It is also water proof[24].

(3) Multiple Purpose Survey Meter RDS-110

RDS-110 made by RADOS Company in Finland is basically a simple Geiger-Muller detector. It is benefiting from advanced electronic circuit. As a microprocessor based GM detector is a multi functional system. It is designed for monitoring gamma, x-ray and beta radiation. It is versatile and durable, therefore ideally suited for a wide range of harsh applications. It is a light weight portable, battery operated piece of equipment, capable of functioning at extreme temperatures. Incorporation of an advanced electronic circuit in this equipment provides the operator : LED digital display, automatic rang indication, freely adjustable levels for dose, dose rates and accumulated dose, setting pre-defined alarm threshold. Measurement range for this survey meter is 0.05 μGy/h to 99.99 mGy/h [25].

On the other hand if we look back at section 2.1, 2.2 and 2.3 then will remain little doubt that RDS-110, over all is the best detector for our studies. The only point to be explained was the accuracy of RDS-110 relative to the other two systems. To assess the accuracy of RDS-110 a pilot study was performed, close to one RD-02 station, an E.R.M (6-80) and one RDS-110 were installed. Environmental gamma dose rate was measured by all three detectors 60 minutes twice a day and for seven days. Average dose rates were calculated and the following figures were obtained **Table 1**. From average dose rates and their SD's in table one there remain no doubt that the performance of RDS-110 is as accurate as RD-02 which is very elaborate detector. Simplicity of operation, practicality, excellent electronic functionality as well as the accuracy of RDS-110 made it our best choice to employ it for our long term study.

Table 1 RDS-110 accuracy compared with E.R.M and RD-02

Equipment	Mean(μGyh^{-1})	Standard Deviation
E.R.M	0.06	0.01
RDS-110	0.07	0.01
Intelligent RD-02	0.07	0.01

With respect to our final conclusion in regards to the selection of RDS-110, dose rate measurement was performed in the following order

a) Five locations were marked on the latest edition of every town's map.
b) A survey meter model RDS-110 was placed on aluminum frame and a tripod one meter above the ground level, horizontally and in the south-north direction.
c) All displayed dose rates on display of the detector were recorded for one hour, this procedure was repeated in three successive days.
d) Mean of all recorded data in step (c) was computed and taken as dose rate of that particular station.
e) Dose rates acquired at step (d) were statistically tested to find out if they were significantly or widely different, to decide whether further investigation was necessary.
f) Computed mean of all five stations in every town was assigned to average dose rate of the specified town.

g) Finally mean dose rate and population of all 24 towns were utilized to calculate population weighted dose rate of the Khorasan County.
h) Step (g) was exactly repeated for other counties.

III. Results

As described in section II, practically huge numbers of dose rates were recorded but step by step they were substantially summarized, to avoid a very bulk table the most important dose rate quantities i.e. maximum, average and minimum dose rates for all 24 towns, plus corresponding population are tabulated in **Table 2.** Population's weighted mean dose rate for Khorasan province is also presented.

Table 2 Environmental gamma dose rate of 24 towns of Khorasan

City/ Town	Population	Minimum dose rate (nGy/h)	Maximum dose rate (nGy/h)	Average dose rate (nGy/h)
Daregaz	78614	56	71	62
Lotf abad	-	-	-	65
Sabzevar	419049	63	77	66
Bojnord	278818	67	82	70
Tabas	59632	63	83	70
Fareaman	77555	68	86	77
Sarakhs	73604	72	87	78
Esfarayen	118334	80	89	83
Torbateh Heydaryeh	340231	78	89	83
Shearvan	200045	69	93	83
Nehbandaan	40010	79	90	84
Chenaraan	106747	74	101	85
Bearjand	308290	70	95	86
Ghochan	152105	73	115	88
Mashhad	2277811	84	99	90
Khaf	92158	86	95	92
Ghayen	126951	85	102	92
Kashmar	185398	83	120	94
Torbateh jaam	210253	80	111	97
Tayebad	127679	89	114	101
Bardaskan	65393	93	115	102
Neyshabour	411235	79	132	102
Ferdows	54920	92	121	108
Gonabaad	103625	92	144	120
Populations weighted average dose rate for Khorasan				87

IV. Discussion and Conclusion

As explained in section II, average dose rate for individual locations in each town looked different, to ensure they were significantly different, they were statistically examined. In some instances average dose rates of two or three stations were significantly different from the others e.g. in Ghonabad average dose rates for stations 1, 2 and 3 are not significantly different, same conclusion is true for stations 4 and 5, but the differences between stations 1, 2 and 3 on one hand and stations 4 and 5 on the other hand are significantly different **Fig. 1**.

Arithmetic average dose rate computed for a county consisting of towns of widely different population dose not take into account the number of people exposed to different dose rates. To take this human factor into account population weighted mean is calculated which is influenced by both elements of dose rate and population **Table 3**.

In **Fig. 2** maximum and minimum out-door dose rates of Khorasan province have been compared with corresponding quantities acquired for some other counties and similar results reported for Hong Kong, UK and Germany. Mazandaran, Azarbayjan, Kurdestan and Khorasan are all located in North central, North West and North East of Iran. Most of the towns in these counties are also situated at high altitudes. On the other hand Sistan-Baluchestan, Kerman and Hormozgan are located from center to South East. Hormozgan in particular is situated at the north coast of Oman sea. An interesting feature of Fig 2 is the fact that maximum dose rate is declining when you move from north to south. The inhabitants of Mazandaran, Azarbayjan, Kurdestan are exposed to higher dose than Hong Kong and UK populations. On the other hand people living in Germany on average receive a higher out-door gamma radiation dose rate than all counties so far studied in Iran.

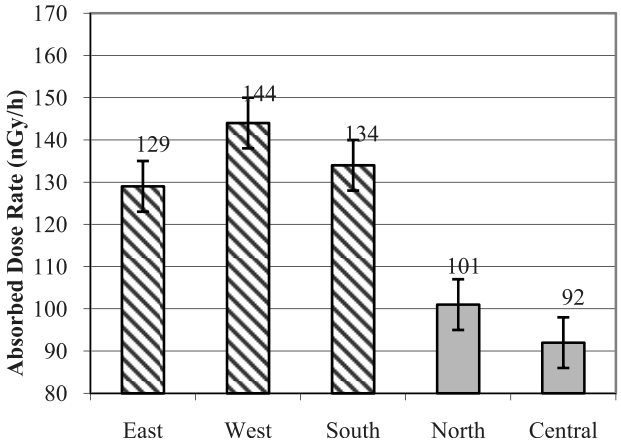

Fig. 1 A typical dose rate of different stations in a town (Gonabad)

Table 3 Average population weighted dose rate for 6 counties in Iran

Province	Population weighted mean (nGy/h)
Systan & blochestan	69
Kerman	96
Khorasan	88
Hormozgan	39
Kordestan	114
Mazandaran	80

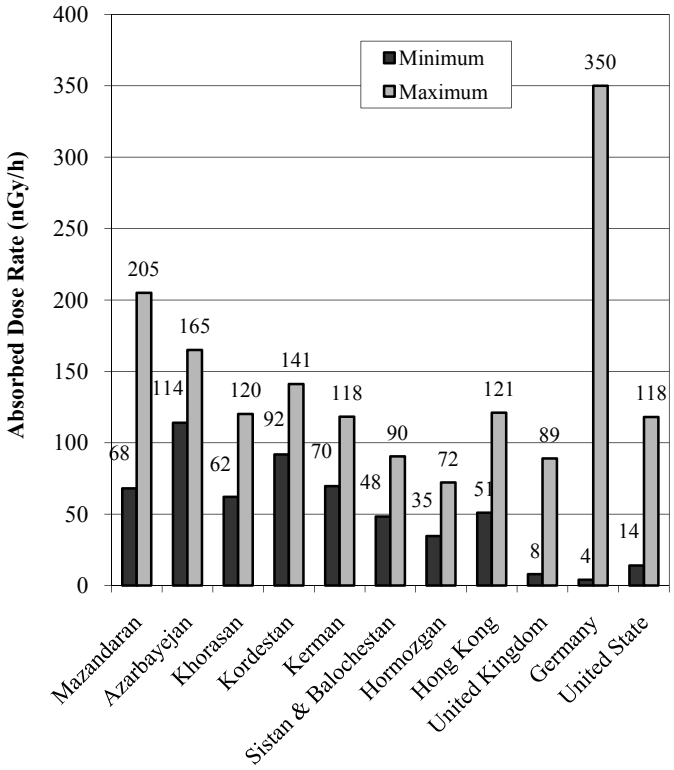

Fig. 2 Environmental gamma dose rate (out-door) for Khorasan province compared with corresponding values for six more counties in Iran and four other countries

Acknowledgement

The authors would like to thank the research council and office of vice president for research affairs of Mashad University of Medical Sciences for their financial support of this work.

References

1) P.A. Karam, S.A. Leslie, 'Calculations of background beta-gamma radiation dose through geologic time'. Health Physics, Vol. 77, No. 6, 662 (1999).
2) P.A. Karam, S.A. Leslie. 'The effects of changing atmospheric oxygen concentrations and background radiation levels on radiogenic DNA damage rates'. Health Physics, Vol. 81, No. 5, 545 (2001).
3) P.A. Karam, 'The high background radiation area in Ramsar Iran: geology, norm, biology, LNT and possible regulatory fun'. WM'o2 Conference, Tucson, A2, 24 (2002).
4) 'Radiation and the nuclear fuel cycle' , World Nuclear Association , 2004 , www.solarstorms.org
5) M.A. Statkiewicz Sherer, P.L. Visconti, E.R. Ritenour, 'Radiation protection in medical radiolography'. 4th Ed., Andrew Allen, 11 (2002).
6) F. P. Bonzi, P. Msaki, I.N. Makundi, 'A survey of background radaiton dose rates and radioactivity in Tanzania'. Health Physics, Vol. 82, No. 1, 80 (2002).
7) F. Bouzorjomehri, M. H. Ehrampoush, 'Gamma background radiation in Yazd province; a preliminary report'. Iran. J. Radiat. Res., Vol. 3, No. 1, 17 (2005).
8) D. Shahbazi Gahrouei, 'Natural background radiation dosimetry in the highest altitude region of Iran'. J. Radiat. Res., Vol. 44, 285 (2003).
9) Lin Yu-Ming, Lin Pei-Hon, 'Natural background radiation dose assessment in Taiwan'. Environment International, Vol. 22, 45 (1996).
10) R. Hewamanna, C.S. Sumithrarachchi, 'Natural radioactivity and gamma dose from Sri Lonkan clay bricks used in building construction'. Applied Radiation and Isotopes, Vol. 54, 365 (2001).
11) Y.K. Abdul Ahad, H.H. Ali, M.M. Abdalla, 'Environmental gamma radiation monitoring using TLD at the Tuwaitha site and other regions of Iraq'. Radiation Protection Dosimetry, Vol. 34, 215 (1990).
12) M. Beitollahi, M. Ghiassi-Nejad, A. Esmaeili, R. Dunker, 'Radiological studies in the hot springs region of Mahallat, central Iran'. Radiation Protection Dosimetry, Vol. 123, No. 4, 505 (2007).
13) M. Ghiassi-Nejad, S.M.J. Mortasari, J.R. Cameron, et al., 'Very high background radiation areas of Ramsar, Iran: preliminary biological studies'. Health Physics, Vol. 82, 87 (2002).
14) B. Khademi, A. Sekhavat, H. Parnianpour, 'Area of natural background radiation in the northern part of Iran'. International Symposium on Areas of High Natural Radioactivity, Brasil, 186 (1975).
15) M. Ghiassi-Nejad, M.M. Beitollahi, N. Fallahian, et al., 'New findings in the very high natural radiation area of Ramsar, Iran'. International Congress Series, Vol. 1276 (2004).
16) M.T. Bahreyni Toossi, M.H. Oroogi, 'An investigation of environmental γ-radiation rate in Mashhad and Rural area'. Iranian Journal of Basic Medical Sciences, Vol. 2, No. 3, 117 (1999).
17) M. T. Bahreyni Toossi, A. Sadeghzadeh, 'Estimation of Environmental Gamma Background Radiation Levels in Azarbayjan'. Iranian Journal of Basic Medical Sciences, Vol. 3, No. 1 (2000).
18) M. Yarahmadi, M.T. Bahreyni Toossi, 'Comparison indoor and outdoor dose rates from environmental radiation in Kurdstan province's towns'. The 6th Iranian Congress of Medical Physics, Mashhad-Iran, 14 (2004).
19) A. Aghamir, M.T. Bahreyni Toossi, 'An assessment of exposure from environmental gamma radiation in cities and hot and mineral spring waters of Mazandaran province'. The 6th Iranian Congress of Medical Physics, Mashhad-Iran, 9 (2004).
20) M.T. Bahreyni Toossi, A. Jomehzadeh, 'Comparison of environmental gamma radiation of Kerman province and indoor gamma dose rate in Kerman city using thermoluminent dosimeter (TLD) and RDS-110'. Quarterly Journal of Hormozgan University of Medical Sciences, Vol. 9, No. 3, 173 (2005).
21) M.T. Bahreyni Toossi, M. Hagh Parast, 'Gachin dwellings on a hot area but with normal background'. IRPA- 2006, Paris (2006).
22) F.W. Spiers, J.A.B. Gibson, I.M.G. Thompson, 'A guide the measurement of environmetal gamma ray dose rate'. BCRU (1981).
23) AAM-90 Area Monitoring System user manual, RADOS Technology Oy, Finland.(1996)
24) Environmental Radiaiton Meter, type 6-80, user manual, Mini-Instruments Inc., England.(1998)
25) RDS-110, Multi-purpose survey meter operating instructions, RADOS Technology Oy, Finland (1995).

Journal of NUCLEAR SCIENCE and TECHNOLOGY, Supplement 5, p. 606–609 (June 2008)

Research on Additional External Exposure Dose Rate Measurement by in-situ HPGe γ spectrometer

JIA Mingyan[1*] and LI Huibin[2*]

Northwest Institute of Nuclear Technology, Xi'an, China, P.O.Box 69-1 Xi'an 710024 P.R.China

Abstract: A spectrometric method for additional exposure dose rate (external dose rate due to γ-ray emitted by artificial nuclides) measurement is introduced. The principle of this method is that: strip off the spectrum attributed to the natural radionuclides from the gamma spectrum collected by in situ HPGe spectrometer , and get the spectrum attributed to the artificial radionuclides , then integrate the stripped spectrum with corresponding spectrum-dose conversion function ($G(E)$ function) values to acquire additional exposure dose rate . Standard spectrums attributed to nuclides in U series、Th series and ^{40}K were calibrated by in situ HPGe spectrometer at airborne pads, and the interference caused by other nuclides was eliminated by the inverse matrix calculations. The natural compositions in the spectrum is stripped according to the standard spectrums. Six standard γ-ray sources were used to acquire the response functions of the HPGe spectrometer, then the $G(E)$ function was calculated by the least square method. Finally, the utility of this method was verified by in situ experiment, and the factors that influence the precision of the results are discussed.

KEYWORDS: HPGe spectrometer, spectrum dose conversion function, stripping method, certification

I. Introduction

In situ γ spectrum measurement plays an important role in environmental radioactivity monitoring. It is mainly used to measure categories and inventories of the artificial radionuclides. This technique was created by Beck et al in 1972[1)], and further developed by ICRU in 1994[2)]. In this method, the in-situ γ ray spectrum, via the analysis of the full absorption peaks, provides a measure of unscattered flux from various radionuclides, then the measured flux can be converted to concentrations or inventories of various nuclides in soil. The disadvantage of this method is that the calculation of calibration factors must be based on known distribution of radionuclides. In some cases, it is difficult to get the distribution function, especially in inhomogeneously contaminated areas and in structured terrains.

This paper introduce a method to calculate additional exposure dose rate by applying spectrum-dose conversion function($G(E)$ function) to spectrum due to artificial radionuclides. In principle, γ-ray spectrum collected by in-situ spectrometer in contaminated sites is consisted of two compositions, i.e. spectrum caused by artificial radionuclides and spectrum due to natural nuclides, including ^{40}K, U and Th series. If the counts corresponding to natural radionuclides can be stripped off from the original spectrum, the remaining is completely caused by artificial nuclides, and is relative to additional exposure dose rate values which can be obtained by applying $G(E)$ function to the stripped spectrum.

*Corresponding Author, Tel No: 086-29-84765047, Fax No: 086-29-83366333, E-mail: huaxiuwang@163.com[1], manxue685@sohu.com[2]

II. Stripped off Spectrums Attributed to Natural Radionuclides

In general, natural radionuclides such as ^{40}K, nuclides of U and Th series can be considered to uniformly distributed in soil, so the shapes of spectrums attributed to these natural radionuclides are steady in different sites measurement, although peak counting rates may change . In order to obtain standard spectrums attributed to ^{40}K, U series and Th series, the spectrometer was calibrated at airborne pads . These pads are concrete blocks individually doped with U, Th and K minerals. One pad Area is 126m^2, and the depth is 50cm.

A closed-end coaxial HPGe detector, the Ge crystal of which is 54.5mm in diameter and 57.1mm long, was used in the study. The crystal is attached to a cryostat having a liquid-nitrogen dewar of 7.5L. The detector was supported 1m high above the ground by a tripod in the center of the pads as shown in **Fig 1**. Four standard spectrums were acquired at U, Th, K and background pads, and the inverse matrix method was used to eliminate the interference caused by impurity nuclides and radiation from the surrounding environment.

Fig.1 Spectrometer calibration at airborne pads

The counts attributed to ^{40}K, nuclides in U and Th series can be stripped off from the original spectrum according to the peak counting proportions between the measured spectrum and the standard spectrums . The counts of 1764.5keV (^{214}Bi) characterizes the nuclides in U series, in the same way, counts of 2614.7keV (^{208}Tl) characterizes Th series and counts of 1460.8keV characterizes ^{40}K. For example, if peak counting of 1460.8keV in one spectrum measured is fivefold to that in standard ^{40}K spectrum, the original spectrum should be stripped off which is fivefold to standard ^{40}K spectrum. For nuclides in Th series and ^{40}K, the same approach are applied. A measured spectrum and standard spectrums to U, Th series and ^{40}K is shown in **Fig. 2**.

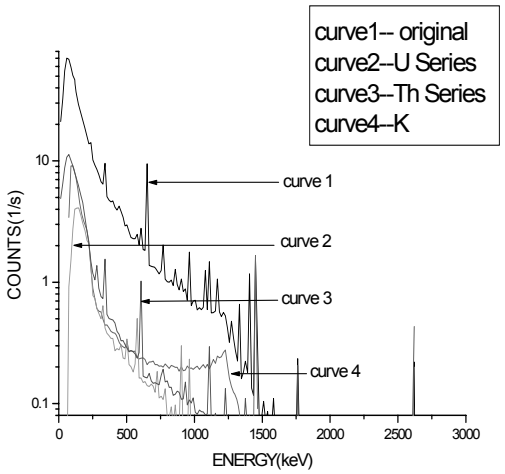

Fig. 2 Sketch of spectrum stripping. Curve 1 is the original spectrum, and the curve 2,3,4 are standard spectrums attributed to U, Th series and ^{40}K.

III. Additional Exposure Dose Rate Calculated by G(E) Function

External exposure dose rate can be simply evaluated by the total counts in a given energy range of the spectrum, but this tedious procedure may not be accuracy, because dose rate value is relative to γ-ray energy. Spectrum-dose conversion function ($G(E)$ function), theoretically, can eliminate the energy dependence of the HPGe crystal in the estimation of dose rate[3]. So the stripped spectrum shown in **Fig. 2** can be converted to additional γ dose rate by applying the $G(E)$ function.

The measured spectrum $F(E)$ can be expressed by the combination of spectrums due to monoenergetic photons:

$$F(E)=\sum N_i f(E,E_i) \quad (1)$$

where, N_i: Number of incident photon of energy E_i.

$f(E,E_i)$: Pulse height distribution of the spectrum per one incident photon of energy E_i,

So the total γ dose rate $\dot{D}$, can be expressed as follows:

$$\begin{aligned}\dot{D}&=\sum \dot{D}_i=\sum\left[N_i\int_0^{E_i} f(E,E_i)G(E)dE\right]\\&=\int_0^{E_i}[N_i f(E,E_i)]G(E)dE\\&=\int_0^{E_{\max}} F(E)G(E)dE\end{aligned} \quad (2)$$

where, $\dot{D}_i$: γ dose rate corresponding to the counting rate of energy E_i.

$E_{\max}$: Maximum energy in the spectrum, in general, $E_{\max}$=3MeV.

$G(E)$ function values can be determined by the least square method using the response functions of the detector.[4] The response functions can be determined either by MC simulation or by monoenergetic γ-ray source calibration. In this paper , the detector was calibrated by six standard sources: ^{241}Am, ^{155}Eu, ^{137}Cs, ^{54}Mn, ^{22}Na and ^{60}Co for the gamma-ray incidence at 90°. Six response functions were acquired from the experiments. Angle response of the detector was negligible, because the ratio of the crystal's diameter to its length is about one, so the angle response effects of the detector only induce little error to the results.

The dose rate corresponding to each response function was calculated by the $G(E)$ function method:

$$\dot{D}_j'=\int_0^{E_i} F_j(E)G(E)dE \quad (3)$$

where, $F_j(E)$: Standard spectrum corresponding to the j-th standard point source

E_i: Maximum γ-ray energy emitted by the j-th standard point source

Otherwise, dose rate due to the j-th standard point source can be calculated by the following equation:

$$\dot{D}_j'=\frac{A_j p_\gamma E}{4\pi r^2}(\mu_{en}/\rho) \quad (4)$$

where, A_j: Radioactivity of j-th standard point source

E: γ-ray energy of the source (keV).

P_γ : γ-ray emission possibility.

μ_{en}/ρ : mass attenuation coefficient.

The relative difference between $\dot{D}'$ and $\dot{D}_j'$ is expressed as follows:

$$S_j=\frac{\dot{D}_j'}{\dot{D}_j}-1 \quad (5)$$

Let the sum of the square of S_j be denoted by S^2.

$$S^2=\sum S_j^2 \quad (6)$$

The $G(E)$ function is expressed as[4]:

$$G(E)=\sum_{i=1}^{K} A_k(\log E)^{k-1} \quad (7)$$

where k is the maximum term number of the polynomial equation, and A_k is the coefficient for k-th term of the polynomial equation. In our calculation, 10 was selected for K.

The principle of the least square method is that: calculate appropriate A_k's values to minimize S^2. The calculation result is shown in **Fig. 3**, and additional γ dose rate calculated for the stripped spectrum is shown in **Fig. 4.** In this energy range, the cosmic dose can be neglected.

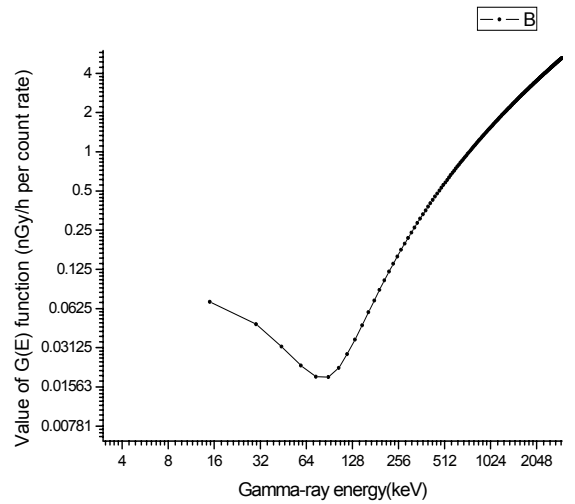

Fig. 3 $G(E)$ function for our HPGe spectrometer

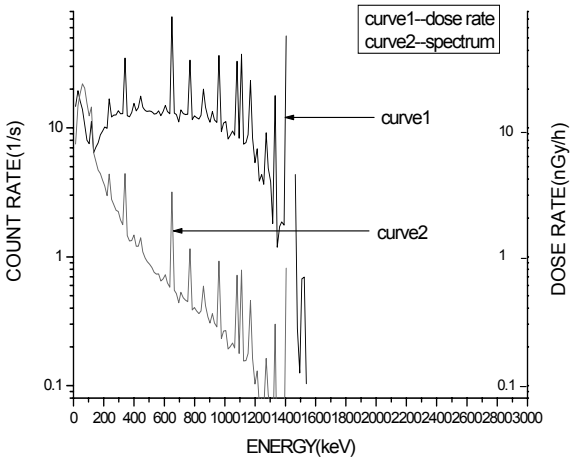

Fig. 4 Additional dose rate calculated by $G(E)$ function. Curve 2 represents the stripped spectrum, curve 1 represents calculated dose rate for each channel.

IV. Verification

In order to verify the utility of the $G(E)$ function and the stripping method, the additional exposure dose rates calculated by this method were compared with those measured by high pressurized ionization chamber which had subtracted dose rates contributed by cosmic ray and natural radionuclides.

The experiment was carried out in a contaminated site. Dose rate caused by cosmic ray was acquired by ionization chamber measurement at a lake surface, which elevation is the same as the contaminated site, and the result is 53nGy/h. The activity calibration factors for natural radionuclides were acquired by the airborne pads calibration, and the dose rates attributed to natural radionuclides were obtained by the following conversion factors (nGy/h per Bq/kg) which convert their activity to the exposure dose rate at a height of one meter above the ground. The value for

^{40}K is 0.0417 ,U series is 0.462 and Th series is 0.604. The additional exposure dose rates acquired by the two methods are listed in **Table.1**. According to the table, we can come to a conclusion that: if an area is seriously contaminated, the deviation of the additional dose rates calculated by the $G(E)$ function and measured by ionization chamber is little. Because the interference of natural radionuclides is slight, the additional dose rates measured by ionization chamber have high degree of precision, so additional dose rate calculated by $G(E)$ function can also be considered to have small error. But if the sites is contaminated slightly, neither the $G(E)$ function method nor the ionization measurement can obtain additional dose rates with high degree of precision. As the additional dose rate is small, the interference from natural radionuclides and the statistical error seriously affect the result.

Table 1 Comparison of additional dose rates acquired by the two methods

Measurement point	Additional exposure dose rate(nGy/h)	
	Calculated by $G(E)$ function	Measured by ionization chamber
1	1699.00	1755.13
2	638.70	777.46
3	265.10	278.52
4	344.30	362.92
5	117.00	115.59
6	27.10	18.79
7	20.60	11.43
8	10.50	N/A
9	5.70	N/A

V. Conclusions

The additional exposure dose rate can be acquired by integrating stripped spectrum with corresponding spectrum dose conversion function ($G(E)$ function) values. The advantage of this method is that: it can provide additional dose rate without the information of the distributions of artificial radionuclides. For the seriously contaminated site, the additional exposure dose rate calculated by this method has high degree of precision. But in slightly contaminated areas, this method may cause more uncertainty.

Reference

1) H.L.Beck, J.A.DeCampo, and C.V.Gogolak, In Situ Ge(Li) and Nai(Tl) Gamma-Ray Spectrometry, HASL-258, Health and Safety Laboratory(HASL), (1972).

2) ICRU.Gamma-Ray Spectrometry in the Environment. ICRU Report 53, International Commission on Radiation Units and Measurements (ICRU),(1994).
3) S.Morichi and I.Miyanaga, " A spectrometric method for measurement of low-level gamma exposure dose," Health physics,12[5],541(1966).
4) H.Ierada, E.Sakai and M.Katagiri, "Environmental gamma-ray exposure rate measured by in situ Ge(Li) spectrometer," Journal of nuclear science and technology, 17[4],281(1980).

Journal of NUCLEAR SCIENCE and TECHNOLOGY, Supplement 5, p. 610–613 (June 2008)

Performance Characteristics of Newly Modified $CaSO_4$:Dy based Indigenous Thermoluminescent Dosimeters for Environmental Radiation Monitoring

M. P. CHOUGAONKAR*, R. A. TAKLE, Y. S. MAYYA, V. D. PURANIK, and H. S. KUSHWAHA

Health, Safety and Environment Group, Bhabha Atomic Research Centre, Mumbai, 400085, INDIA

Environmental gamma radiation monitoring around the nuclear installations in India is being carried out for over three decades. This programme was essentially based on powder based Thermoluminescent Dosimeters (TLDs) using naturally occurring calcium fluoride (Fluorite) powder. Being powder based, it was labor intensive and to cater to the increasing demand for monitoring new stations, it was necessary to go for automatic TLD reader system. This was achieved by modifying the TLD cards suitably and using the automated PC based TLD badge TLD reader system indigenously developed and being used for personal dosimetry in India. This paper discusses the modifications that were carried out to make the TLDs suitable for environmental gamma monitoring using TLDs.

Performance characterisation of the TLDs like accuracy, precision and energy dependence etc were carried out to see the efficacy of the system for use in the environmental gamma radiation monitoring. In addition, inter-comparison with the existing TLD system, both deployed simultaneously in the field was also carried out. It was found that the new TLD exhibit the accuracy of 89-96 % of the various delivered doses in the laboratory while the precision was observed to be within 4% for all the doses delivered. The gamma radiation levels as measured using two TLD systems were found to match very well with each other. The paper also discusses the results.

KEYWORDS: TL dosimeters, $CaSO_4$:Dy, TLD reader, IIED, energy independence

I. Introduction

Radiation monitoring programme in the environs of all the Department of Atomic Energy (DAE) units constitutes an important component of the nuclear industry in India. It monitors the radioactive releases, solid, liquid or gaseous waste if any, to the environment. It also assesses the adequacy of the controls, set by the international bodies like International Atomic Energy Agency (IAEA) and in Indian context, Atomic Energy Regulatory Board (AERB) on the release of radioactive materials to the environment. The programme assures the public at large that the nuclear industry does not add to the radiation levels in the environs of the establishment. In addition, radiation dosimetry in regions where the natural radiation levels are higher than the surrounding regions, is also important to study the effects of the elevated radiation levels on the human health and a possible correlation between them.

Environmental gamma radiation monitoring, using Thermoluminescent Dosimeters (TLDs) around all the nuclear installations in India is being carried out for over three decades [1,2]. The TLDs have also been used in the indoor dosimetry of the High Background Radiation Areas (HBRAs) in the southwestern state of Kerala in India [3].

These programmes have been essentially based on powder based Thermoluminescent Dosimeters (TLDs) using naturally occurring calcium fluoride powder. Fifty mg of the processed calcium fluoride powder in the particle size range 75-150 μm was filled in two brass capsules of 8mm length & 3mm ID through a constant volume vibrator dispenser. Two such capsules sealed in watertight packet made one TLD (**Fig. 1**).

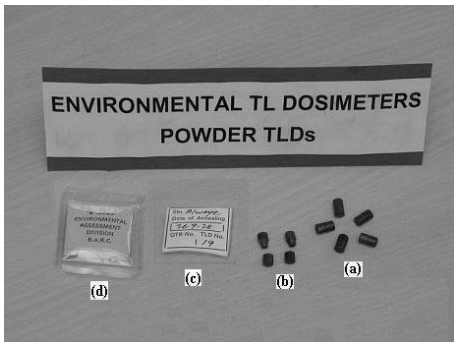

Fig. 1 Photograph of a typical powder based TL dosimeter using brass filled CaF_2 powder. (a) Brass capsules, (b) Brass capsules opened, (c) TLD packet and (d) TLD packed in PVC; ready for deployment.

This TLD was found to be quite satisfactory for environmental gamma radiation monitoring in India and participation in many International Inter-omparisons of Environmental Dosimeters (IIEDs) proved the efficacy of this system (**Fig. 2**)[4].

However, being powder based, this system was labor intensive and could not cater to increased requirement of environmental monitoring and other R&D activities like population dosimetry in the HBRAs in India. In order to meet the increased demand for monitoring new stations, it was necessary to go for automatic TLD reader system. This was achieved by using an indigenously developed automated PC based TLD badge TLD reader system. This system, used in personal monitoring purposes, uses three element TLD

*Corresponding Author, Tel No.: +91 222 559 8275, E-Mail: mpckar@hotmail.com

card each being used for beta, X-rays and gamma radiation respectively [5]. The preliminary studies with these TLDs without any modifications indicated that the Lowest Detectable Dose (LDD) was about 250 μGy. In addition, there is only one element used for gamma radiation monitoring. Few modifications were therefore carried out in the TLDs and were tested for environmental gamma radiation measurements. The TLDs were subjected to rigorous laboratory tests. What follows in the paper is the results of the tests that were carried out and also the performance of the TLDs *vis a vis* powder based TLDs.

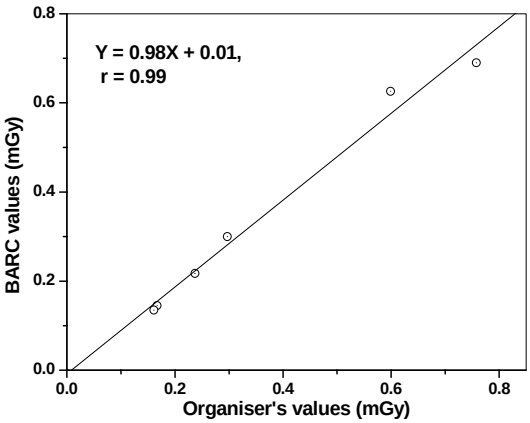

Fig. 2 Results of different International Inter-comparisons of Environmental Dosimeters.

II. Materials and Methods

1. Phosphor

$CaSO_4$: Dy phosphor, first prepared by Yamashita et al[6] by recrystallisation method has been found to be quite useful in TL Dosimetry and is regularly used in personal monitoring in India. This phosphor uses 0.05% mole/mole concentration of Dysprosium in the host lattice of $CaSO_4$. Although quite satisfactory in personal monitoring, it was found that the confidence levels in environmental gamma radiation monitoring were not satisfactory due mainly to its lowest detectable dose LDD[7].

Previous studies[8] indicated that increase in the dopant concentration increased the TL sensitivity in this phosphor and peaked at about 0.2 % (mole/mole). The phosphor containing 0.2 % Dy was therefore used in the new dosimeters. The phosphor was mixed with teflon powder in the ratio of 1:3 and a discs of 12 mm diameter were made so that they can be read on PC based automatic TLD badge reader Two such discs were mounted on a machine identifiable TLD card and were encased in a plastic TLD cassette with 1 mm copper filters on both sides of the card (**Fig. 3**). The automatic TLD badge reader is an indigenously developed reader system that has been described elsewhere.

In order to assess the efficacy of the modified dosimeters, following tests were carried out on the dosimeters.

Sixty freshly annealed TLDs were taken and the background readings were recorded using the automatic TLD badge reader [9]. Average background readings and the standard deviation were determined.

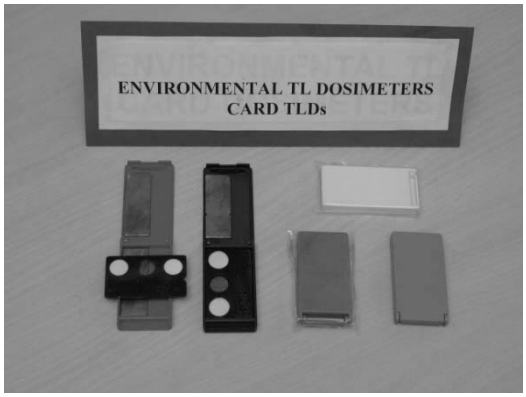

Fig. 3 A typical photograph of Card based TLD using $CaSO_4$: Dy phosphor.

The TLDs were then used for determination of calibration factor. Ten TLDs each were exposed to a standard Cs-137 gamma-source (662 keV), traceable to IAEA primary standards, for calibration exposures of 88,176,264 and 352 μGy respectively. Irradiation was performed on a plastic table at a sample to source distance of 50 cm.

Ten more freshly annealed TLDs were also exposed to another ^{137}Cs gamma source, corrected regularly for the dose rate and used routinely for TLD calibration, for known dose and the values were read off. These readings were used in the studies pertaining the accuracy and precision of the TLDs.

$CaSO_4$ based TLDs are known to exhibit energy dependence if proper care is not taken. The dosimeters, as described above, are designed in such a way that the phosphor discs are covered on both sides by a 1mm thick copper filter. The energy dependence of the arrangement was assessed by exposing 10 TLDs to 88 μGy of X-ray/gamma radiation of various energies. Three sets of readings were taken, i) only bare cards, ii) cards only with plastic cassettes and iii) cards with 1mm copper filters in the plastic cassettes. In each case, the TL response for each energy, either X-ray or gamma radiation was compared with that due to ^{137}Cs source.

III. Results and Discussion

1. Calibration Factor

The dose response curve drawn using the TLD output (counts) against the exposure imparted is as shown in **Fig. 4** below.

It is observed from the figure that the dose response is linear in the range up to 350 μGy, the range useful for routine environmental gamma radiation monitoring. The slope of the correlation line was found to be 2.07 counts/μGy and the inverse of the slope 1/ 2.07 = 0.483 (μGy/count) yielded the calibration factor as seen in Figure**.**

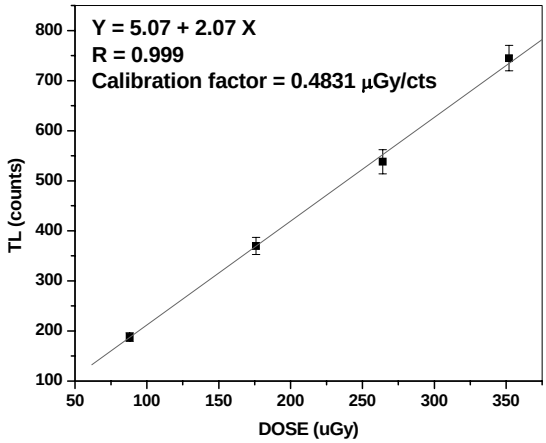

Fig. 4 Dose response curve of the $CaSO_4$: Dy based TLDs. Inverse of the slope gives the calibration factor.

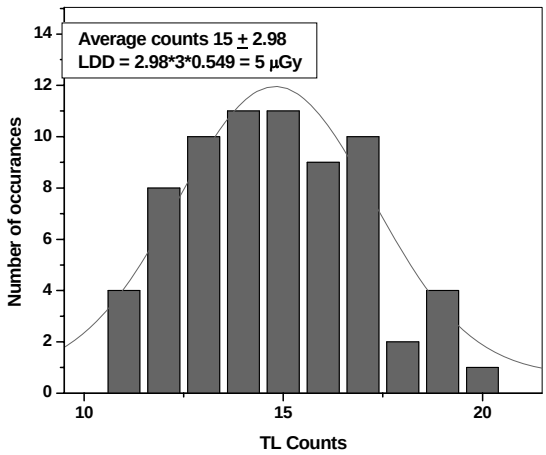

Fig. 5 Distribution of background TL signal of 77 freshly annealed TLDs. 90% of the TLDs are seen to have the background between 15± 2.98. The standard deviation of 2.98 gives the LDD of 5 μGy.

2. Lowest detectable Dose (LDD)

Average background reading of the 77 freshly annealed TLDs was observed to be 15 ± 2.98 counts. Taking three times the standard deviation of readings corresponding to the zero dose, and multiplying it by the calibration factor. The LDD was found to be 5 μGy and is depicted in **Fig. 5**.

3. Energy Independence

TL response of the TLDs to the same exposure of various energies, used in three sets as described in the previous section, was normalised to that of ^{137}Cs respectively. The normalised response thus obtained was plotted **(Fig. 6)**. It is seen from the graph that the copper filter of 1 mm thickness was quite suitable.

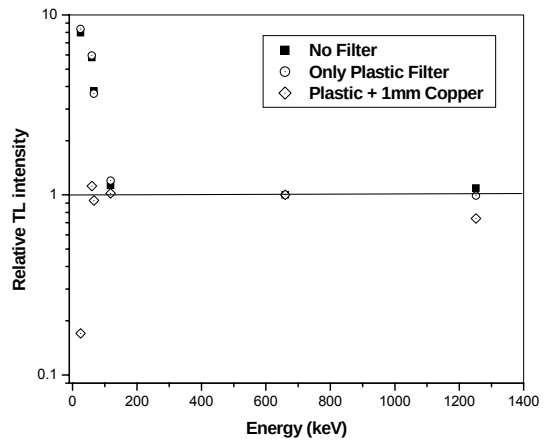

Fig. 6 Energy dependence of TLDs. The TLDs with copper filter of 1 mm thickness is seen to be sufficient to make the TLDs almost energy independent of the gamma/X-ray energy.

4. Accuracy and Precision

The calibration factor obtained as discussed earlier was used to evaluate the TLD readings recorded from the other set of TLDs exposed to another source. Accuracy and precision were then evaluated from the readings **(Table 1).** American National Standard Institute criteria for environmental TL dosimeters (ANSI N545) specify that the field results should be within 30% of the delivered values. It is seen from the table that the accuracy of all the values is well within the limit specified in ANSI N545. The precision was found to be about 5% of the delivered value.

5. Fading of the TL Signal

The $CaSO_4$: Dy based TLDs have been studied for fading and it has been reported that the fading is typically 1% per month. Considering that the duration of environmental gamma radiation monitoring is three months, this suits the needs.

Table 1 Determination of accuracy and precision of the TLD readings.

Delivered Dose (μGy)	Observed dose (μGy)	Precision %	Accuracy %
126	123 ± 5.3	4	2
189	180 ± 8.8	5	5
252	234 ± 10.9	5	7

6. Field Test

The field tests carried out by deploying these TLDs together with CaF_2 powder based TLDs indicate that the readings match quite well. As seen in **Fig. 7**, the correlation between two sets of TLD readings is quite well with the slope of 1.00 (expected unity) and regression coefficient of 0.99. This indicates that the modified TLDs are as good as the CaF_2 powder based TLDs that were being used in the environmental gamma radiation monitoring for over two decades.

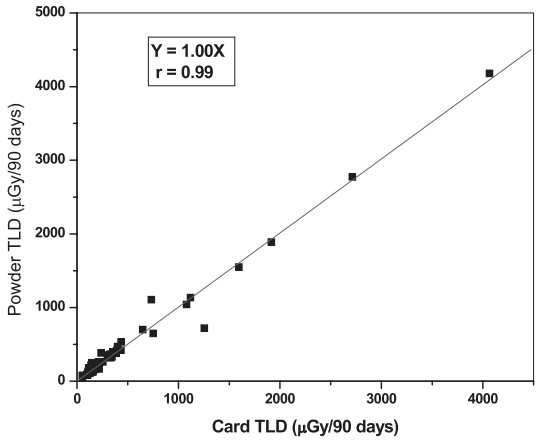

Fig. 7 Intercomparison of the gamma radiation levels obtained using two different TLDs. The slope of 1.00 (expected unity) indicates the excellent matching between the modified TLDs and the ones that are in use for over three decades.

IV. Conclusions

It is seen from the discussion above that the newly modified TL Dosimeters

1. Exhibit the lowest detectable dose (LDD) of 5 μGy
2. With 1mm thick copper filter are almost energy independent.
3. Show precision and accuracy of the TLDs are within 5% and 6% respectively.
4. Perform well vis a vis the powder based TLDs.

References

1) K.S.V Nambi, "Environmental radiation surveillance using thermoluminescent dosimeters," BARC report, BARC/I-575 (1979).
2) K.S.V Nambi, V. N. Bapat, M. David, V. K. Sundaram, C. M. Sunta and S. D. Soman, "Country-wide environmental radiation monitoring using TLDs," Radiat.Prot.Dosim. 28(1), 31-38, (1987).
3) M. P. Chougaonkar, Application of TL dosimetry in epidemiological studies in HBRAs. Proc. NCLA-2006, Ed. S. V. Godbole et al, pp 92-96 (2006).
4) M. P. Chougaonkar and A. S. Basu "Environmental radiation dosimetry using TLDs: quality assurance in performance; Proc. National Seminar on Luminescence and its Applications," (NSLA-2001) at Osmania University, Hederabad, India. Jan. 17-18, 2001pp 151-154 (2001).
5) K.G.Vohra, R.C.Bhatt, B.C.Bhatt, A.S.Pradhan, A.R.Lakshmanan and S.S.Shastry "Personnel dosimeter TLD badge based on $CaSO_4$:Dy Teflon TLD disc," Health Phys. 38(1980), 193-197.
6) T. Yamashita, N. Nada, H Onishi and S. Kitamura "Calcium sulphate phosphor activated by rare earth," Proc. 2nd Int. Conf. Lum. Dod. Gatlinburg, T.N. 4-7.
7) P. G. Shetty,, M. P. Chougaonkar, Munish Kumar, Y. S Mayya,. O. P. Massand and V. D Puranik. "Intercomparison between CaF_2-based environmental TLDs and $CaSO_4$: Dy personnel monitoring TLDs," Proc. International Conference on Luminescence and its Applications (ICLA –2004) pp 227-229, (2004).
8) K. Ayyangar, A. R. Lakshmanan, Bhuwan chandra and K. Ramdas "A comparison of thermal neutron and gamma ray sensitivities of caoomon TLD materials," Phys. Med. Bio. 19, 665-676, 1974.
9) S. Kannan, P. Ratna and M. S. Kulkarni "A new TLD badge with machine readable ID for fully automated readout," Rad. Prot and Env. 26, 251-253 (2003)

Journal of NUCLEAR SCIENCE and TECHNOLOGY, Supplement 5, p. 614–618 (June 2008)

Evaluation of the Transfer Parameters of Radionuclides in China

LI Jianguo[1*] and SHANG Zhaorong[2]

[1]*China Institute for Radiation Protection, P.O. Box 120, Taiyuan, China*
[2]*State Environmental Protection Administration, P.O. Box 8088, Beijing, China*

The transfer parameters involved in models to calculate the population dose from radioactive releases are compiled and evaluated. The data are mainly drawn from literatures in China, which are derived from laboratory experiments, field studies, or paired values from environmental monitoring measurements. The natural radionuclides involved are U, Th, and ^{226}Ra, ^{210}Po, ^{210}Pb, etc., and the artificial radionuclides are ^{90}Sr, ^{137}Cs, ^{131}I, ^{60}Co. The methodology in selecting and evaluating the data is discussed. Further research suggestions are proposed.

KEYWORDS: transfer parameters, radionuclides, evaluation

I. Introduction

In models to calculate doses to an individual on population from environmental radioactive sources or radionuclides released from nuclear facilities, transfer parameters are used to predict concentrations in human food chain. Transfer parameter values are highly variable. For instance, soil-plant transfer factors of terrestrial environment depend on climatic characteristics where they are derived, soil properties, plant species, agricultural practice and other interrelated factors.

In 1982, IAEA published default values of transfer parameters used to estimate the radiation dose of the critical inhabitant group[1)]. In 1994, IAEA and IUR (International Union of Radioecologists) organized the Joint Research Project to collect and evaluate transfer factors in literatures. The data are drawn from different resources, such as the research cooperation of radionuclide in the soil-plant systems of some European countries, studies on the 50's and 60's nuclear weapon test fallouts of North America countries in the last century, controlled radioactive release from nuclear facilities, experimental values both in natural and laboratory conditions, observation from the transfer behavior of stable isotopes, and the data from atmospheric fallout of Chernobyl nuclear accident in 1986. As the results, the "Handbook of parameter values for the prediction of radionuclide transfer in temperate environments" was published[2)].

After the Chernobyl nuclear accident in former Soviet Union in 1986, IAEA initiated the research project "the Validation of Models for the Transfer of Radionuclides in Terrestrial, Urban and Aquatic Environments" in 1988, divided into four work groups: the Terrestrial Working Group, the Urban Working Group, Multiple Pathway Working group, and Aquatic Working Group, and published each Working Group's achievements by the IAEA technical reports[3-6)]. The modelling of resuspension, seasonality, interception on vegetation, losses in food processing, and the transfer of radionuclides in marine environment are studied.

In recent years，with the increase of nuclear facilities in tropic and subtropic countries, the limitation of "the Handbook of parameter values for the prediction of radionuclide transfer in temperate environments"[2)] is obvious. In 1999, IAEA and FAO jointly initiated the research project "Classification of soil systems on the basis of transfer factors of radionuclides from soil to reference plants (1999 ~ 2003)"[7)]. Meanwhile the revision of the Handbook[2)] has been carrying on by IAEA.

The research on transfer parameters started from the 60's of last century in China, but no systematic analysis of the achievements. In the practice of radiation environmental impact assessment of nuclear facilities, for lack of site-specific data, transfer parameters from foreign literature are generally adopted, one of the examples is the "Radiation Environmental Impact Assessment of the Nuclear Industry in China in the Three Decades (1955~1985)"[8)].

Afterwards, the environmental assessments of nuclear facilities are facing the similar question. For the transfer parameter values are highly varied with environmental conditions, it's necessary to compile and evaluate existing data and provide expected values with background information.

II. Methodology

1. The Transfer Process of Radionuclides in Food Chains

In the models to estimate the dose received by an individual or population group from ingestion of radionuclides in food (both terrestrial and aquatic food chains), the following processes are involved[9)]:

(a)Deposition by dry or wet process;
(b)Initial interception and retention by vegetation surfaces;
(c)Translocation to the edible tissues of vegetation;
(d)Post-deposition retention by vegetation and soil surfaces;
(e)Uptake by roots;
(f)Adhesion of soil particles on to vegetation surfaces;
(g)Direct ingestion of surface soil by humans or grazing animals;

*Corresponding Author, Tel No.: +86-351-2203517, Fax No.: +86-351-7020407, E-Mail; lijg@cirp.org.cn

Table 1 Transfer parameters of radionuclides involved in terrestrial and aquatic food chains

Parameters	Units	Descriptions
Bv	(Bq/kg plant tissue)/(Bq/kg dry soil)	Soil-to-plant concentration factor, the uptake of radionuclide from soil by edible parts of crops;
f	-	Interception coefficient, defined as the fraction of deposited activity intercepted and initially retained by vegetation.
TLF	-	Translocation factor, defined as the ratio of the activity in the edible parts in 1 m2 soil area (or activity concentration in edible parts, Bq/kg) at harvest time and the activity initially retained on foliage of the same area (Bq/m2).
th	a	The time internal between harvest and consumption of the food.
Yv	kg/m^2	The effective biomass of crops at harvest.
ρ	kg/m^2	The effective surface density for the soil.
λes	a-1	The removal rate constant for physical loss by weathering.
Fa	d/kg or d/L	The average fraction of the animal's daily nuclide intake present in each kg or L of animal product.
Qf	kg/d	The daily consumed amount of forage by an animal.
tf	a	The average transit time from slaughtering or milking to consumption.
Bp	L/kg	Equilibrium ratio of the concentration of a radionuclide in aquatic food p to it's dissolved concentration in water known as the bioaccumulation factor.
Kd	L/kg	The ratio of radionucides in the solid and liquid phases.
Fr	-	The total amount of a radionuclide in processed food divided by the total amount of the radionuclide in the original raw food.
Pe	-	Processing efficiency, the ratio of kg for prepared food to the kg of raw product.

(h)Transfer of radionuclieds in soil, air, water and vegetation into the milk and meat of grazing animals;
(i)Transfer of radionuclides in surface water to the terrestrial system by spray irrigation.
(j)Transfer of radionuclides in surface water to sediment and to aquatic biota.

The transfer parameters mainly involved are soil-to-plant transfer factor (*Bv*), transfer coefficient for animal products (*Fa*), interception coefficient(*R*), translocation coefficient (*TLF*), concentration factors for freshwater fish(*Bp*) etc., and the factors which are related to agriculture and local areas, such as effective biomass of crops at harvest(*Yv*), effective surface density for the soil(ρ), the time interval between harvest and consumption of the food(th), and so on. The units and brief definition of these parameters are listed in **Table 1**.

2. Data Analysis

The data have been analyzed with the objective of estimating an expected value for a given parameter and of providing an indication of the extent of uncertainty about this estimate[2]. The expected value is taken to be a value that is considered "typical" or most likely to occur, the uncertainty assigned to an expected values is given either as minimum and maximum value based on 1 95% confidence interval, or as a range of minimum an d maximum values occurring in the literature.

In some cases the expected values are given without a statement of uncertainty or a range because of the limited data. The expected value in these cases must be used with caution.

Bv (soil-to-plant transfer factor) values were given with arithmetic mean and empirical standard deviation for experimental data. For the distribution of *Bv* were transformed to a logarithmic normal distribution[10)11)], the expected values were given also with geometric mean and the lower 95% and upper 95% confidence limit. Besides, the background information including soil types, location (for paired data from environmental monitoring), originations (eg. Laboratory or field studied).

For literature values of transfer parameter published in recent years in China, the arithmetic mean and standard difference are generally provided[11, 12]. But in the early literatures, the estimates or similar information were often absent. Therefore necessary data analysis has to be carried on in possible situation [13-15].

3. Consideration in Selecting Transfer Parameters

For the Paired data from the field experiments or the environmental monitoring (paired values), following principle are considered:

A. The data derived from representative plant species and soil type in local area are selected;

B. The sampling of soil and plant samples is synchronous (in the same location and at the same time);

C. The information including soil type, physiochemical characteristics, climatic conditions are provided as long as possible;

D. Unified data statistical method is adopted.

Table 2 The Expected *Bv* values of natural U in rice based on different soil species

Unit: (Bq/kg dry plants)/（Bq/kg dry soil）

N	TF		Geo.S.D.	95% confident		Soil species, location	Reference
	Geo-mean	Average±S.D		Upper limit	Lower limit		
70	3.00×10^{-5}	8.00×10^{-5}	1.36	4.68×10^{-4}	2.0×10^{-6}	Red Earths(A13), Chenchou, Hunan Province	[22]
62	6.30×10^{-4}	1.44×10^{-3}	1.48	1.23×10^{-2}	3.24×10^{-5}	Red Earths(A13), Hengyang, Hunan Province	[22]
10		2.75×10^{-3} $\pm2.11\times10^{-3}$				Red Earths(A13), Field Experiments	[22]
17	1.20×10^{-4}	3.35×10^{-4}	1.53	2.56×10^{-3}	5.6×10^{-6}	Yellow Earths(A21), Yiyang, Hunan Province	[22]
11	1.81×10^{-3}	3.36×10^{-3}	1.45	3.32×10^{-2}	9.9×10^{-5}	Publish Soils(G23), Jiajiang, Sichuan Province	[22]
60	1.09×10^{-3}	1.23×10^{-3}	5.40×10^{-1}	3.21×10^{-3}	3.7×10^{-4}	Yellow Earths(A21), Quzhou, Zhejiang Province	[22]
18	4.86×10^{-3}	7.55×10^{-3}	8.06×10^{-1}	2.43×10^{-2}	9.69×10^{-4}	Gray Desert Soil(F11), Lanzhou, Gansu Province.	[22]
65		7.61×10^{-4} $\pm1.98\times10^{-4}$				Red Earths(A13), Field experiment, Ganzhou, Jianxi Province	[22]
23	8.81×10^{-4}	2.52×10^{-3}	1.25	1.08×10^{-2}	7.21×10^{-5}	Red Earths(A13), Ganzhou, Jiangxi Province	[22]
31	1.91×10^{-4}	4.95×10^{-4}	1.63	4.96×10^{-3}	7.37×10^{-6}	Latosols(A11), Nanxiong, Guangdong Province	[22]

For the data derived from laboratory and field experiments, following principles are considered:

A. The experiment conditions and the data obtained are satisfied to the transfer parameter's requirements;

B. The number of parallel experimental samples should be at least 3;

D. For the experiments simulating the long-term pollution, it's necessary to consider the balance condition of radioactivity.

It should be emphasized that the estimates of transfer parameters are analyzed in unified data statistical method, the parameter expression must be consistent. For usage of the estimates of transfer parameters, the background information including sample number, involved soil type, the physiochemical properties of soil (including soil ingredient, organic content, ion exchange capacity, the pH, exchangeable content of K, soil moisture, etc.), meteorological parameters during the experimental period are provided if possible.

The estimate of a transfer parameter is the judgment based on the knowing of their variation. Therefore the estimate is only a reference value. When lacks of site-specific values, the estimates may be used in consideration of the background information, eg., the origination of the data, in order to reduce the uncertainty of parameter

III. Evaluation of Transfer Parameters

1. Terrestrial Transfer Coefficient

For expected values of *Bv* for natural radionuclides of U, Th, ^{226}Ra, ^{210}Po, ^{210}Pb, and artificial radionuclides of ^{90}Sr, ^{137}Cs, ^{131}I, ^{60}Co, the involved plants are cereals, vegetables, fruits, tea, and grass, etc.

As the important background information, soil species are provided depending upon the China soil classification and code[16], in which the soils are classified into 60 soil species. For example, the expected *Bv* values of rice are provided with *Red earths* (A13, the Chinese National Standard Soil Code)[16], *Yellow earths*(A21), *Brown earths*(B21), *Castanozems* (D21), *Gray desert soils* (F11) and *Gray-brown desert soils* (F12). As an example, the *Bv* data of natural U in rice are given in **Table 2**.

Some 4000 pairs of *Bv* data compiled from environmental monitoring measurements around the country are analyzed for transfer parameters.

2. Transfer factors in Animals

The intake of radionuclides by animals depends on animal species, mass, age and growth rate of the animal, and the digestibility of feed. The radionuclides considered for intake by animals maybe fresh or stored in forage, drinking water, and soil adhered on plant surfaces for grazing animals.

Data obtained for transfer parameters of animals both from laboratory experimental researches and environmental monitoring measurements are sparse in China.

Paired data of transfer parameters for animals (sheep, etc.) are drawn from environmental monitoring measurements of ^{137}Cs[11]. An important foodstuff for the animals are grass, the expected values of transfer parameter of ^{90}Sr and ^{137}Cs for grass are also compiled and provided.

For experimental data, the absorption and accumulation of ^{90}Sr, ^{125}I were studied in poultry (Yellow-feather broiler and Beijing-White Layers) by feeding experiments[17,18].

For the complex of the experiments, equilibrium of radioactivity rarely occurs in animals and in the daily feed.

3. Bioaccumulation factors in aquatic organism

Radionuclides discharged into the aquatic environment are also assimilated by living organisms. The transfer of radionuclides from water, through various trophic levels of aquatic life, those organisms consumed by humans is condensed into one parameter-the bioaccumulation factor *Bp*. This parameter is highly variable depending on the concentration in suspended sediment, chemical composition of the water, chemical state of the raionuclide, and the characteristics of the aquatic organism.

Expected values of *Bp* for natural U, ^{226}Ra, ^{210}Po, ^{90}Sr and ^{137}Cs in aquatic plant, fish, shrimp and waterfowl are provided[19]. The data are from environmental monitoring measurements and field studies in China.

Experimental data are also compiled, including *Bp* values of ^{147}Pm in aquatic fish (*Basilewsky, Ctenopharyngodon idellus, Carassius auratus*) and plant (*Lemnaminor*)[20]. The transfer of ^{147}Pm in the aquatic food chain composed by the 5 aquatics are studied.

4. Bioaccumulation factors in marine organism

Through investigation of radioactivity in marine ecosystem of Daya Bay before and after the operation of the Nuclear Power Plant, the migration and accumulation of radionuclides including ^{110m}Ag, ^{90}Sr, ^{137}Cs etc. from the Nuclear Power Plant were studied[22]. The *Bp* of ^{110m}Ag, ^{90}Sr and ^{137}Cs for mollusk (*Perna viridis, Chlamys sp.etc.*), seaweed (*Laminaria japonica, Sargassum sp., Sargassum fusiforme, Porphyra sp., etc.*), and crustacean (*Penaeus penicuatus, Acetes chinensis etc.*) are provided.

There are 7 types of Marine species considered in the evaluation transfer parameters, including seaweed, phytoplankton, the zooplankton, the crustacean, the mollusk and the fish.

When the expected values derived from temperate zone are used in the tropical zone, special caution is necessary, Consideration of the sampling sea area and the season are helpful to use the estimates of accumulation factor. Site-specific data are always the first choice if possible.

IV. Conclusions

As the result of compilation and evaluation of transfer parameters for environmental assessment of nuclear facilities in China, the "Handbook of Radioecological Transfer parameters" [21] was published in China in 2006. The aim is to provide expected values of transfer parameters for environmental assessment of nuclear facitities in China. When domestic data are absent, the data from IAEA publications[2,9] and other literatures have to be adopted.

It is strongly suggested that the data of the "Handbook of Radioecological Transfer Parameters"[21] to be used as default values only if the site specific data are not available.

In some fields for the gap of understanding, further researches are suggested to conduct in the future. eg., the transfer parameters of radionuclides in Chinese food cooking processing. And the accumulation of radionuclides discharged from nuclear power plants in economic marine species located in Chinese Coastal sea waters, for example, the transfer of radionuclides in *Porphyra sp.*, *Penaeus oenicuatus, Acetes chinensis,* etc.

To meet the needs to construct nuclear power stations in the inland areas of China, further researches should be focused on the transfer behavior of radiounclides in specific river ecosystems, in crops by irrigation, distribution coefficient (Kd) of radionuclides in water and sediments.

Acknowledgement

This work was sponsored by National Natural Science foundation of China. The Project authorization number is 10375101.

References

1) IAEA Safety Series No.57, Generic Models and Parameters for Assessing the Environmental Transfer of Radionuclides from Rountine releases,1982
2) IAEA Technical Reports Series No.364, Handbook of Parameters for the Prediction of Radionuclide Transfer in Temperate Environments. 1994
3) IAEA Technical Reports Series No.647, Modelling of Resuspension, Seasonality and Losses during Food Processing. First Report of the VAMP Terrestrial Working Group Vienna, 1992
4) IAEA Technical Reports Series No.760, Modelling the Deposition of Airborne Radionuclides into Urban Environment. First Report of the VAMP Urban Group, 1994
5) IAEA Technical Reports Series No.857, Modelling of Radionuclides Interception and Loss Processes in Vegetation and of Transfer in Semi-natural Ecosystems. Second report on the VAMP Terrestrial Working Group, IAEA,Vienna,1996
6) IAEA Technical Reports Series No.442, IAEA. Sediment Distribution Coefficients and Concentration Factors for Biota in the Marine Environment. IAEA,Vienna, 2004
7) IAEA Technical Reports Series No.1497, Classification of Soil Systems on the Basis of Transfer Factors of Radionuclides from Soil to Reference Plants. IAEA, 2006
8) Pan Ziqiang et al. Radiation Environmental Impact Assessment of the Nuclear Industry in China in the Three Decades (1955~1985), IBSN 7-5022-3125-8/TL-1001,Atomic Energy Press, Beijing, 2004.4
9) IAEA. Safety Reports Series No.19. Generic Models for Use in Assessing the Impact of Discharges of Radioactive Substances to the Environment, IAEA Vienna, 2001
10) C.Sheppard, W.G. Evenden. Characteristics of Plant Concentration Ratio Assessed in 64-site Field Survey of 23 Elements. J. Environ. Radioactivity (11):15-36,1990
11) Qin Suyun, Qin Yong et al. Study for Transfer of ^{90}Sr, ^{137}Cs, Natural U, ^{226}Ra and ^{239}Pu in Terrestrial Foodchains. Radiation Protection 15:241-252,1995
12) Li Jianguo, Guo Zede. In-Situ Study on the Transfer of

13) Pollutants in the Environment around the Tailings in China. Radiation Protection 22(1):9-14, 2002
14) Zhao Wenhu, Hou Lanxin, Xu Shiming. Study on the ^{90}Sr Absorption by Agricultural Plants Grown in Soil from Daya Bay Qinshan Area. CNIC-00490, 1991
15) Li Chuanzhao, Zhao Wenhu, Xu Shiming. Translocation, Accumulation and Distribution of ^{110m}Ag in Crops and Soils. Acta Agriculturae Nueleatae Sinica 9(4):230-234, 1995
16) Zhao Wenhu, Xu Shiming, Hou Lanxin. The Contamination on Farm Products from ^{125}I. Cnic-00372, 1995
17) China Soil Classification and Code, Chinese National Standard, GB/T17209-2000, China Standard Press. 2000.8
18) Shang Zhaorong et al. Study on Absorption, Accumulation and Distribution of ^{90}Sr in Yellow-Feather Broiler. CNIC-00752. 1993
19) Wanf Bing-Kui, Zhao Miao-zhen, Jin Zi-yu. Distribution and Accumulation of ^{125}I in Chicken and Egg. Acta Agriculturae Zhejiangensis 12(5), 2000
20) Qin Suyun, Li Shuqin, Zhou Caiyun. On the Concentration factors of Some Radionuclides in Aquatic Organisms in Freshwater Environment. Radiation Protection 15(5):330-337,1995
21) Chen Zuyi, Cheng Wei, Zhang ligan. Study on Bioconcentration of ^{147}Pm (RE) in Aquatic Food Chain. CNIC-01295,1998
22) Li Jianguo, Shang Zhaorong et al. Handbook of Radioecological Transfer Parameters (Chinese Edition). IBSN 7-5022-3565-5, Atomic Energy Press, Beijing, 2006.6.
23) Zhou Caiyun, Li Jianguo, Qi Yong et al. Variation of Radioactivity in Marine Ecosystem of Daya Bay before and after the Operation of Daya Bay Nclear Power Plant. The Chinese Academy of Sciences, Marine Biology Research Station at Daya Bay, Annual Research ReportsVol.2. ISBN 7-03-006731-2/P-1059, Sciences Press, 1998.5

Journal of NUCLEAR SCIENCE and TECHNOLOGY, Supplement 5, p. 619–622 (June 2008)

Environmental Gamma Radiation Monitoring Around Nuclear Power Stations in India, an Indian Scenario

M. P. CHOUGAONKAR*, P. G. SHETTY, Y. S. MAYYA, V. D. PURANIK, M. L. JOSHI, and H. S. KUSHWAHA

Health, Safety and Environment Group, Bhabha Atomic Research Centre, Mumbai, 400085, INDIA

There are 17 operating nuclear power reactors in India at 6 sites with an installed capacity of approximately 4120 MWe of electricity. Apart from two reactors in Tarapur Atomic Power Station (TAPS), which use enriched uranium and are based on boiling water reactor (BWR) technology, all the other reactors at various power stations use natural uranium as fuel, are moderated and cooled by heavy water and are Pressurised Heavy Water Reactors (PHWR). Environs of all the power stations in India are monitored for gamma radiation on regular basis using Thermoluminescent Dosimeters (TLDs). The gamma radiation levels thus measured are regularly compared with the pre-operational levels. The data generated for all the stations during the past years was subjected to various analyses like comparison of the annual levels with those during the pre operational levels, distribution studies, regressions with the possible contributors etc. This paper discusses the environmental gamma radiation levels based on the analyses of all data generated for all the power stations during the years up to 2005. Comparisons of the annual radiation levels with those during the pre operational data indicates that none of the stations show any increase in the environmental gamma radiation levels.

KEYWORDS: environmental radiation, primordial radioactivity, Monitoring, nuclear power stations, TL dosimeters, ^{41}Ar,

I. Introduction

India has 17 nuclear power reactors operating at 6 sites with an installed capacity of 4120 MWe of electricity. Apart from Tarapur Atomic Power Station (TAPS 1&2), which has two boiling water reactors using enriched uranium as fuel, all the other reactors are Pressurized Heavy Water Reactors (PHWRs) using natural uranium as fuel, heavy water as coolant and moderator.

The environmental gamma radiation-monitoring programme, using Thermoluminescent Dosimeters (TLDs), has been in existence in India for more than three decades and the pre-operational environmental gamma radiation levels in the environs of all the power station sites have been monitored in the past. The continuous gamma radiation monitoring is being carried out at these sites using calcium fluoride based TLDs. The methodology of preparation of TLDs and the protocol of analysis has been standardised[1].

This paper gives the analysis of the results of the environmental gamma radiation levels at four sites where PHWR based Nuclear Power Stations are operating. The paper presents analyses for the four sites as representative, however the similar analysis is carried out for all the six sites.

II. Materials and Methods

The TL Dosimeters being used in the environmental gamma radiation surveys of nuclear power stations in India contain CaF_2 (Natural) powder that has been found to be similar to Manufacture Belge de Lamps et de Material Electronique (MBLE) fluorite.

This powder is thoroughly cleaned, sieved between particle size 75-150 μm and annealed to remove the previous dose history. Fifty mg of this powder is filled in brass capsule of 1.5 mm wall thickness. Two such capsules, sealed in PVC packet constitute a TLD as shown in **Fig. 1**. These TLDs have been thoroughly characterised based on the ANSI N545 criteria for the environmental radiation monitoring using TLDs[2] and the results are reproduced in **Table 1**. In addition, participation in six International Inter-comparisons of Environmental Dosimeters (IIEDs), organised by US Department of Energy (US DoE) during 1984-2001, have shown that the accuracy of these dosimeters in field deployment is better than 15%, very much within the ANSI criteria of "field results should be within 30% of the delivered values".

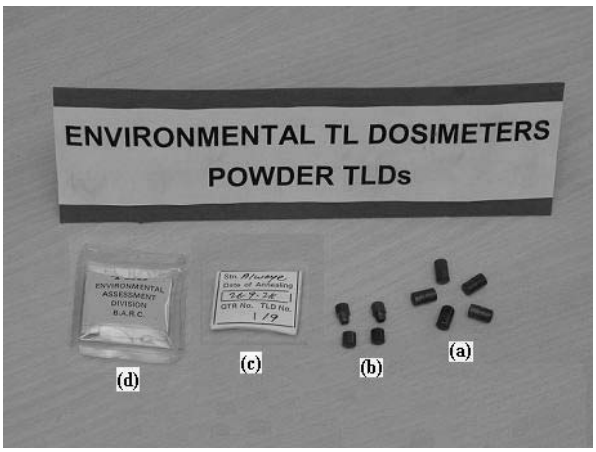

Fig. 1 Photograph of a typical powder based TL dosimeter using brass capsules filled with CaF_2 powder. (a) brass capsules, (b) brass capsules opened, (c) TLD packet and (d) TLD packed in PVC; ready for deployment.

*Corresponding Author, Tel No: +91 222 559 8275,E-Mail: mpckar@hotmail.com

Table 1 Performance characteristics of the environmental TLD using natural CaF_2 powder.[2)]

	Characteristics	Performance
1	Energy dependence	± 20 % between 50 and 1250 keV.
2	Environmental exposure response	± 1 %of the true exposure using Ra-226 calibration.
3	Fading	3 % in 3 months of continuous exposure.
4	Directional response	Nearly isotropic.
5	Self-dose rate	26.8 μGy /year.
6	Precision	± 5 %.
7	Accuracy (1-100 μGy)	± 10 %.

The freshly prepared TLDs are mailed from the laboratory to various stations and are deployed by the station staff on quarterly basis, the exposed TLDs being replaced by the next batch of the TLDs. The exposed TLDs are sent back to laboratory for evaluation. Lead pot doses, transit doses etc are properly accounted in the protocol standardised. The data thus generated over the years is subjected to various analyses on a regular basis to examine the rise in environmental gamma radiation levels if any.

III. Results and Discussion

1. Determination of Baseline Gamma Radiation Levels:

Apart from determining the baseline gamma radiation levels in the region, this exercise was also carried out to assess whether the region exhibited radiation levels attributable to man made radiation during the pre operational survey. Soil samples from all the locations, where TLDs were deployed, were collected and the annual dose calculated for the primordial radioactivity data using UNSCEAR 2000 dose conversion factors (DCF). Correlation between dose due to primordial radioactivity and that measured by TLDs[3)] during the period 1980-1987 was then obtained. The Y intercept at zero dose due to primordial radioactivity in this correlation can be attributed to the sum of sky shine, cosmic ray dose, self dose, dose due to airborne dose and manmade radioactivity if any.

Considering that the dose due to airborne radioactivity is practically uniform in the region[4)], it was treated as that measured by TLD as due to primordial radioactivity. Similarly, contributions due to self-dose (based on Table 2) and sky-shine dose (10% of the terrestrial dose,[5)]) were appropriately accounted for during the correlation. As seen in **Fig. 2**, the Y intercept of 0.29 ± 0.07 mGy/a in the case of Rajasthan Atomic Power Station (RAPS) could then be attributed to the sum of cosmic ray dose and that due to the manmade radiations if any. Sadasivan et al[6)] carried out detailed studies on the soil radioactivity in India and observed that the region showed the concentration of 110 ± 2 Bq/m^2 of ^{137}Cs amounting to only tens of nGy/a and thus matched well with cosmic ray dose value of 0.29 mGy/a.[2)] in the terrain. Although the dose response of the cosmic rays in TLDs is not uniform for all the energies, the cosmic ray dose does not vary significantly within the small region of 15km and the exercise implied that there is no manmade radioactivity present in the environs under study.

Yus et al [7)] developed a novel method to separate manmade radiation levels in the environs of a nuclear facility. While the method can work satisfactorily in a facility in operation, manmade radiations during pre operational phase is expected to be insignificant, if any, and as such the method was not adopted during the survey.

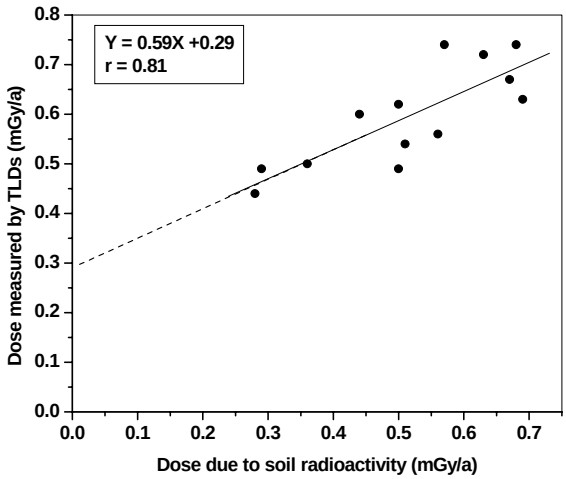

Fig. 2 Correlation between doses calculated based on primordial soil radioactivity (X axis) and that as measured using TL dosimeters (Y axis). Y intercept at zero doses due to soil radioactivity should match the cosmic ray component if there is no contribution due to the human activities in the environment.

Similar exercise was also carried out during the pre operational survey in the environs of Kakrapar Atomic Power Station (KAPS). The pre operational gamma radiation survey in this region during the period 1986- 1992[8)] yielded the average of 0.52 ± 0.13 mGy/a. The soil radioactivity analysis indicated the dose levels due to primordial soil radioactivity in the region was 0.25 ± 0.06 mGy/a. The ^{137}Cs concentration in the region[6)] was found to be 2 ± 0 Bq/m^2, negligibly small, thus giving the cosmic ray component of 0.27 mGy/a. This matches very well with the value of 0.26 mGy/a[2)] and indicated the absence of any manmade radioactivity during the preoperational survey. This gave the base line value of 0.52 ± 0.13 mGy/a for the region before any nuclear power operations began. The corresponding levels during the period of operations up to the year 2002 were observed to be 0.53 ± 0.08 mGy/a, matching well with the preoperational values.

2. Estimation of Dose Contribution due to ^{41}Ar Release:

The effect of release of ^{41}Ar in the environment was assessed as follows. The dose contribution due to Argon release from the stack was evaluated at a given location using Gaussian Plume Model (GPM) considering the local terrain, wind velocities and directions etc. The dose value thus calculated was correlated with those measured using TLDs. In the case of most of the locations, away from the stack, this correlation was found to be poor with negligible

statistical significance thereby indicating that the contribution of ^{41}Ar releases to the environmental gamma radiation levels at far off locations was insignificant. The best correlation that could be obtained was at a location within the 1.6km radius as shown in **Fig. 3**[3]**.** The Y intercept at zero doses due to ^{41}Ar release (X=0) in **Fig. 3** was observed to be about 0.60 ± 0.045 mGy/a, which could be taken as the natural background level at the location. The overall average gamma radiation levels in the environs of RAPS during the years 1982-2005 has been found to be 0.63 ± 0.15 mGy/a which matches reasonably well considering the limitations of the plume models. The annual gamma radiation level at this location during the same period has been found to be to be 0.93 ± 0.32 mGy/a. The contribution due to ^{41}Ar dose thus comes to be about 0.3 mGy/a. It may be emphasised here that with the design modifications in the later PHWR reactors production of ^{41}Ar was substantially reduced. This contribution became negligible and could not be discerned in the case of all the other NPPs using TLDs.

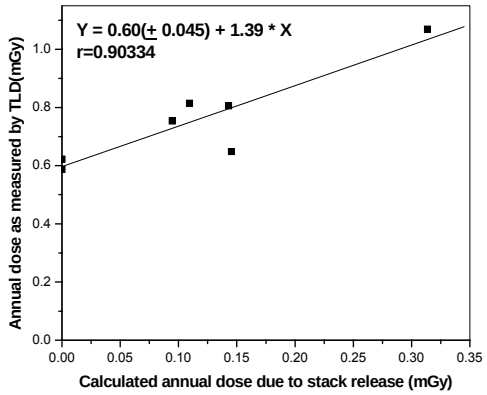

Fig. 3 Correlation between dose due to gaseous releases from the stack and that as measured using TLDs. The Y intercept at zero stack release (X=0) should correspond to the natural background level at the location. Anything above this value is the contribution due to the stack release

3. Monitoring of the Prevalent Gamma Radiation Levels:

Regular monitoring of the various locations gives the indication whether there has been any unusual rise in the radiation level at the location. Detailed investigations can then follow to ascertain the causes for the same. The average annual gamma dose levels during the period 1989-2005, based on the 22 TLD locations that are situated beyond the radius of 1.6 km (exclusion zone) in Narora Atomic Power Station (NAPS), is found to be 1.2 ± 0.12 mGy/a. The pre operational levels in the region have been evaluated for the period Jan.1987 to March 1989[9] and the average of 1.2 ± 0.27 mGy/a during this period matches well with 1.2 ± 0.12 mGy/a during the period 1989-2005. The effect of ^{41}Ar release from stack even within the exclusion zone could not be discerned during this period and this is attributed to the design improvements in this NPP. A typical gamma radiation dose variation during 1989-2005 at a location situated at 6.4 km NW is shown in **Fig. 4**. It is seen that there is no abnormal change in the level during any of the year under survey. It is observed that the variation in the radiation levels at this location is about 10%. This is typical of all the locations that are being monitored in the environs of the power stations.

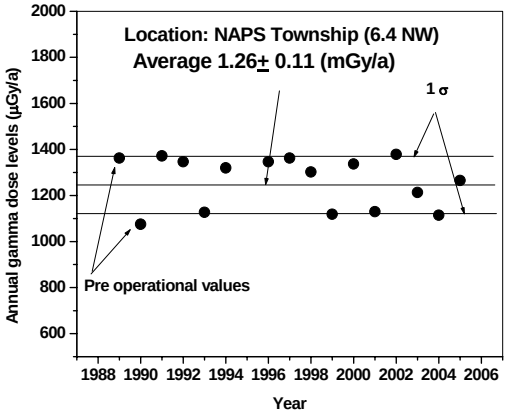

Fig. 4 Annual gamma radiation levels at a township 6.4km west of NAPS. The values (mGy/a) are seen to be within one standard deviation limit, indicating that the levels at this location are steady showing no increase during the period of monitoring.

4. Seasonal Variations in the Gamma Radiation Levels:

The 4 monitoring quarters are adjusted in such a way that four seasons in India are covered separately by the monitoring cycles. Seasonal variation in gamma radiation levels at a location can be prominent particularly when the dosimetry is carried out indoors in the cold countries. It may be emphasised that all the locations in the survey are outdoors. India being the country with temperate climate, significant seasonal variation is not expected. Monitoring of seasonal variation in the gamma radiation levels at various locations do not show any major variations. **Fig. 5** shows typical analysis carried out for a location on the boarder of exclusion zone at KAPS.

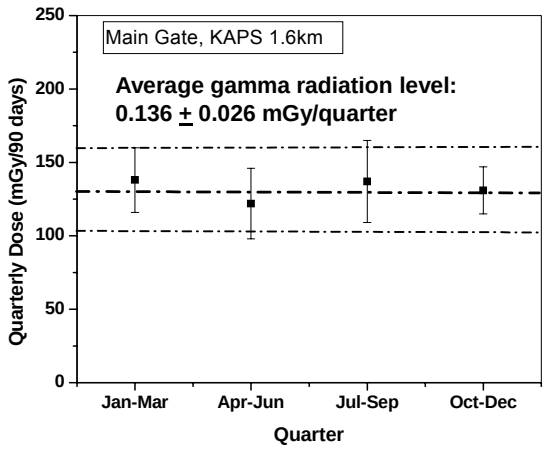

Fig. 5 A typical plot showing seasonal variations, if any, at a location in the environs of KAPS. Seasonal variations are seen to be too miniscule considering the wide variations in the gamma radiation levels at the location during respective quarters.

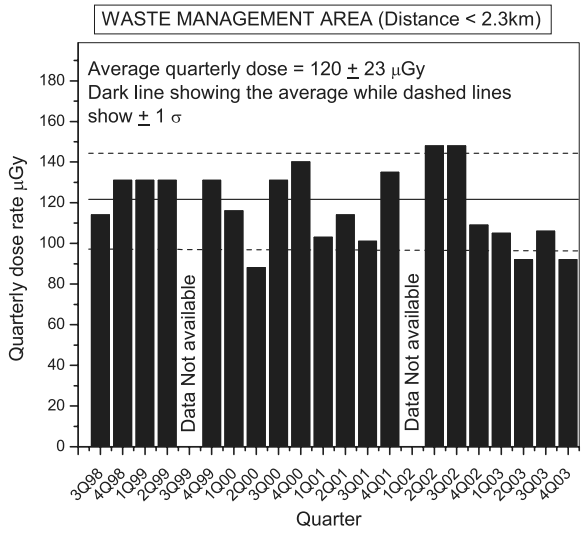

Fig.6: Quarterly gamma radiation levels at a location less than 2.3 km from stack at KGS.

Twenty-seven locations were monitored during the pre-operational survey in the environs of Kaiga Generating Station (KGS). The average gamma radiation levels of 0.50 ± 0.09 mGy/a was observed in the region during the pre-operational survey during 1989-90. After the operations of the power station started, the corresponding value was observed to be 0.51 ± 0.11 mGy/a for the locations.

The effect of seasonal variation, if any, is also shown in **Fig. 6.** No pattern of seasonal variation in the levels could be observed at the location.

As seen in **Fig. 4**, the variation in the gamma radiation levels at a given location over time is about 10%. However, if overall average of the environs in a power station site is calculated, it is observed to be more than 10% as seen in **Table 2.** While the general background of the region is an indication of the soil radioactivity parameters, the variation in the background as shown in the third column is an indication of the location to location non uniformity in the radioactivity contents of the soil. Relative percent error evaluated and shown in the last column highlights this aspect of the environmental radiation levels around the Indian NPPs.

Table 2 Comparison of General Background between some of the power stations under DAE and KAIGA.

Station	General Background	SD/mean*100
KGS	0.51±0.11 mGy/a	21.6%
KAPS	0.53±0.08 mGy/a	15.1%
RAPS	0.63±0.15 mGy/a	23.8%
NAPP	1.2 ±0.12 mGy/a	10.0%

IV. Conclusions

The environs of the PHWR reactors that have been operating in India for the generation of electricity, are regularly monitored for rise in the gamma radiation levels, if any, using TL dosimeters. The various analyses that are carried out on the data generated over the years indicate that the environs of the nuclear power stations do not show any increase in the background gamma radiation levels at the locations that were monitored.

Acknowledgments

The programme of environmental gamma radiation monitoring using TLDs in India has been in progress for over two decades. The constant support by all the staff of environmental surveillance laboratories at various NPPs in India is gratefully acknowledged.

References

1) K.S.V Nambi, et al., "Environmental radiation surveillance using thermoluminescence dosimeters," BARC report, BARC/I-575 (1979).
2) K. S. V. Nambi., V. N Bapat., M. David., V. K Sundaram., C. M. Sunta and S. D. Soman. Countrywide environmental radiation monitoring using TLDs Radiat. Prot. Dosim. **28** (1) 31 - 38 (1987).
3) A. S. Basu, V. N. Bapat, M. P. Chougaonkar, K. S. V. Nambi and R. P. Garg. 'Quarterly radiation monitoring results for the period 1988-1996 in RAPS region using TLDs and summarised analysis for the period 1982-1996. BARC report No. BARC/1998/E/021 (1998).
4) H. Yamanishi,. T. Iida, and Y. Ikebe, Measurement of regional dostribution of Radon 222 concentration. J. Nucl. Sci. Technol **28** (4) 331-338 (1991).
5) S. Minato, Monte Carlo Calculation of Gamma Radiation Field due to Precipitation Washout of Radon Daughters from the Atmosphere to the Ground Surface. J. Jpn. Health Phys. **15**, 19-24 (1980)
6) S. Sadasivan; V.K. ShukIa, S. Chinnaesakki, S. J. Sartandel, Natural and fallout radioactivity measurement in Indian soils. Journal of Radioanalytical and Nuclear Chemistry, Vol. 256, No.3 (2003) 603-607
7) R. A. Yus, M. Ogawa, Y. Ikebe, T. Ida, T. Nagaoka, R. Sakamoto and H. Obayashi. Passive method for separating elevated photon dose from background in the vicinity of a nuclear facility. Rad. Prot. Dosim. **64** (2), 233-237 (1996)
8) N. K Mehta, M. R Menon, V. K Shukla, V. D. Vashi and K. S. V., Nambi 'Preoperational environmental radiation survey around Kakrapar nuclear power project' Nat. Symp. on safety of nuclear power project plants and other sites, BARC Bombay, (1992).
9) A. S. Basu, M. P. Chougaonkar, Y. S. Mayya, S. Sadasivan and L. N. Sharma. 'Environmental radiation monitoring results for the period 1989-1999 in NAPS region using TLDs. BARC Report No. BARC/2001/E/011 (2001).

Journal of NUCLEAR SCIENCE and TECHNOLOGY, Supplement 5, p. 623–626 (June 2008)

Challenges in Promoting Radiation Safety Culture

Noriah MOD ALI*

Secondary Standard Dosimetry Laboratory, Malaysian Nuclear Agency, Bangi, 43000 KAJANG, Selangor, Malaysia

Safety has quickly become an industry performance measure, and the emphasis on its reliability has always been part of a strategic commitment. This paper presents an approach taken by Malaysian Nuclear Agency (Nuclear Malaysia) and authority to develop and implement safety culture for industries that uses radioactive material and radiation sources. Maintaining and improving safety culture is a continuous process. There is a need to establish a program to measure, review and audit health and safety performance against predetermined standards. Proper safety audit will help to identify the non-compliance of safety culture as well as the deviation of management, individual and policy level commitment; review of radiation protection program and activities should be preceded.

KEYWORDS: safety culture, safety audit, continuous process

I. Introduction

Many of the challenges in radiation industry have the potential to influence the safety culture in the workplace. Radiation safety is based on a whole set of regulations and standards, design solutions, operating instructions, safety culture, training, the work of regulatory bodies and other factors, all of which contribute to the control of the occupational exposures and prevention of the release of radioactive materials into the environment.

The introduction of the Atomic Energy Licensing Act, followed by the establishment of the Atomic Energy Licensing Board (AELB) in 1984 are serious initiatives taken by the Malaysian Government to regulate, safeguard and monitor the ionizing radiation activities in Malaysia. In addition, AELB is to complement the functions of Malaysian Nuclear Agency (formerly known as Malaysian Institute for Nuclear Technology Research (MINT)) in promoting the peaceful uses of nuclear technology. Since radiation issues are of national interest, the government has taken proactive approaches by formulating radiation safety strategies, whereby due consideration is given to the application of nuclear technology in various economic sectors without compromising on radiation safety standard.

Maintaining and improving safety culture requires continuous action and commitment. There is a need to establish a program to measure, review and audit health and safety performance against predetermined standards. Proper safety audit will help to identify the non-compliance of safety culture as well as the deviation of management, individual and policy level commitment, the audit and review of radiation protection program and activities should be preceded. Personnel attitudes and habits are generally intangible but the deviations of personnel attitudes and habits through the safety culture also can be tangible through radiation safety audit.

*Corresponding Author, Tel No: +60-3-89282961, Fax No: +60-3-89250575, E-Mail: noriaha@nuclearmalaysia.gov.my

II. Remarks on Safety Culture

One important component of safety, particularly in the nuclear industry, is radiation safety for employees and local communities. Nuclear Malaysia and AELB strives to keep radiation doses as low as reasonably achievable (ALARA) for workers that use radiation sources in Malaysia. This means going beyond compliance with regulatory limits to further reduce exposure for employees and the public. There are also adequate arrangements on education, training and public information and resources for these, as well as appropriate means of informing the public, its representatives and the information media about health and safety concerns. Facilities and services for radiation protection and safety must be well established at the national level. These include laboratories for personal dosimetry and environmental monitoring, and calibration and intercomparison of radiation measuring equipment; they could also include central registries for radiation dose records and information on equipment reliability.

In Malaysia, radiation industries are only small-sized organizations or teams of workers using radiation sources. In 2007, there are about 1,800 different workplaces involved with ionizing radiation, with about 15,000 radiation workers from 3 categories of job activities, namely medical, industrial and non-destructive testing (NDT). Approximately 43% of the total workers are from the industrial, 51% from medical and 6% from NDT sectors. Industrial radiographers are among the most highly exposed group of workers as compared to others. The nature of their work, the strength of the sources and the energy of radiation used in radiography works contributes to the high exposure that was received.[1,2] **Table 1** provides a detailed breakdown of exposure in the area of occupational groups. The annual effective dose received by industrial radiographers is higher than other radiation workers. The pattern shows a significant decrease in the average annual individual doses in industrial and medical sector with increasing number of workers from 1996 to 2006.[1]

The lower in average doses received in radiation industries in Malaysia may not be sustainable in the face of changes in work requirements. In specific work that involves high routine exposure, safety relies largely on procedures and human performance. Despite national efforts to improve occupational safety and health performance, many companies continue to experience unnecessarily high rates of occupational accidents.

Table 2 lists the number of incident and accidents in the radiation industries in Malaysia. Analyses of accidents have identified the major cause as failure to follow procedures, especially with regards to the use of proper dosimeter and personal protective equipment. Findings from the surveys on several facilities using ionizing radiation showed that internal safety audit is the most common aspect ignored in almost all facilities. Inadequate training and the limited availability of information on hazards and how to deal with them further compound these constraints. Similar comments are also relevant to the use of gauge sources in general industry, and the wider issue of source security is becoming a significant international concern with lost sources becoming a hazard to working groups who are not normally exposed to radiation. Current management practice demands that organization inculcate culture of safety to protect the workers, public and the environment from the hazards of radiation.

III. Stages of Development of Safety Culture

Safety has a role of growing importance in nuclear regulation, and also changed the regulatory program from one that addressed problems after the fact, to one that is more proactive in monitoring current safety and performance trends. The International Nuclear Safety Advisory Group (INSAG) [3] described two general components of safety culture: a framework in the organizations that is created by management, and an attitude of staff at all levels in responding to and benefiting from that framework. The achievement of a strong safety culture starts, therefore, with the approach and attitudes of the senior management in all organizations. Managers ensure not only that their staffs understand the significance of their duties and that they are continuously motivated towards high level of personal performance, but also they are themselves fully aware of their own responsibility towards safety (**Table 3**).

Table 1 Distribution of Accumulative Doses among Occupational Category, 2006

Accumulative dose (mSv)	Occupational Category		
	Industrial	Medical	NDT
0	418	5581	6516
0.1 – 5.0	266	373	390
5.1- 20.0	177	8	3
20.1- 50.0	33	8	2
> 50.0	6	1	-
No. Of User	900	5971	7911
Collective man (man-Sv)	3937.82	1074.78	1977.25
Average dos (mSv)	4.38	0.18	0.25

Table 2 Type of accident/incident involving use of ionizing radiation, 2000- 2006

Year	Number of overdose	Type of accident/incident
2000	6	Source stuck Lost of source Irradiator failure
2001	6	Source stuck Lost of source Incident on site
2002	4	Source stuck Incident on site
2003	3	Source stuck Premise on fire
2004	3	Source stuck Lost of source
2005	5	Source stuck Lost of source Irradiator failure
2006	7	Source stuck Incident on site
2007	2	Irradiator failure Incident on site

A good safety culture creates an environment for success. Understanding the basis of a strong safety culture and the tools to make it work will help us all be successful**.** Fostering a strong safety culture and providing systematic defense in depth are two of the most important strategies that are employed. Among elements to consider it include provision of competence staff as an important element for strong safety culture. Radiation Protection Officers are also challenged with building a radiation safety culture in diverse organizations. This includes regulatory audit processes and ongoing development of safety programs and training. Appropriate training of the workers at all levels is a fundamental building block in the attainment of a good radiation protection safety culture. Updating of training and refresher courses are also known to contribute to a good radiation safety culture. Of particular interest will be sharing the experiences of different types of radiation safety programs from small organization to larger consolidated facilities.

1. Actions Towards Safety Culture

The prime responsibility for safety and protection rests with the owner or the operator. National authorities are necessary to boost the development and implementation of radiological safety and security in the organizations responsible for the uses of radiation sources. The objective of the action program is greater awareness by managers and workers of the benefits of a safety culture, with a view to the more widespread adoption of the safety culture approach. A practical guide will also be developed to foster a commitment by managers and workers to the development of a safety culture approach at the enterprise level. These elements are already stressed in the license requirement and again will be taught and reminded in national courses, workshops and seminars to promote radiation safety including internal safety and health audits by workers and managers at the enterprise level**.**

Rapid development in the application of ionizing radiation has created a new opportunity in training needs. Training program offered by Nuclear Malaysia is seen as one of the catalyst for the proper use and implementation of radiation safety, as stipulated by the regulation. It is designed to respond to the needs arising from the legislative requirements, in line with the enforcement of the Act and in assisting organizations that uses ionizing radiation in their progress toward higher stages of development of safety culture. Hence, those who deal with ionizing radiation, regardless of their economic activities, are required to attend the recognized training. A training program is designed or tailored to meet the needs of customers. In this regards, Nuclear Malaysia has provided all these opportunities to cater for the changing needs of customers. With suitable training approaches, dedicated trainers, state of the art training facilities, the training has attracted numerous customers from various industries and institutions of higher learning both local and abroad. To improve safety performance in an organization, those involved in radiation activities are required to undergo continuous professional education (CPE) to refresh and enhance their knowledge, and improve skills in radiation related areas.

Establishment of Malaysian Radiation Protection Association (MARPA) on 15th September 2002 provide the advancing national and international meetings and forums to discuss all aspects of radiation protection to members and beneficial to the public. MARPA supports initiative by cooperation with governmental organizations and the authority dealing with education and training in radiation protection. This includes fostering, sponsoring and organizing scientific meeting, conferences, courses and seminars at national and international level.

Table 3 Elements of radiation safety culture

Policy level commitment

- Statement of safety policy
- Management structure
- Resources
- Self-regulation

↓

Managers commitment

- Definitions of responsibilities
- Definition and control of safety practices
- Qualifications and training
- Audits, review and comparison

↓

Individual commitment

- Questioning attitude
- Rigorous and prudent approach
- Communication

2. Developments and Continuous Improvement of the Safety Culture

The effectiveness of the safety culture can be improved if radiation safety audit is performed on the system. Radiation safety audits are an in-house means of ensuring radiation safety compliance at all times. It is a systematic and independent examination to determine whether radiation safety activities and related result comply with planned arrangement and whether these arrangements are implemented (**Fig 1**). The aim of the reviews should be to identify deficiencies unnecessary redundancies and to take appropriate corrective action. The interval each review should be dependent on the operations, the magnitude of the doses routinely, the risk of exposure,

and other operational parameters. The review should include an examination of facilities and equipment and of staff, procedures, and systems, including individual behavior.

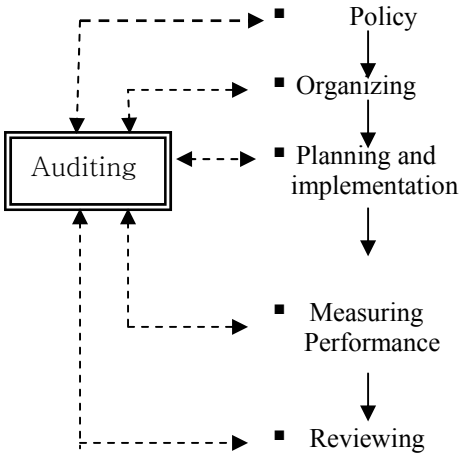

Fig.1 Role of audit in radiation safety program

The systematic application of the principles and the appropriate strategies to ensure the safe management of technologies involving radiation can be further improved through implementing self-assessment or audit on the system. [3,4]. Opportunities for improvement raised during the audit can be carefully considered and used to improve the implementation of the existing systems in each and every radiation facility in Malaysia whenever appropriate. Nuclear Malaysia has pioneered and conducted training for internal auditing of the radiation safety in the past three years for the public and private sectors. The radiation safety audit course is developed with modules describing the content of the audit trainings and the performance of internal audit in organization dealing with nuclear technology. Through this course, radiation protection officers will able to conduct self-audit in their premise. The main aim of the audit is to:

- Maintain facilities and equipment in a safe operating condition
- Provide a safe working environment for all employees and assess the level of emergency readiness
- Ensure that all procedures and activities are conducted in a safe and prudent manner
- Ensure adherence to the content of the safety manual.

AELB is presently encouraging organizations dealing with nuclear technology to slowly and voluntarily adopt the Radiation Safety Management System, in line with requirement of the Occupational Safety and Health, OSH (Safety & Health Committee) Regulation 1996. The OSH Regulations specifically stipulates the need to take into consideration on safety audit to protect the safety of the employees. In realizing this need, Nuclear Malaysia has initiated a course on Integrated Radiation Safety Management, IRSMS, which is aimed to highlight the integration IAEA, and AELB standard and requirement into the OSH management. Through this integration, it is able to manage a variety of hazards on environmental, safety and health and by promoting safe behavior at all levels of workers.

As a structured system, IRSMS is seen to be a competitive and sustainable product. The course is aimed to provide the basis of integration into OSH management to ensure adequate protection of workers, the public and the environment and encourage licensee to manage radiation safety based on performance, and not on compliance culture, with the final objective of professing a safety culture through self regulation. There is a significant improvement observed in the IRSMS as compared to the current Radiation Protection Program. This will certainly benefit an organization with ultimate goals of continuously striving for a healthy, accident-free and environmentally sound workplace and community, while providing the technical support needed to meet the national mission.

IV. Conclusions

The number of radiation sources in use today is very large and their uses range from simple to highly complex. An approach based on actions by Nuclear Malaysia, regulatory body and related association maybe helpful to facilitate the implementation of safety culture in organizations or companies working with radiation sources in Malaysia. In particular, this approach would be useful to prevent accidents and strengthen overall safety framework within which the control of all radiation risks from such sources is accommodated. The introduction of radiation safety audit and Integrated Radiation Safety Management, IRSMS are seen as the as a competitive product to meet the current and seen future needs in sustainability of radiation safety. As a result, safety culture, which has been a vital element on safety can be improved and utilized to promote changes from good safety performance leading to excellence.

The association, MARPA, plays a major role to provide a suitable environment for cross communications, technical updating and learning on safety issues. In the area of radiation risk, it is important that lessons learned from managing the safety of one type of radiation source, so that good practices are used as widely as possible. In this way, the safety of individual industries and society in general can be enhanced for the common good.

References

1) Noriah Mod Ali, Trends in Occupational Exposure in Malaysia, 11th International Congress of the International radiation protection Association, Madrid, Spain, 23rd-28th May 2004.
2) Noriah M.A., Gaining Competitive Advantage in personal Dosimetry through ISO 9001 Certification, Radiat. Prot. Dosimetry, ncl381v1, 2006.
3) International Nuclear Advisory Group, Key Practical Issues in Strengthening Safety Culture INSAG-15, Vienna, 2002.
4) IAEA Safety Standards, Management Systems for Technical Services in Radiation Safety, DS 315, IAEA2005.
5) Radiation Safety Management System- Specifications, AELB, Malaysia, 2005.

Journal of NUCLEAR SCIENCE and TECHNOLOGY, Supplement 5, p. 627–670 (June 2008)

The Seasonal Variation of Radon Concentration in the Atmosphere of Chichi-jima Island in the Pacific Ocean

Katsuhiro YOSHIOKA*

Shimane Prefecture Institute of Public Health and Environmental Science, 582-1, Nishihamasada-cho, Matsue, Shimane, 690-0122, Japan

We continuously measured the radon concentration from April 2001 to December 2004 in Chichi-jima Is. We expect that the radon concentration at Chichi-jima Is. would be influenced only by the air mass transported through the long distance. The hourly values had very large variations, ranging from 0.2 to 6.0 Bqm^{-3}. No diurnal periodicity was found in the variation of the radon concentration. We found that the monthly averages of the radon concentration had a clear long term pattern, showing the highest in the winter and the lowest in the summer. To analyze the radon long time variation, an arriving air mass is grouped into five sectors according to the backward trajectory. Sector Ⅰ is the sea areas surrounding Chichi-jima Is. Sector Ⅱ including Philippines, Indonesia and the southeast Asia is spread the southwestern Pacific Ocean from Chichi-jima Is. and sector Ⅴ is spread the northeastern way to the southeast. Sector Ⅲ includes China, Mongolia, Korea and the western Japan region and sector Ⅳ two regions of the eastern Siberia and the eastern Japan. The radon long time variation showed a high positive correlation between the number of arrivals of the continental air mass, while strong negative correlation between the maritime air mass.

KEYWORDS: radon, long-term variation, seasonal variation, diurnal variation, backward trajectory, Pacific Ocean, Chichi-jima Is., continental air mass, maritime air mass

I. Introduction

Radon-222 (called as radon hereafter), an inactive radioactive gas nuclide in the uranium series nuclides, is constantly released into the air from the earth's surface. Because radium concentration in the continental crust is higher than in the ocean, the radon flux is larger on the land than on the ocean, and its concentration in the atmospheric boundary layer is higher over the land by over 100 times than the one over the ocean.[1)]

The air mass also carries the radon escaped from the soil of the continent to the atmosphere over the Pacific Ocean. Because Chichi-jima Is. is small area and the atmospheric gamma radiation is low level, radon escaping from the soil there is supposed to be small amount.[2)] The island is located in the Pacific Ocean, approximately 1000km away from Tokyo and 2500km and 1800km from Beijing and Shanghai in China, respectively. Because of its isolated location, it is safe to assume that the radon concentration in the air there is low. We expect that the time variation of the radon concentration at Chichi-jima Is. would be influenced only by the air mass transported through the long distance. The continental air mass reaching Chichi-jima Is. is mixed with maritime air mass during the transportation. Therefore, the radon concentration is expected to be determined by the transportation time of the air mass.[3)]

We monitored the radon concentration in the atmosphere at Chichi-jima Is. over the long period and studied the long time variation, which is caused by the air mass coming from the Eurasian continent and/or the central area of the Pacific Ocean.

*Corresponding Author, Tel No: +81-852-36-8186, Fax No: +81-852-36-8171, E-Mail: yosiokaf@f8.dion.ne.jp

II. Measurement Method

1. Location of the Measurement

The atmospheric radon concentration was measured at 5m height on the ground in the central area of Chichi-jima Is. (240m above sea level, N 27.07, E 142.22) from April 2001 to December 2004, as shown in **Fig. 1.**

2. Equipment to Measure Radon Concentration

Radon concentration was continuously measured by an electrostatic radon sensor. This sensor is described in detail in the paper of the developer, Iida.[4)] We continuously counted the number of alpha particles from radon's decay products, Po-218 and -214, in the sucked air. Continuous hourly values of radon concentration were calculated from the counts.

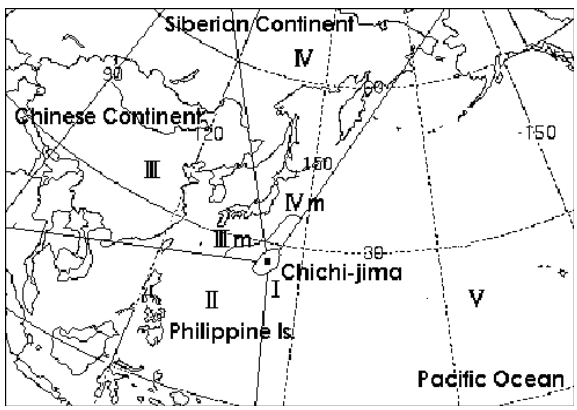

Fig. 1 Location and sectional map of backward trajectory at Chichi-jima Is. in the Pacific Ocean

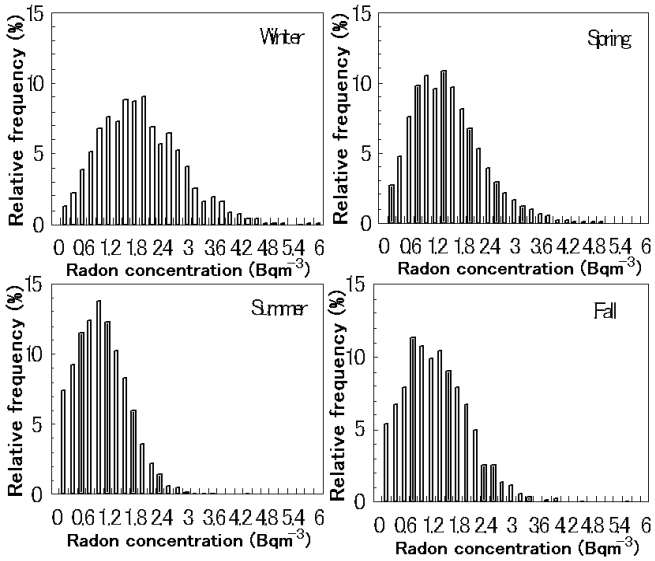

Fig. 2 Frequency distributions of radon concentration at Chichi-jima Is. in every season

III. Results and Discussion

1. Seasonal Variation of Frequency Distribution of Radon Concentration -Hourly Values

Fig. 2 shows the seasonal variation of frequency distributions of the radon concentration measured hourly from January to December 2003. The variation range of frequency distribution of the radon concentration varied widely in the summer and winter. The mode and variation range in summer were, respectively, 1.0 Bqm^{-3} and 0.2-3.6 Bqm^{-3}, and in winter, those were 2.0 Bqm^{-3} and 0.2-6.0 Bqm^{-3}, which were about two times larger in the mode at the summer. In the spring and fall, the modes are 1.2 Bqm^{-3} and 1.0 Bqm^{-3}, and the variation ranges are 0.2-5.0 Bqm^{-3} and about 0.2-4.0 Bqm^{-3}, respectively.

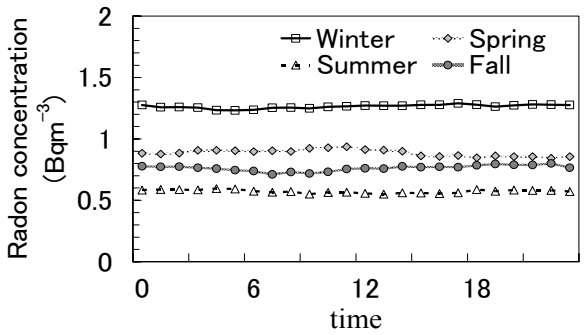

Fig. 3 Diurnal variations of radon concentration in every season at Chichi-jima Is. from DEC 2002 to NOV 2003

2. Amplitude of Diurnal Variation of Radon Concentration

Monthly diurnal variation data were obtained by calculating each hourly average from 00:00 to 23:00 for all the days in the month. **Fig. 3** shows the amplitudes of diurnal variation of the winter (DEC-FEB), spring (MAR-MAY), summer (JUN-AUG), and fall (SEP-NOV), calculated based on the data taken from December 2002 to November 2003. The amplitude of diurnal variation was very small, and no periodicity was seen in every season. In the atmospheric boundary layer of Chichi-jima Is., the mixing and diffusion of the air could be very different from that on the continents.[5)]

The fact that the dose rate of atmospheric gamma radiation and Ra-226 concentration in the soil are low suggests that very little amount of radon is released from the surface of Chichi-jima Is.[6)] Because Chichi-jima Is. has limited land area, the quantity of land air is also small, so that the land air can be constantly mixed with maritime air in the surface boundary layer even at night. Because the inversion layer cannot be build up in the surface boundary layer, radon does not stay and diffuses to the upper layer in the night. As the result, the increase of radon concentration cannot be seen.[7)] Therefore, as in **Fig. 3**, the amplitude of diurnal variation of the radon concentration could be approximated to 0.

3. Seasonal Variation of Monthly Average of Radon Concentration

Fig. 4 clearly shows the seasonal variation with a yearly cycle pattern in the long-term monthly average of radon concentration. The radon concentration rapidly increased from October in the fall, reached a maximum in January to February during the winter, started decreasing sharply from March in the spring, and bottomed from June to August during the summer. Since the lowest value in the summer was about 0.7 Bqm^{-3} every year, the value was considered to be the background level in the area of the Pacific Ocean surrounding Chichi-jima Is.

The southern wind was found most frequently, followed by the eastern wind, while western and northern wind was not recorded often. The range of monthly average of the wind velocity was as little as 2-4 ms^{-1}, and the wind velocity was lower in the summer than in the winter.

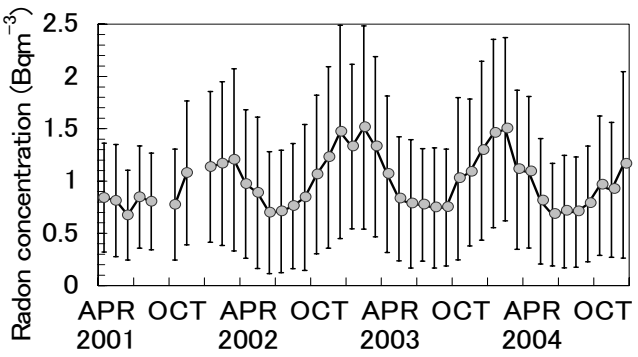

Fig. 4 Seasonal variation of monthly averages of radon concentration at Chichi-jima Is. from APR 2001 to DEC 2004

4. Relationship between Seasonal Variation of Radon Concentration and Advection Course of Air Mass

As discussed in III.2, the radon originated from Chichi-jima's soil was assumed to be very small amount; therefore, the radon concentration of the air mass brought by the long-distance transport is going to be discussed hereafter. In

China and Korea, there are many areas of high radon concentration, and in many places, the measurement values more than 20 Bqm^{-3} have been reported in the surface layer at about 1m high.[8-9] High radon concentration was also found in Siberia.[10] In Japan, locations with higher radon concentration are found in the western region than in the eastern region.[6] Because a continental air mass has high radon concentration, the air mass coming from China and Siberia would have higher radon concentration than the maritime air mass.

On the other hand, very low radon concentration has been reported on the remote islands in the Pacific, such as the Hawaii Islands.[3, 11] Low values have been reported in the Indonesian islands, too.[12] Because, in theory, the radon concentration of air mass is influenced by the mixing ratio of the continental air mass and maritime air mass during the traveling path, we set up zones contain one of the following areas: China, Siberian area, one group of the Philippine Islands, the southeast Asia, and the Indonesian Islands, and the Pacific Ocean, in order to analyze the backward trajectories of air mass.

The backward trajectories at 00 UTC and 12 every day were calculated using the HYSPLIT4 model of NOAA ARL,[13-14] and the courses of advection ascending for 5 days were estimated. Using the sectional map (**Fig. 1**), the estimated advection courses for 5 days prior to the arrival were classified into types I to V. In types III and IV air masses, the radon concentration decreases because of mixing with the maritime air. Among such air mass, those which travel in IIIm or IVm areas for more than 1 day before the arrival were grouped as type IIIm and IVm in order to discuss the difference in the advection time on the ocean. In order to estimate the effect of radon escaping from Chichi-jima's soil, the air mass which stayed in area I for more than 1 day before its arrival were categorized as type I.

Fig. 5 shows the seasonal variations of the frequency distributions of air mass types from April 2001 to December 2004. In the winter, types III and IV air masses are many frequencies and in the summer, type V is many. Type I is arriving through the year and type II is many frequencies in the rainy season before the summer.

(1) Variation of Radon Concentration according to Advection Course of Air Mass

The average radon concentration was computed during the time from 0 to 11 and 12 to 23 JST, at which the air mass arrived. Then, the each average radon concentration was calculated in the every arriving air mass type.

Fig. 6 shows the average radon concentration by the arriving air mass from April 2001 to December 2004. The radon concentrations of types III and IV air masses were significantly higher than those of types I, II and V, which show the influence of long traveling time over the land.

The radon concentration of type III air mass was about 1.9 and 1.8 times higher than those of types V and II respectively and it clearly shows the difference between the continental air mass and the maritime air mass. Type III air mass showed about 1.1 times higher concentration than type IV, suggesting the difference between China and Siberian areas and the traveling time of air mass. Type II air mass coming from the Indonesian islands, the Southeast Asia, and the Philippines islands gave slightly higher radon concentration than that of type V, which comes for the central area of the Pacific Ocean. This supports the influence of the land area under the traveling path. The radon concentration of type I air mass was about 1.2 times and about 1.1 times higher than those of types V and II, respectively. This fact verifies the influence of self radon in Chichi-jima.

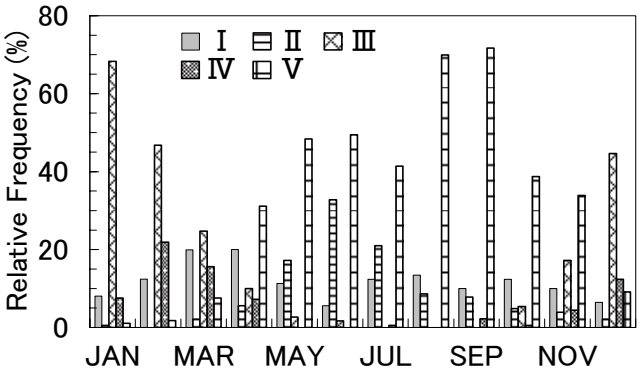

Fig. 5 Seasonal variations of frequency distributions of air mass types at Chichi-jima Island

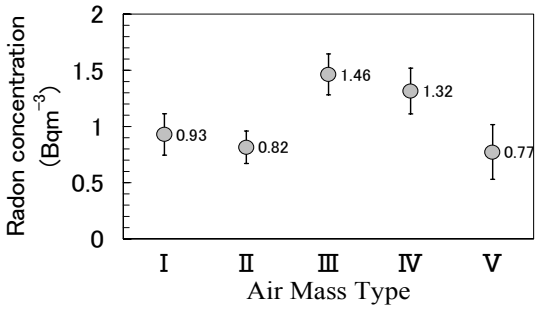

Fig. 6 Radon concentration of each type of air mass at Chichi-jima Island

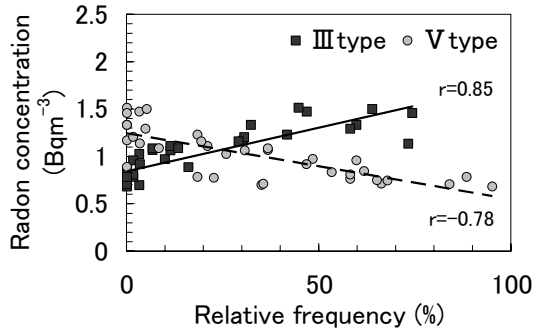

Fig. 7 Correlation between monthly average of radon concentration and monthly frequency of types III and V air mass from JAN 2002 to DEC 2004

The concentrations of types IIIm and IVm air mass were about 0.8 times lower than types III and IV, respectively, indicating the difference of the concentration caused by the time difference (about one day) in the mixing with the maritime air..

(2) Correlation between Monthly Averages of Radon Concentration and Arrival Frequencies of Air Mass

Fig. 7 shows correlations among monthly averages of radon concentration, and the monthly arrivals of type III air mass, as well as those of type V air mass. There is a positive correlation between the monthly radon concentration and the arrivals of type III air mass with a correlation coefficient; r=0.85, but a negative correlation was found between the arrivals of type V air mass with r=-0.78. From these results, it is obvious that the increase of type III air mass resulted in the highest concentration in the winter, which is shown in the seasonal variation. The results also clearly show that the lowest concentration in the summer depends on the increase of type V air mass.

IV. Conclusions

We continuously measured the radon concentration from April 2001 to December 2004 in Chichi-jima Is. The hourly values had very large variations, ranging from 0.2 to 6.0 Bqm^{-3}. Radon concentrations above 4 Bqm^{-3} were less than 1 %, and it mainly distributed between 0.2 and 4.0 Bqm^{-3}.

No diurnal periodicity was found in the time variation of the radon concentration, we presumed that the difference between the atmospheric stability at day and night was small and the air in the island was always mixed with the air mass over the ocean. No apparent diurnal variation of the radon concentration was found; therefore, it was expected that radon escaped from Chichi-jima's soil was very little. We found that the monthly averages of the radon concentration had a clear long term pattern, showing the highest in the winter and the lowest in the summer.

Grouping under 5 types of advection courses of the backward trajectories of arriving air masses, we discussed the seasonal variation in the radon concentration and the arrival frequency. It was found that types III and IV air masses had high radon concentration and mostly arrived in the winter, while types II and V air masses had low concentration and arrived in the summer. A high positive correlation coefficient was found between the monthly averages of radon concentration and the number of arrivals of type III air mass, while strong negative correlation was found for the type V air mass. This means the seasonal variation was strongly influenced by the air mass originated from China in the Eurasian continent and the Pacific Ocean.

Type I air mass, on which Chichi-jima Is. influences, showed the low radon concentration. Therefore, the influence of radon originated in Chichi-jima Is. was small and the atmosphere in this area was well mixed with the arriving air mass.

Acknowledgement

The author greatly appreciates Prof. M. Uematsu, The University of Tokyo Ocean Research Institute, to obtain the long-term observation. Mr. T. Yoshiyama, the National Space Development Agency Ogasawara pursuit place, Dr. S. Koga and Dr. N. Kaneyasu, Advanced Industrial Science and Technology are greatly thanked for the maintenance of measurement equipment. Mr. T. Konishi, Mr. K. Watai and Mr. K. Nagase, Ohyokokenkogyo Co., LTD., are thanked to set up and adjust of equipment. The author is grateful to the NOAA Air Resources Laboratory for the provision of HYSPLIT model and/or the READY website (http://www.arl.noaa.gov/ready.html) used in this paper.

References

1) S.D.Schery; "Progress on Global ^{222}Rn Flux Maps and Recommendations for Future Research", 1st International expert meeting on sources and measurements of natural radionuclides applied to climate and air quality studies, 3-5 JUN., 2003.
2) S. Minato, "Gamma Ray Dose Rate due to Rocks in Japan", RADIOISOTOPES, **54**, 79-84, 2005.
3) S. Whittlestone, E. Robinson, S. Ryan, "Radon at the Mauna Loa Observatory. Transport from distant continents", Atmos. Environ., **26A** [2], 251-260, 1992.
4) T. Iida, "An Electrostatic Radon Monitor for the Continuous Measurement of Environmental Radon", ATMOSPHERIC RADON FAMILIES AND ENVIRONMENTAL RADIOACTIVITY, 65－73, 1985, [in Japanese].
5) T. Asai, "Local Meteorology", University of Tokyo Press, Tokyo, 99-131, 1996.
6) JAPAN CHEMICAL ANALYSIS CENTER, Environmental Radioactivity and Radiation Data Base, http://search.kankyo-hoshano.go.jp/
7) R.E.Larson, W.A.Hoppel, "Radon 222 measurements below 4km as related to atmospheric convection", Pure and Applied Geophysics (Historical Archive), **105**[1], 900-906, 1973.
8) J. CHENG, Q. GUO, T. REN, "Radon Levels in China", J.Nucl.Sci.Technol., **39**[6], 695-699, 2002.
9) W.H.Chung and S.Tokonami, "Preliminary Survey on Radon and Thoron Concentrations in Korea", Radiat. Prot. Dosim., **80**, 423-426, 1998
10) J.Moriizumi et al., "The Temporal Variation in Atmospheric Radon-222 Concentrations in West Siberian Forest: High Concentrations in Snow Covered Season", SEVENTH INTERNATIONAL WORKSHOP on GEOLOGICAL ASPECTS of RADON RISK MAPPING, 2004.
11) Wilkning MH, "Radon-222 on the island of Hawaii", Health Phys., **58**[19], 77-80, 1990.
12) G.W. Berger, A.J. Van Bennekom and H.J. Kloosterhuis, "Radon profiles in the Indonesian archipelago", Netherlands J.of Sea Res., **22**[4], 395-402, 1988.
13) R.R.Draxler and G.D.Rolph; HYSPLIT (HYbrid Single-Particle Lagrangian Integrated Trajectory) Model access via NOAA ARL READY Website (http://www.arl.noaa.gov/ready/hysplit4.html). NOAA Air Resources Laboratory, Silver Spring, MD., 2003.
14) G.D.Rolph; Real-time Environmental Applications and Display system (READY) Website (http://www.arl.noaa.gov/ready/hysplit4.html). NOAA Air Resources Laboratory, Silver Spring, MD., 2003.

Journal of NUCLEAR SCIENCE and TECHNOLOGY, Supplement 5, p. 631–634 (June 2008)

Investigation of Aliquot Representativeness in the Radiochemical analysis and Gamma Measurement of Contaminated Soil Sample

JIN Yuren*, LI Weiping, LI Ling, and XU Hui

Northwest Institute of Nuclear Technoloty, Xi'an,710024,China

Abstract. In the present paper, the size of the soil particle and the weight of the aliquot submitted to gamma measurement or radiochemical analysis, while fulfilled the requirement of representativeness, were investigated experimentally. The radioactive contaminated soil sample was pulverized, ^{239}Pu was separated and determined by isotope dilution introduced coupled plasma mass spectroscopy, and gamma emitters, ^{241}Am and ^{137}Cs etc were measured by the gamma spectrometry. The dependence of the time taken during the milling and consequent mesh size, and the relationship between the weight of aliquot for radiochemical analysis and the mesh size of the soil were established, under the supposed representativeness criteria of (1) the relative standard deviation (RSD) less than 20% and (2) the deviation from certificated value (DCV) less than 10%. An empirical equation of the aliquot weight and size was fitted, by which the optimum size is 40mesh when circa 180 g is used for gamma measurement, and the preference size is 150 mesh when the aliquot for the radioanalysis around 2 g soil is scooped for assay. These results could be used in the assay of the soil samples in the radiological survey.

KEYWORDS: representativeness, radiochemical analysis, contaminated soil, plutonium-239, americium-241

I. Introduction

Release of anthropogenic radioactivity in the environment happens mainly due to atmospheric nuclear tests and various nuclear events. The contamination characterization such as the category of radioactive nuclides, their activity concentration and the vertical distribution profile in the soil, are generally accomplished by collecting the soil at the site followed by pretreatment such as dry, milling and sieving, laboratorial analysis and measurement. Gamma measurement is the main technique for γ emitting nuclides, whereas, radiochemical analysis is essential to some primary contaminants of concern with little or non-gamma emitter such as ^{238}Pu, ^{239}Pu, ^{240}Pu and ^{90}Sr. In the case of radiological survey for a broad area, a great number of soil samples would be collected, and the homogeneity of soil samples is time consuming.The determination of plutonium and strontium in soil involves tedious radiochemical procedures, including conversion of the analytes associated with the matrix into acid soluble form, radiochemical separation from the components of the soil, purification and preparation of the source. In general, the error of the analytical results comes firstly from the process of soil collection(sampling representativeness), then from the process of analysis, including aliquot representativeness and the error of the measurement. Many of investigations concerned about how to obtain representative samples in the radiochemical analysis of the radioactive contaminated soil, whereas, few of studies focus on the aliquot representativeness. The representativeness of the aliquot depend mainly on the three aspects (1) inter-contamination during samples pretreatment, (2) the uniformity of the sample and (3) the representative of the aliquot using for analysis. Inter-contamination should be strictly controlled during experiment, and the uniformity of the sample could be accomplished by homogenizing. The present paper aims to reveal the relationship of the weight of the aliquot and the particle size of the sub-sample that has been homogenized by milling and sieving.

*Corresponding Author, Tel No: 086-29-84765047, Fax No: :086-29-83366333, E-mail: Email: jinyuren@sohu.com

II. Experimental Methods

To fulfill the requirement of data quality, a definite weight of aliquot using for radiochemical analysis or gamma measurement there exist a maximum particle size, and vice versa, for a definite particle size of the sample being analyzed, there exist a minimum weight of aliquot using for analysis, as has been revealed by empirical equation, $m = Kd^{\alpha}$ .Where, m is the minimum weight of the aliquot, kg, d is the particle size, mm, K is the sample splitting factor, α is the exponential item. The contaminated soil collected from polluted area was pulverized to a definite size. By analyzing the concentration of plutonium in the aliquots, the representative weight of the aliquot corresponding to a definite particle size was obtained, and the data was fitted in order to obtain empirical factor K and α. The supposed criteria of the representativeness of the aliquot including two item, (1) the relative standard deviation (RSD) of the concentration of ^{239}Pu of the replicated aliquot for a sub-sample is less than 20% and (2) the deviation of the mean concentration from the certificated value(DCV) is less than 10%.

The RSD and DCV were obtained by the following procedure. The soil sample was mixed and quartered. Each quarter was milled and sieved through one of screens with mesh size of 100, 150, 200, and 300 respectively to get sub-sample used for investigation. To each homogenized sub-sample, five classes of the aliquot weight (as listed in **Table**

1) were designed and the weight of the aliquots was strictly controlled during weighting with its deviation less than 0.1%. For each class, 6 replicated aliquots were taken for the analysis of the concentration of ^{239}Pu which was determined by acid leaching followed by isotope dilution and ICP-MS measurement, and then RSDs were calculated. For the calculation of DCVs, the certificated concentration of ^{239}Pu in the soil sample was obtained by analyzing 6 replicated aliquots of the sub-sample of mesh size 300, in this case, the aliquot was totally dissolved using microwave acid digestion.

Table 1 The weight of the aliquot designed for each sub-sample

Mesh size (mesh)	100	150	200	300
Five classes of designed weight of the aliquot (g)	0.1	0.1	0.1	0.1
	0.3	0.3	0.3	0.3
	0.9	0.9	0.9	0.9
	4	3	3	2
	15	10	6	4

1. Measurement of Gamma Emitter

The sandy soil sample collected at a contaminated site was dried in an oven at 105℃ for at least 4h, ground using a ball mill, and sieved through a screen of 40 mesh. The aliquot about 180 g was filled into 110 ml plastic containers for the measurement of ^{137}Cs and ^{241}Am by gamma-spectrometry using high purity germanium detectors with multichannel analyzers from Canberra and analytical software "Genie 2000". Energy and efficiency calibration of the detector was carried out using a certified γ-source. The relative efficiency of the Ge-detector was 50% the resolution measured as FWHM was 1.90 keV at 1332 keV[1)].

2. Determination of ^{239}Pu

The measurement of ^{239}Pu was performed on the double focusing inductively coupled plasma mass spectrometer (Finnigan MAT Element). The aliquot was spiked using a certificated ^{242}Pu solution and then placed into a muffle furnace and ashed at a temperature of 500℃ for at least 12 h. If the weight of the aliquot was less than 10 g, 0.2g $FeCl_3 6H_2O$ should be added. All the chemicals and reagents used in the experiment were of analytical grade. The water used was deionized Milli-Q 18.2 MΩ.

(1) Acid leaching

The ashed aliquot of soil was conditioned with 10 to 100 ml of aqua regia depending on the weight of soil. The mixture was kept overnight in a beaker covered with a watch glass. This mixture was heated to mild boiling for 2 h on a hot plate. Then the mixture was cooled, centrifuged. The supernatant was stored, and fresh 25ml 8 mol/l HNO_3 was added to the centrifuge tube for washing the matrix. The process was repeated until the leachate was clear, and all the resultant liquid was combined. The resulted leachate was evaporated to near dryness. The residue was used for the isolation and purification of ^{239}Pu (the procedure used will be described in section (3).

(2) Microwave acid digestion

Microwave acid digestion was used for totally digestion of soil samples. In the experiments, Mars 5 microwave digestion system was used. The aliquot (weight less than 0.5 g soil) was placed into each vessel jointly with 2ml 65% HNO_3 5 ml 35% HCl and 3 ml 48% HF. The vessels were covered and installed in the rotor. When the digestion was finished and vessels had cooled, the digestion solution was passed to a glass beaker. The vessels were washed with concentrated nitric acid and deionized water, and the washings were added to the beaker containing the sample. 5 ml of 70% $HClO_4$ were added to each beaker. Finally, the sample was evaporated to dryness over a hot-plate. The residue was treated with 50 ml 60% HNO_3 and evaporated to dryness again. The residue was used for further isolation and purification of ^{239}Pu.

(3) Isolation and Purification

Plutonium was isolated by iron hydroxide coprecipitation and its oxidation state was adjusted with NaS_2O_4 - $NaNO_2$ [2)]. The purification of plutonium was accomplished by conventional anion exchange resin [3)].

The residue of leachate or digestion solution was dissolved diluted to ~200 ml with 0.5 mol/L HCl, the pH of the solution was adjusted 7.5~8 with 12.5% $NH_3 \cdot H_2O$ and the ^{239}Pu was coprecipitated with iron hydroxides. The mixture was centrifuged and the supernatant was discarded; 20 ml 6mol/lNaOH was added and stirred for 5 min, then diluted with deionized water to the volume of ~200 ml; stirred, centrifuged and discarded the supernatant. The precipitation was dissolved and diluted with deionized water to the volume of ~120ml, then 150mg NaS_2O_4 was added. The mixture was sporadically stirred for around 1h to adjust the valence of Pu to Pu (III), and then the pH of the solution was adjusted to 10 with 6mol/l NaOH again, followed by centrifuging. The supernatant was discarded and the precipitation was dissolved with a few ml of 9 mol/l HCl. The resultant solution was transferred into a graduated glass centrifuge tube, and 14 mol/L HNO_3 was added(Vs/V_{HNO3}=1:1.3), then, 50 mg $NaNO_2$ was added to stabilize the Pu oxidation state at Pu(IV) and the resulted solution was submitted for the anion exchange purification of plutonium.

The solution was passed through an anion exchange column (8cm×0.75cm) containing the resin Dowex 1×4 100-200, where Pu (IV) was retained. The adsorbed plutonium was purified from uranium and thorium by washing the column with 40 ml 8 mol/L HNO_3, and 60 ml10 mol/L HCl respectively, 10 ml 3 mol/l HNO_3 was used to rinse the column. Plutonium was eluted with 0.025 mol/l $H_2C_2O_4$ - 0.15 mol/l HNO_3, and the eluate was used for ICP-MS measurement directly.

(4) ICP-MS Measurement

The measurement and quantification of ^{239}Pu were carried out by isotope dilution ICP-MS[4].A Finnigan MAT ELEMENT high resolution ICP-MS was used. The mass resolution was 300. The sample solution was injected using

an Aridus membrane desolvator.The sensitivity was tuned to approximately 2×10^5cps per ppb ^{238}U.

A blank (2% nitric acid) procedure was performed in advance of sample analysis. The signal intensity at m/z 238 was monitored, incase unsatisfactory separation of uranium was encountered. The count rate of m/z239 originated from ^{238}U and the mass bias coefficient were determined before or after the measurement of each sample. The limit of the determination for ^{239}Pu in soil is 40fg.

III. Results and discussion

1. The Preferable Mesh Size

The soil samples were firstly homogenized by mixing, and split into four parts, then each part was ground using a small ball mill and sieved thoroughly through 100, 150, 200 and 300 mesh screen, respectively. The time used in the milling (and sieving) was recorded. **Fig. 1** shows the dependence of time to get 100 g homogenized sub-sample and its particle size (characterized as the mesh size of the screen). The time needed to grind the soil till totally sieved through 150 mesh is a little longer than that through 100 mesh. The milling time increased dramatically when the particle size is larger than 200mesh. and when the mesh size is 300, the milling time rise up to unendurable 14 h. Therefore, the preferable particle size 150 mesh was recommended.

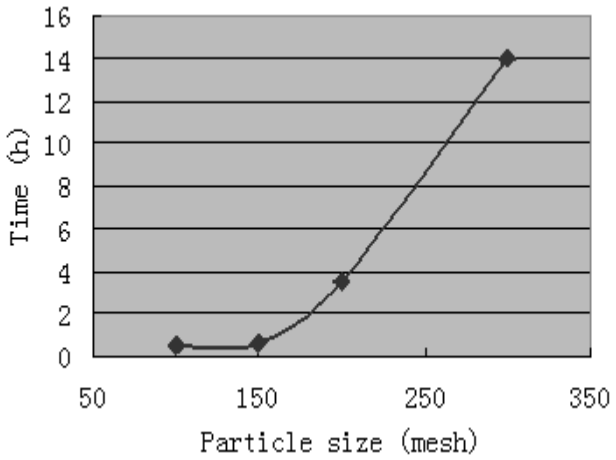

Fig 1 The time used for milling 100 g soil to sieve through thoroughly the corresponding mesh size screen.

2. Acid Leaching Recovery

When the weight of the aliquot is greater than 0.5 g, it is difficult to dissolve the soil completely by microwave acid digestion, whereas acid leaching is convenient. Therefore the aliquots used for the radiochemical analysis of plutonium were digested by acid leaching. The concentration of ^{239}Pu obtained by the acid leaching was calibrated using the chemical recovery. Replicate aliquots of the sub-sample with particle size 300mesh were digested by acid leaching as well as by microwave acid digestion respectively. The concentration of ^{239}Pu was analyzed as described above. The recovery of plutonium by acid leaching was calculated by the mean results from acid leaching divided by that from microwave acid digestion assuming that the soil dissolution of the latter was complete. The results show that the acid leaching recovery of ^{239}Pu by acid leaching was 82 %(1±15%, n=6).

3. Minimum Weight of Aliquot

Fig. 2 shows the RSD and DCV with the weight of the aliquot for the sub-sample of which particle size is 300 mesh. Curve 1 is the dependence of the RSD on the weight, and curve 2 is the relationship of the DCV with the weight of the aliquot. According to the supposed criteria of aliquot representativeness, the minimum weight of the aliquot is around 0.5 g for the sample with particle size of 300 mesh. Correspondingly, the representative minimum weight of the aliquot for particle size 200 mesh is 1.0 g, for 150 mesh is 2.0 g and for 100 mesh is 9.0 g. The equation for the minimum representative weight of aliquot m (in kg) and the particle size (sieve size), d (in mm) was fitted by using these results, $m = 1.6d^{2.8}$ (**Eq. 1**), and yielded a coefficient of determination $r^2 = 0.980$, the fitted curve is shown in **Fig. 3**. As the experimental results show that the minimum representative weight of the aliquot is 2 g, when the particle size of the sub-sample for radiochemical analysis is 150 mesh.

When the weight of aliquot used for gamma measurement was ~180 g, according to **Eq. 1**, the particle size of the sub-sample should not be less than 33 mesh. In our experiments, the contaminated soil samples used for gamma measurement were pulverized to sieve through 40 mesh size screen to fulfill the requirement of the representativeness. In order to validate the representativeness of the gamma measurement aliquots, three contaminated soil samples were pulverized and sieved through 40 mesh size screen, and eight replicate samples for each soil sample were filled for gamma measurement. The results and the RSD listed in **Table 2** show that the precision is satisfactory.

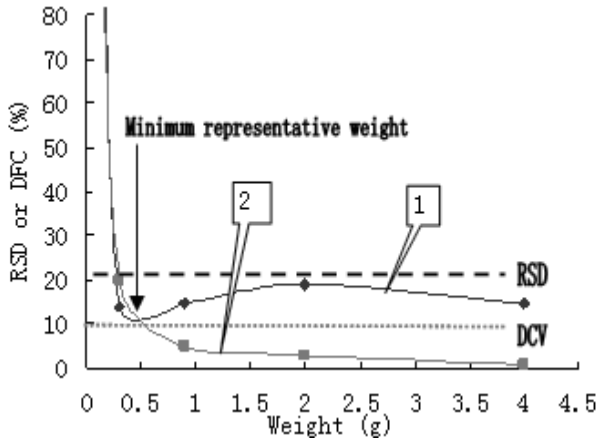

Fig 2 The relationship of the RSD and the DCV with the weight of the aliquot. The particle size of the sub-sample is 300mesh. Curve 1—RSD, Curve 2—DCV.

Table 2 The precision of gamma measurement., The weight of the aliquot is about 180 g.

Title of the soil sample	Number of aliquot	^{137}Cs (Bq/kg)	^{241}Am (Bq/kg)
S013	S013-A	151	16.4
	S013-B	149	16.4
	S013-C	153	16.8
	S013-D	151	17.1
	S013-E	150	16.6
	S013-F	147	16.0
	S013-G	140	14.9
	S013-H	141	14.9
RSD (%)		3.2	5.1
S020	S020-A	108	10.5
	S020-B	116	10.8
	S020-C	113	10.6
	S020-D	107	9.65
	S020-E	94.6	9.76
	S020-F	115	11.2
	S020-G	109	10.1
	S020-H	115	11.0
RSD (%)		6.4	5.4
S033	S033-A	80.4	11.4
	S033-B	93.5	11.9
	S033-C	90.9	11.7
	S033-D	89.7	12.2
	S033-E	92.6	12.2
	S033-F	91.9	11.9
	S033-G	90.6	11.6
	S033-H	91.3	11.9
RSD (%)		4.6	2.3

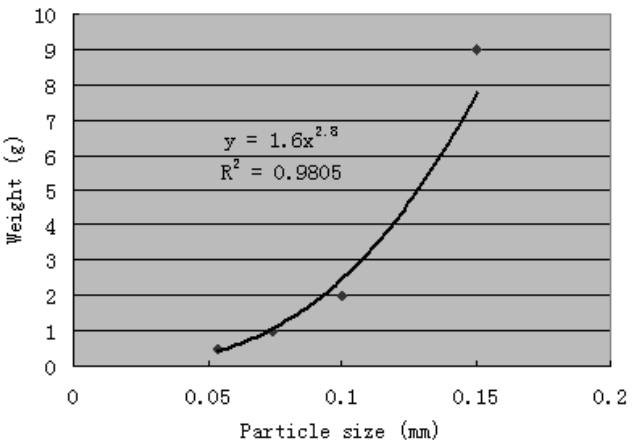

Fig 3 The dependence of the minimum representative weight of aliquot on the particle size of the sub-sample.

IV. Conclusions

The results show that the preference particle size for radiochemical analysis is 150 mesh and the corresponding minimum weight of the aliquot is 2 g. The soil sample should be milled and pass through a screen with mesh size of 40 mesh when the aliquot weight for gamma measurement is 180 g, these results could be used in the assay of soil samples in the radiological survey.

References

1) J. M. Zang, Q.L. Shi, T. Bai, Y.R Jin, D.M.Li. Radioactivity Determination of Several Manmade Radionuclides in Soil Samples by γ Spectrometry. Journal of Isotopes, 18 (1,2), 102-107(2005).(in Chinese)
2) Q.J. Chen, A. Aarkfog, S. P. Nielsen, H. Dahlgaard, B. Lind, A.K.Kolstad and Y. Yu. Procedures for Determination of ^{239,240}Pu, ^{241}Am, ^{237}Np, ^{234,238}U, ^{228,230,232}Th, ^{99}Tc and ^{210}Pb-^{210}Po in Environmental Materials, RisØ National Laboratory, Roskilde,Denmark, RisØ-R-1263(2001)
3) M.P. Rubio Montero, A. Martín Sánchez, M.T. Crespo Vázquez, J.L. GascÓn Murillo, Analysis of plutonium in soil samples. Applied Radiation and Isotopes 53, 259-264 (2000).
4) Y.R. Jin, J.F. Gao, J.F. Bai, G.Q. Zhou, L Li, J.C. Xie,J.F. Wu, X.H.Wang , F.R. Zhu. Determination of plutonium in the Air by Isotopic Dilution ICP-MS After TNOA Extraction Chromatographic Separation. In Environmental Radiochemical Analysis II. Ed. Peter Warwick, The Royal society of Chemistry, UK. PP263-272(2003).

Journal of NUCLEAR SCIENCE and TECHNOLOGY, Supplement 5, p. 635–638 (June 2008)

Environmental Radiation Measurements And Comprehensive Impact Assessment Around A Nuclear Power Plant Site In Kaiga, India

P.M.RAVI[1*], T.K.REJI[1], M.S. VISHNU[1], A.G. HEGDE[1], M.L.JOSHI[1], and H.S. KUSHWAHA[2]

[1]*Health Physics Division, Health, Safety and Environment Group, Bhabha Atomic Research Centre, Trombay, Mumbai, India – 400 085.*
[2]*Health, Safety and Environment Group, BARC*

This paper presents the results of environmental monitoring of Kaiga site and impact assessment due to the operation of two PHWR type reactors. Measurements of radionuclides were carried out in atmospheric, terrestrial and aquatic environmental compartments using state-of art techniques and radiological impact due to external exposure, ingestion, inhalation and skin absorption pathways to individual member of public evaluated. A hypothetical case of OBT intake through contamination of crops due to tritium is also considered. The paper also presents the results of estimation of Site Specific Transfer Factors required for the impact assessment modeling. The parameters required for dose evaluation and respective uncertainties for each parameter were attributed. The dose distribution was estimated using parameter uncertainty analysis from all the pathways and for all the major radionuclides. Dose distribution was found to be lognormal and ranges from 0.2 – 5.8 $\mu Sv.a^{-1}$ (at 95% Confidence) with a mean value of 1.1 $\mu Sv.a^{-1}$ in the year 2006. Since the upper limit of 95% confidence level is below the regulatory limit, violation of the limit is highly unlikely. Statistical analysis of ^{137}Cs concentration in soil and sediment samples indicate that there is no build up of ^{137}Cs in the environment as compared to pre-operational value ($p<0.001$).

KEYWORDS : environmental impact assessment, public dose, transfer factors

I. Introduction

Two units (each of 220 MWe) of Pressurized Heavy Water Reactor (PHWR) type nuclear reactors are operational at Kaiga site since 2000, while two more similar units are likely to be operational by the end of 2007. Gaseous effluents consisting mainly of Tritium, Argon-41 and Fission Product Noble Gases (FPNG) are released through a stack of height 100m to the environment after ensuring regulatory compliance. Liquid effluents after necessary treatment and ensuring regulatory compliance are released to Kadra reservoir, the fresh water body, near the site. The hilly terrain, forest ecosystem and the reservoir ecosystem around the site makes the environmental impact assessment very complicated and challenging. The basic purposes of environmental monitoring around a nuclear power plant are to demonstrate that

1. The dose to the member of public is well within the internationally acceptable limits.
2. The operating power plants will not lead to any unacceptable radioactivity build up in the environment.

This paper presents the results of environmental monitoring carried out during the operational period of the plants and compares with the pre-operational data. The impact assessment was carried out using the results of analysis of in situ samples collected from environmental matrices and also using environmental modeling. The paper presents the results of estimation of site specific parameters for environmental modeling.

*Corresponding Author: Tel No: +91-08382-254092, Fax No: +91-08382-264025 E-Mail: pmravi@npcil.co.in

II. Materials and Methods

Our regular environmental monitoring program covers up to a radial distance of 30km from plant site. However this paper presents the results of radiological impact assessment to the critical population.

As per the site meteorological conditions, annual averaged χ/Q values are maximum at South West (SW), West (W) and South of South west (SSW) sectors[1)]. (χ/Q (Dilution Factor) is defined as the ground level air concentration of a radionuclide per unit release). The village within these sectors and closer to plant site is Hartuga, which is also located in the downstream of Kadra reservoir.

As far as Tritium is concerned, the critical population is that of Hartuga and the critical pathways are inhalation of contaminated air, ingestion of water. Argon-41 and Fission Product Noble Gases (FPNG) are chemically inert and act only as an external hazard. Air samples from Hartuga village and water samples from Kadra reservoir near Hartuga were collected on a weekly basis using standard procedures[2)]. Soil and sediment samples were collected from villages and estimated for ^{137}Cs. Tritium was estimated using a Liquid Scintillation Counting system. During the period 1999-2003, a Liquid Scintillation Counting System with a Figure of merit (E^2/B) of 180 was used for Tritium analysis. From 2004 onwards, an Ultra Low Level Liquid Scintillation Counting System PACKARD 3170TR with a Figure of merit (E^2/B) of 1400 is operational. A High Purity Germanium (HPGe) Detector (Oxford make, 15% relative efficiency, Minimum Detection Limit of 70 mBq (^{137}Cs) for a counting time of 60000 sec) was used for Gamma ray spectrometric measurements.

III. Results and Discussions

The radiological impact in public domain around the reactor are contributed from internal dose due to tritium and external dose due to ^{41}Ar and FPNG. Tritium released as HTO will exist in environment as HTO and Organically Bound Tritium (OBT). OBT exhibits longer residence time in organisms than HTO[3].

1. Activity in Air and Water

Table 1 shows estimated tritium activity in the air samples and water samples taken from Hartuga village during the years 2002-2006.

Table 1 Tritium activity in air and water near Hartuga village

Year	Activity in air ($Bq.m^{-3}$)			Activity in water ($Bq.l^{-1}$)		
	No. of samples	GM	GSD	No. of samples	GM	GSD
2002	50	1.6	2	51	58.7	1.4
2003	49	1.2	1.5	48	51.0	1.2
2004	59	0.5	2.7	50	17.7	1.0
2005	63	0.7	3.0	48	16.2	1.3
2006	61	0.8	2.9	46	17.6	1.8

GM-Geometric Mean , GSD-Geometric Standard Deviation

The observed tritium concentration in air and water were either below detection limit or slightly above the detection limit. The lower GM values observed after 2004 can be attributed to the improved sensitivity of the system.

2. Hypothetical Tritium Concentration in Rice

Rice is the major food item consumed by the villagers in their daily diet. Hence intake of contaminated rice is one of the pathways through which tritium can enter into human body. In view of its long retention period in plant, OBT is the major dose contributor through ingestion pathway of dietary items. Our environmental monitoring program could not assess any tritium activity in rice samples. Maximum possible OBT concentration in rice is calculated in the hypothetical case of exposure of rice plant to tritiated air and irrigation with tritiated water. Mean air concentration of tritium at Hartuga and mean water concentration of tritium in Kadra reservoir near Hartuga were used for the calculation of dose. Following empirical equation is used for the estimation of OBT concentration in rice.

$$C_{OBT} = [C_{iw} R_{pw} + C_{a,m} R_{pa})*W_C * R_{OH}] \quad (1)$$

where C_{OBT} is the concentration of OBT in rice ($Bq.kg^{-1}$), $C_{a,m}$ is the average concentration of HTO in air moisture ($Bq.l^{-1}$). R_{pa} represents the Transfer Factor which describes the activity transfer from air to plant. R_{pw} is the transfer factor which describes the transfer of HTO to plant from irrigation water. W_c is the Water content of vegetation ($l.kg^{-1}$), R_{OH} is the transfer factor representing the Transfer from HTO to OBT.

3. Estimation of Site Specific Transfer Factors R_{pa} and R_{pw}

Various types of plant growing near reactor premises were used for the estimation. Spot air samples taken twice in a week and leaf samples of the plants taken once in a week were analyzed for air moisture tritium activity and plant moisture tritium activity respectively. R_{pa} was calculated by the following equation

$$R_{Pa} = \frac{\text{Av. HTO Conc. in plant water}}{\text{Av. HTO Conc. in air moisture}} \quad (2)$$

The site specific value of R_{pa} was found to be within the range of 0.3-1.8 with a mean of 0.9.

Mango plants in pots were irrigated with tritiated water of known concentration. Plants were allowed to grow in well ventilated area and soil was covered with plastic bag so that air borne tritium will not influence the uptake. Tritium concentration in leaf water and soil water were estimated. R_{PW} was calculated using following equation

$$R_{PW} = \frac{\text{Av. HTO Conc. plant water}}{\text{Av. HTO Conc. in irrigation water}} \quad (3)$$

R_{pw} values varied from 0.1 to 0.5 with a mean of 0.3 during the experiment.

4. Estimation of R_{OH}

Experiments are planned at Kaiga to estimate the site specific values of R_{OH} . However for this paper, we have used the literature value of 1.6 ± 0.5[4].

5. Dose Evaluation

The Annual dose from inhalation pathway $(Da)_{inh}$ is calculated using the following equation

$$(Da)_{inh} = 1.5(C_{a,m} * \rho * BR * (DCF)_{HTO} \quad (4)$$

where BR is the breathing rate in $m^3.a^{-1}$ and ρ is the moisture content of air in $l.m^{-3}$. $(DCF)_{HTO}$ is the dose conversion factor for HTO. Multiplication factor of 1.5 is to account the contribution through skin absorption[5] .

The Annual dose from water intake pathway $(Dw)_{ing}$ is calculated using the following equation.

$$((Dw)_{ing} = Cw * Iw * (DCF)_{HTO} \quad (5)$$

where Cw is the concentration of Tritium in water ($Bq.l^{-1}$) and Iw is the water intake rate ($l.a^{-1}$).

The hypothetical dose to the members of the public due to consumption of contaminated food $(D_R)_{ing}$ is calculated using the following equation

$$(D_R)_{ing} = (C_{iw}R_{pw} + C_{a,m}R_{pa})*W_C*R_{OH}*I_R*(DCF)_{OBT} \quad (6)$$

Table 2 Parameter distribution assignments

Symbol	Parameter (Units)	Distribution type	Mean	Standard Deviation	
Ca,m	Conc. in Atm. Moisture ($Bq.l^{-1}$)	LN	68.5	74	
ρ	Mean Absolute humidity ($l.m^{-3}$)	N	0.02	0.005	
BR[5)]	Breathing Rate ($m^3.a^{-1}$)	N	13000	1560	
$(DCF)_{HTO}$	Dose Conversion Factor, HTO ($Sv.Bq^{-1}.a^{-1}$)		1.8E-11[10)]		
$(DCF)_{OBT}$	Dose Conversion Factor, OBT ($Sv.Bq^{-1}.a^{-1}$)		4.2E-11[10)]		
Cw	Conc. in drinking water ($Bq.l^{-1}$)	LN	23.8	29.3	
Iw	Water Intake Rate ($l.a^{-1}$)	N	906	58	
C_{IW}	Conc. in irrigation water ($Bq.l^{-1}$)	LN	23.8	29.3	
R_{OH}	Ratio OBT to HTO in plant	N	1.6	0.5	
I_R	Intake rate of rice ($kg.a^{-1}$)	N	249	42	
			Mean	Min	Max
R_{pa}	Ratio Plant to air HTO	T	0.9	0.3	1.8
R_{pw}	Ratio plant to water HTO	T	0.3	0.1	0.5
W_C	Water content in vegetation ($l.kg^{-1}$)	T	0.0798	0.06	0.14

Distributions: LN- Log Normal, N - Normal , T- Triangular

Table 3 Dose computation

Pathway	Computed Dose ($\mu Sv.a^{-1}$)			
	Mean	Standard deviation	95% Confidence Level	
			Lower Confidence Limit	Upper Confidence Limit
Inhalation and skin absorption	0.3	1.2	0.2	0.4
Drinking water	0.2	1.3	0.1	0.4
Ingestion of contaminated food (Hypothetical)	0.02	1.5	0.007	0.04
External –^{41}Ar and FPNG	0.6	2.3	0.1	3.0
Total Dose	1.1	2.3	0.2	5.8

Annual External dose from ^{41}Ar and FPNG were calculated by the following equation[6)].

$$D_{ext}\,(Sv) = \Psi * WDE / 3600 \quad (7)$$

where Ψ is the annual ground level time integrated concentration ($Bq\text{-}s.m^{-3}$) and WDE ($Sv.h^{-1}$ per $Bq.m^{-3}$) is the Weighted Dose Equivalent from a semi-infinite cloud to total body per unit air concentration, 3600 is the number of seconds per hour. Ψ is obtained from sector averaged χ/Q values and total Release. WDE values for ^{41}Ar and FPNG were taken from Reference 6.

From the above equations, it is clear that the variability in the calculated dose depends upon the variability in the input parameters mentioned in the equation. The variability in the input parameters arises due to uncertainty in estimation of each parameter. Suitable distributions were attributed to take into account these variabilities. A quantitative uncertainty analysis was performed with the measured data using 'parameter uncertainty analysis'[7)]. The uncertainty in the estimation of dose can be calculated from an estimate of uncertainty in each of the parameters used in the dose assessment equations. The parameters used for the dose evaluation, with respective assigned distribution, are described in **Table 2**. The estimated dose distribution from all the pathways and for all the major radio nuclides during the year 2006 is lognormal and ranges from 0.2–5.8$\mu Sv.a^{-1}$ (at 95% Confidence) with a mean value of 1.1 μSv **(Table 3)**. As per the statistical principle, if the 95% upper confidence limit is below the standard, it is likely that the standard will not be violated[7)]. The upper limit of 95% confidence level annual dose is very much lower than the internationally accepted regulatory limit[8)] of 1000 $\mu Sv.a^{-1}$

6. Build up of Environmental Radioactivity

Soil and sediment samples collected from Hartuga were analyzed for ^{137}Cs to estimate any build up of activity over the pre-operational values. The Pre –operational ^{137}Cs activity in soil sample ranged from 2.2-34.6 $Bq.(Kg\ dry\ wt)^{-1}$ with a geometric mean of 9.1 $Bq.(Kg\ dry\ wt)^{-1}$ while

operational value ranged from Below Detection Limit to 23.4 Bq.(Kg dry wt)$^{-1}$ with a geometric mean of 5.1 Bq.(Kg dry wt)$^{-1}$. The Pre –operational ^{137}Cs activity in sediment sample ranged from 1.2-5.9 Bq.(Kg dry wt)$^{-1}$ with a geometric mean of 2.6, while operational values ranged from Below Detection Limit to 5.4 with a geometric mean of 1.3. Statistical analysis (t test) of ^{137}Cs concentration in soil and sediment samples obtained during various years including preoperational and operational phases indicated that there is no statistically significant build up of ^{137}Cs in the environment as compared to pre-operational values[9].

IV. Conclusions

The rigorous statistical analysis of the dose data clearly indicate the estimated dose from all the pathways and for all the major radio nuclides during the year 2006 ranges from 0.2 – 5.8 μSv.a^{-1} (at 95% Confidence) with a mean value of 1.1 μSv.a^{-1}, which is much less compared to the internationally acceptable limits to the member of the public. Statistical analysis (t test) of ^{137}Cs concentration in soil and sediment samples obtained during various years including operational and preoperational phase indicated that there is no statistically significant build up of ^{137}Cs in the environment as compared to pre-operational value ($p<0.001$).

Acknowledgement

The authors would like to thank Mr. G. Nageswara Rao, Executive Director(O), NPCIL, Mr. Harsh Kapoor, Site Director, Kaiga 1-4, Mr. K. Ramamurthy, Station Director, Kaiga 3&4 and Mr. V.V. Sanathkumar, Station Director, Kaiga 1&2 for their support and encouragement. Authors thank all staff of ESL, KGS for their valuable suggestions and discussions.

References

1) Annual Report for 2001 on Off-site Environmental and Micro meteorological Studies at Kaiga Site BARC/2002/I/01,Bhabha Atomic Research Centre, Mumbai, India (2002).
2) Environmental Radiological Laboratory Procedure Manual, Health Physics Division, Bhabha Atomic Research Centre, Mumbai, India (1998).
3) S.Diabate and S.Strack, Organically Bound Tritium, Health Physics ***65***,(6), (1993) pp 698-712
4) F. Pointurier, N.Baglan, G.Alanic, A method for the determination of low level OBT activities in environmental samples. Applied Radiation and Isotopes, ***61***(2004) pp 293-298.
5) D.M.Hamby, A Probabilistic Estimation of Atmospheric Tritium Dose, Health Physics ***65***,(1), (1993) pp 33-40.
6) Manual of dose evaluation from atmospheric releases, B.A.R.C.-1412, Bhabha Atomic Research Centre, Mumbai, India (1988).
7) J.S.Hammonds, F.O.Hoffman, S.M.Bartel An introductory guide to uncertainty analysis in environmental and health risk assessment, ES/ER/TM-35/R1 (1994).
8) International Commission on Radiological Protection, 1990 Recommendations of the International Commission On Radiological Protection, Publication No.60, Pergamon Press, Oxford and New York(1991).
9) Report on the Pre-operational Environmental Radiological and Micrometeorological Studies around Kaiga Atomic Power Project Site, BARC/1999/E/023, Bhabha Atomic Research Centre, Mumbai, India (1999).
10) International Commission on Radiological Protection, Dose Coefficients for Intakes of Radio nuclides by Workers, Pub No.68, Elsevier Science, Oxford (1994).

Journal of NUCLEAR SCIENCE and TECHNOLOGY, Supplement 5, p. 639–642 (June 2008)

Seasonal Variation in Radon Concentration in the Atmosphere Simultaneously Measured in Donghae on Korean Peninsula, Matsue on Shimane Peninsula, and Oki Island in the Sea of Japan

Katsuhiro YOSHIOKA[1*], and Takao IIDA[2], and Yoon Shin KIM[3]

[1]*Shimane Prefecture Institute of Public Health & Environmental Science*
[2]*Nagoya University Graduate School/School of Engineering*
[3]*Hanyang University/Department of Occupational & Environmental Medicine*

We measured simultaneously radon concentration in the atmosphere at Donghae, Oki Island and Matsue. In Donghae, radon concentration had peaks in the winter and summer and lower values in the spring. It was the highest in the winter and lowest in the summer in Oki Island, in Matsue, the highest in the fall and lowest in the summer. The timing and frequency of arrival air mass from the ocean and the land were different among the three measuring points. The highest values in Donghae and Oki Island were because of effects of radon flow from Eurasian continent in the winter. The inversion layer often formed in the atmospheric boundary layer over the land area around the Sea of Japan caused the peak values in the summer in Donghae. The atmosphere over Oki Island is always mixed with that over the ocean because the island is small. Radon escaping from the ground of the island does not stay with the surface layer even at night; therefore, diurnal variation was almost none throughout the year. Air mass with low radon concentration coming from the Pacific Ocean caused the lowest values in the summer. In Matsue, the peak was found in the fall in which occurrences of surface inversion layer is most common in the year.

Keywords: radon, seasonal variation, diurnal variation, backward trajectory, Donghae, Oki Island, Matsue, Korean Peninsula, Shimane Peninsula, Sea of Japan, continental air mass, maritime air mass

I. Introduction

Radon-222 (radon hereafter), a decay product from radium-226, is a chemically inactive radioactive gas nuclide with 3.823 days of half-life. Because radon cannot be washed away by rainfalls and is chemically stable during transportation, it has been used as a tracer of continental air mass in the long distance transportation process.[1)] Radon concentration in the maritime air is much lower than that in the air over the land because the radium concentration in the sea water is less than 0.01% of that in the earth's crust.[2)] It is well known that radon concentration shows diurnal and seasonal variations with large amplitude.[3)]

We measured radon concentration in the atmosphere simultaneously at three sites around the Sea of Japan. Because the Sea of Japan was low radon exhalation rate, we expected that synchronized temporal variations between the results in Donghae and Oki Island, which would be characterized by air mass coming from the Eurasian continent. Geographical conditions cause difference of amplitude and periodicity in the temporal variation, between a remote island in the Ocean and the inland. In this study, we discussed on the simultaneous results focusing on radon transported from distant regions and radon originated near the measuring sites. Areas located on the eastern extremity of the Eurasian continent and surrounding the Sea of Japan have wide-area pollution problem, such as "yellow sand" and acid rain, *etc*. This study can provide useful knowledge to solve diffusing air pollutants due to the long range transportation by finding out the cause of variation in radon concentration in the atmosphere.

II. Locations of Measurements and Sensor to Measure Radon Concentration

1. Locations of Measurements

Fig. 1 shows three locations to make the simultaneous measurements. The sample air was continuously taken at the heights of 15, 30 and 20 m at Donghae on the east coast of Korean peninsula (37.30 N, 129.08 E, 50 m from the sea shore), Matsue on Shimane peninsula (35.27 N, 133.04 E, 8 km from the sea shore), and Oki Island in the Sea of Japan (36.15 N, 133.15 E, top of the mountain with altitude of 580m), respectively. Distance between Donghae and other two places is about 400 km and that between Oki Island and Matsue is 70 km. Data were recorded from October 1999 to September 2000 in Donghae and from January 1999 to December 2000 in Oki Island and Matsue.

2. Sensor to Measure Radon Concentration in the Air

Radon concentration was continuously measured by an electrostatic radon sensor. We continuously counted the number of alpha particles from radon's decay products, Po-218 and -214, in the sucked air. Continuous hourly values of radon concentration were calculated from the counts. This sensor is described in detail in the paper of the developer, Iida.[4)]

*Corresponding Author, Tel No: +81-852-36-8186, Fax No:+81-852-36-8171, E-Mail: yosiokaf@f8.dion.ne.jp

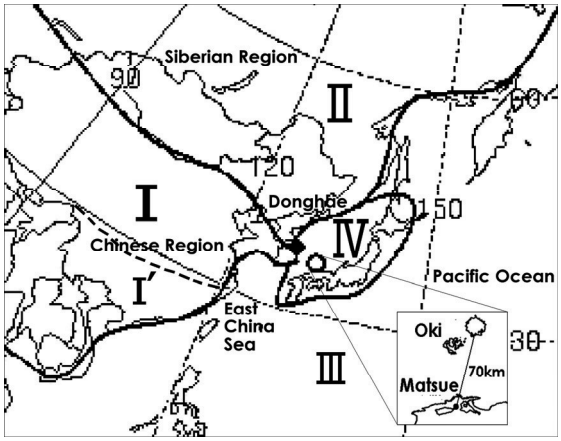

Fig. 1 Locations of radon measurement sites and classification diagram of backward trajectory at Donghae in Korean Peninsula, Oki Island in the Sea of Japan and Matsue in Shimane Peninsula.

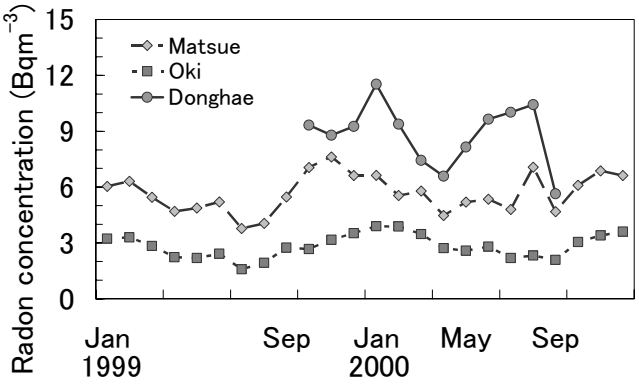

Fig. 2 Seasonal variations of monthly averages of radon concentration from JAN 1999 to DEC 2000 at Donghae, Oki Island and Matsue.

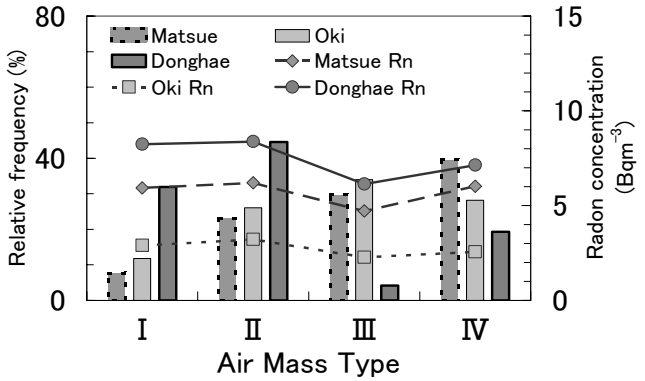

Fig. 3 Distributions of frequencies of air mass types and average values of radon concentration due to air mass types.

III. Comparison of Time Variations of Radon Concentration in the Atmosphere

1. Long Term Variations in Radon Concentration at the Three Locations

Fig. 2 shows monthly averages of radon concentration from January 1999 to December 2000. The maximum values were 11.5 Bqm^{-3}, 3.9 Bqm^{-3}, and 7.6 Bqm^{-3} at Donghae, Oki Island, and Matsue, respectively. Clear seasonal pattern, high in the winter and low in the summer, was found in Oki Island, in Matsue, it was high in the fall and low in the summer. In Donghae, two peaks were found, one in the winter and another in the summer, while it was low in the spring. The highest value was about twice of the lowest value. We think the high concentration was observed in Donghae because the bedrock consists of granite and it is near the Eurasian continent.[5)]

Differences in radon concentration among three locations were strongly affected by radium concentration in the earth's crust and geographical conditions, i.e. distribution of the land and the sea. We supposed that the concentration depended on the mixing ratio of air from the ocean and the inland. Therefore, we will discuss on the effects of radon transported from the distant Eurasian continent and radon originated from the measurement region, which depends on changes in vertical convection.

2. Estimating Effects of Radon Transported from Distant Locations

To discuss effects of radon transported from distant locations on the seasonal variations at three locations, we calculated backward trajectory paths of arriving air mass at 00 UTC and 12 daily.[6-7)] The backward trajectory paths were grouped according to the zones in **Fig. 1**, and the frequency distribution was discussed. According to the geography, the entire area was divided into the Eurasian continent, next into China and Siberia, the Pacific Ocean, and the Sea of Japan (including the Japanese Islands). Matsue and Oki Island were considered to be in the same area as Donghae (**Fig. 1**). Frequency distribution of the arriving air mass and average radon concentration due to each air mass type are shown in **Fig. 3**. In Oki Island and Matsue, no difference was found in the frequency distribution. On the other hand, in Donghae, the distribution was different from other places. In Donghae, fewer arrivals of type III air mass (maritime) and type IV air mass (from the Sea of Japan and the Japanese Islands) than those from the continent were observed.

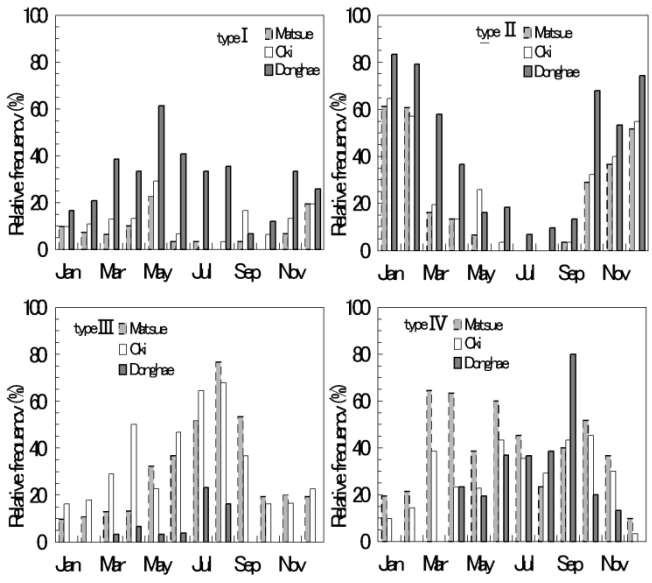

Fig. 4 Seasonal variations of frequencies of air mass types at Donghae, Matsue and Oki Island.

Patterns of radon concentration in each air mass type were the same at three locations: low concentration at the arrivals of types III and IV air mass and high for types I and II. It has been reported that radon concentration is generally high on the land than on the sea.[2, 8-10] Because mixing of the air mass originated from the land and the ocean depends on the geographical location of the measurement points, we think it is reasonable to assume that radon concentration become high when air mass arrives from the continent.

Next, we discussed the seasonal variation of the air mass type and radon concentration at the three locations**. Fig. 4** shows the seasonal variation of the different types at each location. The seasonal variation observed in Donghae was clearly different from those in Oki Island and Matsue for all air mass types. In Donghae, types I and II of continental air mass arrived throughout the year. Among arriving air mass, type I air mass was more than 30 % from March to August (spring and summer), about 30% in November and December, and about 20% in January and February (winter), while it was low 10% in September and October. Type II air mass was high of 40- 80% in January to April, October to December and about 5-20 % in May to September. Type III air mass (maritime) was about 20% in July and August and less than 10 % from March to June, and type IV air mass (maritime) was 40 - 80 % from July to September and 15 - 20 % in April and May and in October and November. On the other hand, in Oki Island and Matsue, types III and IV arrived dominantly, and type II air mass arrived in the same pattern as Donghae except in the summer. Arrivals of type I air mass were low and its maximum was 30% in May. Type III air mass arrived at 25 - 75 % from April to September and about 20% in the rest of the year. Type IV air mass was 20 - 65% from March to October and 10 - 20% in the winter.

Comparing the seasonal variation of air mass arrival frequency and that of radon concentration, the peak values of radon concentration in Oki Island and Matsue were observed in the winter when air mass from the continent was dominant, and the concentration was low because of air mass originated from the ocean is dominant in the summer. This is the same result as Yoshioka, *et al*.[11], and they explains that the peak concentration was shifted to the fall due to the influence of the surface inversion layer in Matsue.

The peak value of radon concentration in the winter of Donghae was influenced the frequencies of land air mass. But in the summer, there was no obvious synchronization between radon concentration and the frequency distribution of arriving air mass, the peak seemed not to be result from the air mass with radon originated in the distant places. The minimum value was observed in the spring when types I and II air mass arrived from the continent frequently, while a few frequencies of type IV arrived in April and May. But among type I air mass arriving at Donghae, almost none comes from southern China (I' area) where radium in the crust and radon in the air are high concentration. This could be one of the reasons of the low radon concentration in Donghae.

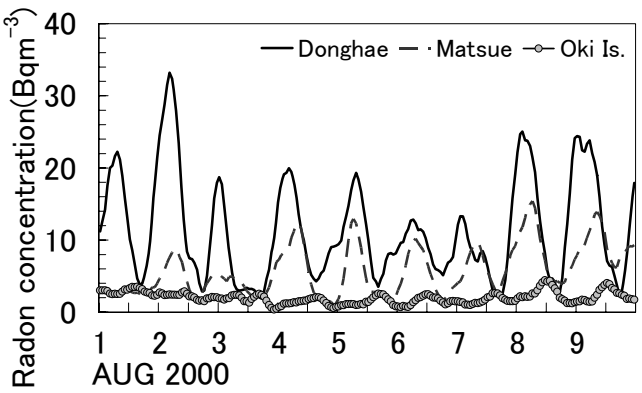

Fig. 5 Time variations of hourly data of radon concentration at Donghae, Matsue and Oki Island in AUG. 2000

3. Determining Factors to Influence the High Level of Radon Concentration observed in the Summer

It is obvious that the transported air mass from distant locations, a phenomenon in which radon stays in the surface boundary layer and by mixing with upper atmosphere with lower radon concentration as the factors to affect radon concentration in the atmosphere.[12] **Fig. 5** shows the time variations in radon concentration in Donghae, Matsue, and Oki Island in August, 2000. On the land in Matsue and Donghae, radon concentration increased in the night and decreased in the daytime and showed a typical diurnal pattern as the time change of convection intensity in the boundary layer. In Oki Island, radon concentration is low due to mixing with low radon air from the ocean and radon production is small because the land area is small. And then, the peak values were always low and no large cyclic pattern could be found. Radon concentration in Matsue decreased to the level near that in Oki Island during the daytime. Even during the daytime, the daily minima in Donghae were often higher than those in Oki Island. We can estimate the background level in Donghae higher than that in Matsue because the vertical profile of radon concentration becomes uniform during the daytime.

Fig. 6 shows the diurnal variations in every season in each location. Amplitude of diurnal variation in Donghae was 10.2 Bqm^{-3} (max) in the summer, 4.2 Bqm^{-3} (min) in the winter, and similar values, 5.4 Bqm^{-3} and 5.0 Bqm^{-3}, in the spring and fall, respectively. In Matsue, the maximum amplitude of 6.7 Bqm^{-3} was found in the fall, and the minimum was 4.1 Bqm^{-3} in the winter. In Donghae, the inversion layer at night increase the radon concentration, so that the daily maximum value was found in the summer and the minimum values were about the same in the spring, summer, and fall. The daily minimum in Donghae in the winter was high, 7.1 Bqm^{-3}. Radon concentration in the upper atmosphere can be high in Donghae because the concentration is high during the daytime in which formation of convective layer is most active. This is one of the reasons for the high radon concentration in the winter.

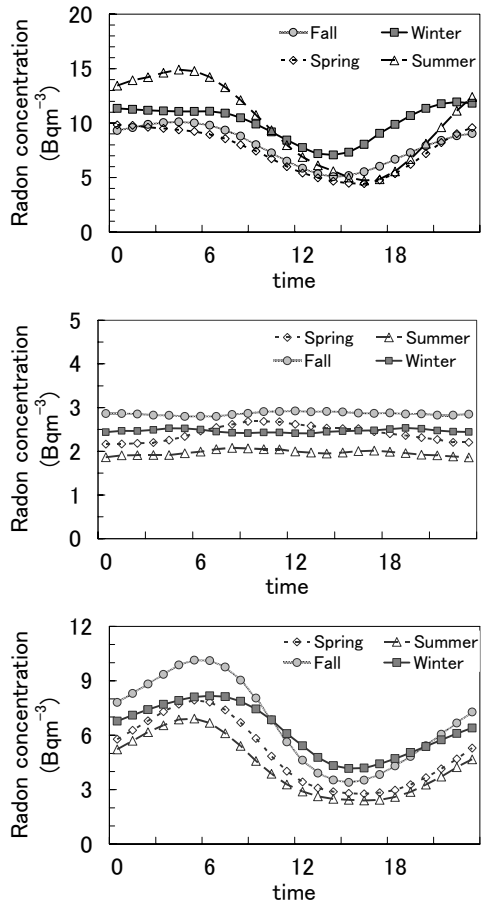

Fig. 6 Diurnal variations of radon concentration at Donghae (upper part), Oki Island (middle part) and Matsue (lower part).

IV. Conclusions

We measured radon concentration in the atmosphere simultaneously in Donghae on Korean Peninsula, Matsue on Shimane Peninsula, and Oki Island in the Sea of Japan and comparatively discussed the temporal variations. Radon concentrations at three locations were largely different. In Donghae, monthly, daily, and hourly averages ranged between 5.6 and 11.5 Bqm^{-3}, between 2.5 and 20.8 Bqm^{-3}, and between 0.8 and 37.7 Bqm^{-3}, respectively. In Matsue, these averages ranged between 3.8 and 7.6 Bqm^{-3}, between 1.5 and 14.5 Bqm^{-3}, and between 0.2 and 23.1 Bqm^{-3}, respectively. In Oki Island, these averages ranged between 1.6 and 3.9 Bqm^{-3}, between 0.7 and 6.0 Bqm^{-3}, and between 0.1 and 8.8 Bqm^{-3}, respectively.

In Donghae, radon concentration showed a unique seasonal pattern, having two peaks: one in the summer and another in the winter. The peaks were caused by the influence of transported radon from the Eurasian continent in the winter and of radon staying at the surface due to the changes in vertical convection in the boundary layer in the summer. The pattern was significantly different from those in Matsue, showing high values in the fall and low values in the summer, and in Oki Island, showing highs in the winter and lows in the summer. Amplitude of diurnal radon concentration was largest in the summer at 10.2 Bqm^{-3} and lowest in the winter at 4.2 Bqm^{-3} in Donghae. They were 6.7 Bqm^{-3} in the fall and 4.1 Bqm^{-3} in the winter in Matsue. In Oki Island, the amplitude was small throughout the year and 0.5 Bqm^{-3} observed in the spring was the largest.

References

1) I.Uno, G.R.Carmichael, D.G.Streets, Y.Tang, J.J.Yienger, S.Satake, Z.Wang, Jung-Hun Woo, S.Guttikunda, M.Uematsu, K.Matsumoto, H.Tanimoto, K.Yoshioka and T.Iida; "Regional chemical weather forecasting system CFORS: Model descriptions and analysis of surface observations at Japanese island stations during the ACE-Asia experiment", J.Geophys. Res., 108(D23), 8668, doi:10.1029/2002JD002845, 2003.
2) S.D.Schery; "Progress on Global 222Rn Flux Maps and Recommendations for Future Research", 1st International expert meeting on sources and measurements of natural radionuclides applied to climate and air quality studies, 3-5 JUN., 2003.
3) T.Hattori and T.Ichiji; "Estimates of seasonal variations of 222Rn from different origins by using the correlation between 222Rn and 212Pb concentrations in air", Proceedings of the 7th Tohwa University International Symposium: Radon and Thorn in the Human Environment, 259-264, 1997.
4) T.Iida; "An Electrostatic Radon Monitor for the Continuous Measurement of Environmental Radon", ATMOSPHERIC RADON FAMILIES AND ENVIRONMENTAL RADIOACTIVITY, 65-73, 1985 [in Japanese].
5) H.K.Je, C.Kang, H.T.Chon; "A Preliminary Study on Soil-Gas Radon Geochemistry According to Different Bedrock Geology in Korea", Environ. Geochem. Health, 21(2), 117-131, 1999
6) R.R.Draxler and G.D.Rolph; HYSPLIT (HYbrid Single-Particle Lagrangian Integrated Trajectory) Model access via NOAA ARL READY Website (http://www.arl.noaa.gov/ready/hysplit4.html). NOAA Air Resources Laboratory, Silver Spring, MD., 2003.
7) G.D.Rolph; Real-time Environmental Applications and Display system (READY) Website (http://www.arl.noaa.gov/ready/hysplit4.html). NOAA Air Resources Laboratory, Silver Spring, MD., 2003.
8) J.Moriizumi et al.; "The Temporal Variation in Atmospheric Radon-222 Concentrations in West Siberian Forest: High Concentrations in Snow Covered Season", SEVENTH INTERNATIONAL WORKSHOP on GEOLOGICAL ASPECTS of RADON RISK MAPPING, 2004.
9) J.Cheng, Q.Guo and T.Ren; "Radon Levels in China", J.Nucl.Sci.Tecnol., 39 (6), 695-699, 2002.
10) Y.S.Kim and T.Iida; "Airborne radon concentrations in different environments in Korea", Proceedings of the 7th Tohwa University International Symposium: Radon and Thorn in the Human Environment, 228-239, 1997.
11) K.Yoshioka, T.Iida; "Major Factors Influencing Long-Term Periodic Variation of the Radon Concentration in the Atmosphere: A Comparative Study between the Ocean and Land Conditions", Hoken Butsuri, 42(1), 53-62, 2007 [in Japanese]
12) K.Yoshioka and T.Iida; "The Diurnal Change in the Vertical Distribution of Atmospheric 222Rn due to Growth and Rise of the Stable Stratification Height in the Atmospheric Boundary Layer", Radioactivity in the Environment, 7, 489-496, 2004.

Journal of NUCLEAR SCIENCE and TECHNOLOGY, Supplement 5, p. 643–646 (June 2008)

Effects of Time Passage and Distance on Distribution of Carbon-14 among Parts of Rice during Growth Period at Korean CANDU Plant

Wook SOHN*, Jun-Hwa CHI, Duck-Won KANG, Gab-Bock LEE, and Woo Tae JEONG

Nuclear Power Laboratory, Korea Electric Power Research Institute, Daejeon, Korea

The pattern of carbon-14 (C-14) distribution among parts of rice growing in the vicinity of the Korean CANDU plant during the growth period was investigated. Six-time samplings of rice and air were performed in seven fields from rice planting to harvest, and the measurements of C-14 content were made by using liquid scintillation counter on the air and each of available parts of the rice such as root, stem, crust and ear. The results illustrated that C-14 showed a relatively even distribution among parts of rice during the growth period implying C-14 accumulation was more dependent on interactions among the parts such as transportation of nutrients than on photosynthesis occurring only in stem that has chlorophyll. Also it was observed that the difference of C-14 concentration between each part of rice and the air decreased with time indicating that the time was needed for C-14 to reach equilibrium between both sides. The radius within which C-14 released from the Wolsong plant could have a significant effect on the C-14 concentrations of the parts was observed to be about 5 km.

KEYWORDS: CANDU, radioactive isotope, carbon-14, distribution, rice, growth period

I. Introduction

Carbon-14 (C-14), a radioactive isotope of carbon, decays to nitrogen-14 by emitting only low energy β-ray (average energy of 49.5 keV), which makes health physicists regard it as an insignificant source of external exposure. On the contrary, C-14 is considered to be one of the most significant sources of internal exposure at nuclear power plants, because C-14 has a relatively long half-life (5730 years) and can be readily absorbed into human body through intake of vegetables where C-14 is assimilated via photosynthesis. [1)]

Generally, the bulk of production of C-14 at nuclear power plants is accounted for by the neutron capture reaction of oxygen-17 ($^{17}O(n, \alpha)^{14}C$) of water present in the primary side of the nuclear power plant. So C-14 can be produced in any type of reactor provided the reactor uses water under neutron flux. However, since the concentration of oxygen-17 of heavy water (0.058%) which CANDU reactors use as both moderator and coolant is higher than that of light water (0.037%) which other reactors use as coolant, CANDU plants experience higher rates of C-14 production and release to the environment than any other type of reactor plant, especially pressurized water reactor one. [2- 4)]

For this reason, the utilities of CANDU plants are required to assess the environmental radioactivity monitoring for C-14 around the plants by their regulators. Currently, the assessments are carried out by determining C-14 contents in some selected crops including rice.[1)] However, since the assessments are generally made on those crops that are sampled at harvest time, the C-14 distribution among parts of the crop during its growth period remains to be examined. Thus, this study aims at investigating such C-14 distribution for rice which was raised near Korean CANDU plant where four CANDU reactors are in operation. Also, the effect of distance from the plant on the C-14 distribution among parts of rice was investigated.

II. Experimental

The locations of the six rice fields in the vicinity of Korean CNADU plant (Wolsong Nuclear Power Plant) that were chosen for sampling in this study are shown in **Fig. 1**. In addition to these sampling fields, another rice field whose distance from the plant is long enough not to be affected by C-14 released from the plant was chosen as a reference field (not shown in **Fig. 1**). The summary of these rice fields is given in **Table 1**. For each rice field, six-time samplings were made during the growth period, i.e., from rice planting to harvest (June 9, July 7, August 11, September 9, September 25 and October 6, 2000).

The sampled rice was divided into parts such as root, stem (including leaf), crust and ear, and then each part was dried naturally in the shade that was well ventilated. Each dried part was pulverized and the resultant powder was burned in order to obtain CO_2 gas from it by using a high pressure combustion system (B.J. Precision Eng. Co., Model: 400). The produced CO_2 gas was then fed to a bottle containg 3M NaOH solution where almost CO_2 gas was converted into CO_3^{2-} ion due to high pH of >12 (**Eq. 1**). The carbon being present in the form of CO_3^{2-} was collected as a precipitate of $BaCO_3$ by pouring an excess amount of a 1N $BaCl_2$ solution into the NaOH solution (**Eq. 2**). The precipitated $BaCO_3$ was filtered and then dried in an oven. The dried $BaCO_3$ was made as powder by pulverization.

*Corresponding Author, Tel No: +82-42-865-5543, Fax No: +82-42-865-5504, E-mail: wsohn@kepri.re.kr

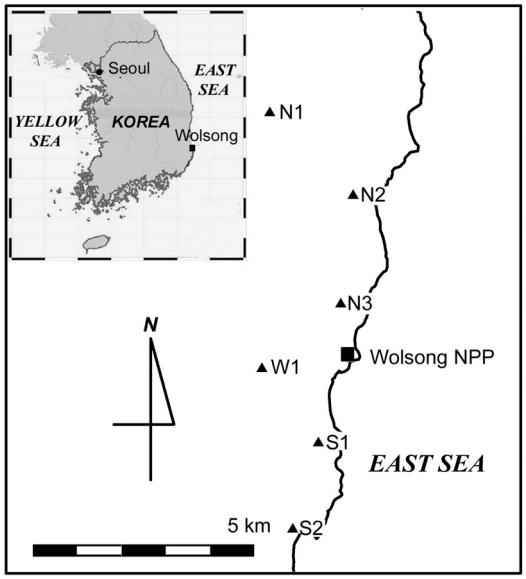

Fig. 1 Locations of the rice fields sampled in this study

$$CO_2(g) + 2NaOH \rightarrow NaCO_3 + H_2O \quad (1)$$

$$Na_2CO_3 + BaCl_2 \rightarrow BaCO_3(\downarrow) + 2NaCl \quad (2)$$

Table 1 Summary of the rice filed sample in this study

Location	Field Code	Distance from the site (km)	Notes
Bonggil-2	N3	1.300	Sampling
Nasan	W1	1.725	″
Eupchen	S1	1.875	″
Bonggil-1	N2	3.600	″
Haseo	S2	3.700	″
Yongdand-2	N1	5.675	″
Bakhyeon	R1	112.237	Reference

The C-14 concentration in the collected $BaCO_3$ powder was determined by using a CO_2 adsorption apparatus shown in **Fig. 2**. The powder was placed at the bottom of the flask, which was purged with nitrogen gas for a while in order to expel CO_2 present inside it. Then the teflon bottle connected at outlet of the silica gel moisture trap was filled with a 20 mL scintillator which was a mixture solution of 10 mL Carbon-sorb® and 10 mL Permafluor-V®. The CO_2 gas that was produced when introducing acid to the flask was trapped on the scintillator. About 2 g of CO_2 was obtained for each collected $BaCO_3$ powder on the scintillator, which was analyzed for C-14 content using a liquid scintillation counter (Wallac, Model: Wallac Quantulus 1220).

The air in each rice field was sampled only at only the last four sampling points by using a passive air sampler consisting of a tray covered with a stainless screen mesh, a rain shield and four legs (**Fig. 3**). The CO_2 in air was collected in a 2M NaOH solution (600 mL) contained in the tray. The subsequent procedure for analyzing C-14 content in the sampled air was the same as for rice samples.

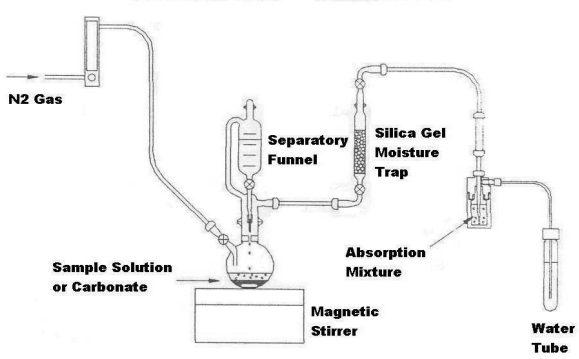

Fig. 2 Schematic of apparatus of Adsorption Counting Method

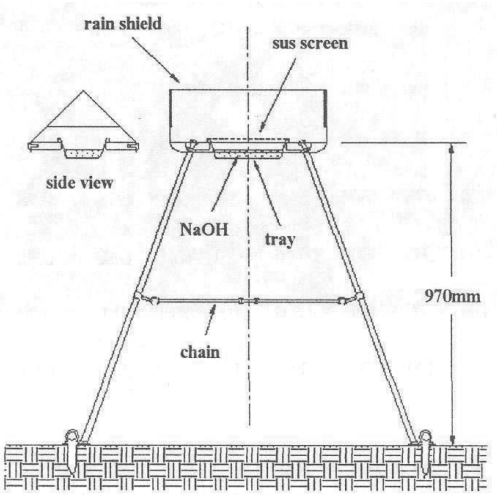

Fig. 3 Schematic of passive air sampler

III. Results & Discussions

Table 2 shows the results of measurements for C-14 contents of the parts of rice and of the air sampled at each rice field. It should be noted that prior to 4th sampling point, collection and thus measurement were possible only for root and stem. Note also that some of the data are missing because of the corresponding measurement failure.

G.M. Milton et al.[5] reported the value of the global background C-14 to be 0.248 Bq/gC. The C-14 levels of the air in all of the fields were measured to be higher than the global value: 0.413 Bq/gC for N3, 0.263 Bq/gC for W1, 0.421 Bq/gC for S1, 0.316 Bq/gC for N1, 0.301 Bq/gC for S2 and 0.270 Bq/gC for N1 Of course, these higher levels can be ascribed to the presence of nuclear power plant.

To investigate a pattern of C-14 distribution among the parts of rice sampled at each field during the growth period, percentages of C-14 contents in all of the parts available were calculated (**Fig. 4**). Note that there is a missing percentage for a specific part in bars such as 5th bar of S1 (ear), 2nd bar of S2 (stem) and 2nd bar of N1 (root) in **Fig. 4** because the corresponding original data in **Table 2** are not available.

Table 2 Results of measurements for C-14 in each part of rice and air sampled at each rice field (Bq/gC).

Code	Part	Sampling 1st	2nd	3rd	4th	5th	6th
N3	Root	0.384	0.962	0.454	0.505	0.374	0.519
	Stem	0.405	0.773	0.375	0.304	0.292	0.549
	Crust				0.321	0.339	0.330
	Ear				0.271	0.437	0.290
	Air				0.350	0.321	0.569
W1	Root	0.351	0.310	0.314	0.284	0.318	0.320
	Stem	0.282	1.231	0.467	0.333	0.299	0.354
	Crust				0.293	0.300	0.391
	Ear				0.343	0.511	0.315
	Air				0.236	0.289	*
S1	Root	0.382	0.333	0.271	0.273	0.297	0.346
	Stem	0.267	0.829	0.362	0.631	0.233	0.322
	Crust				0.281	0.339	0.388
	Ear				0.286	*	0.373
	Air				0.389	0.453	0.453
N2	Root	0.421	0.398	0.535	0.356	0.324	0.476
	Stem	0.337	1.670	0.349	0.363	0.269	0.359
	Crust				0.298	0.312	0.310
	Ear				0.292	0.489	0.326
	Air				0.395	0.297	0.256
S2	Root	0.313	0.303	0.271	0.318	0.222	0.407
	Stem	0.275	*	0.268	0.281	0.277	0.304
	Crust				0.241	0.301	0.360
	Ear				0.266	0.427	0.313
	Air				0.296	0.339	0.268
N1	Root	0.304	*	0.372	0.370	0.333	0.335
	Stem	0.272	0.442	0.293	0.325	0.259	0.327
	Crust				0.275	0.352	0.327
	Ear				0.298	0.363	0.363
	Air				0.291	0.271	0.248
R1	Root	0.250	0.268	0.208	0.279	0.252	0.323
	Stem	0.265	0.467	0.262	0.349	0.253	0.314
	Crust				0.318	0.284	0.304
	Ear				0.291	0.370	0.298
	Air				0.268	0.319	0.255

* No data was obtained because of measurement failure.
** The value of the global background C-14 is 0.248 Bq/gC.

It can be seen from **Fig. 4** that C-14 shows a relatively even distribution among the parts considered throughout the growth period, in particular from 4th to 6th sampling points. This result suggests that the C-14 distribution depends more on interactions among the parts such as transportation of nutrients than on photosynthesis occurring only in stem that has chlorophyll (if photosynthesis was the most influential factor then the percentage of the stem should have been the biggest).

Fig. 5 illustrates the difference in C-14 concentration between each part of rice samples and air. The three kinds of marks in **Fig. 5**, a solid circle, a open circle and a open rectangular designate such differences for all the parts of rice sampled at 4th, 5th and 6th sampling point, respectively. The data for 1st, 2nd and 3rd sampling points are not included since air sampling started at the 4th sampling point. A horizontal line would occur when all the parts have an identical concentration of C-14. Thus, three horizontal lines of rice fields S2, N1 and R1 support the same result that was derived from **Fig. 4**: C-14 is distributed evenly among the parts. Also, the tendency is recognized in these fields that the difference decreases with time bringing about equilibrium between both sides at 6th sampling point (the difference is almost zero at this point). This can be explained by the time needed for the equilibrium to be established. Such tendency, on the other hand, cannot be observed in other fields, suggesting a potential existence of effects of other factors such as wind direction, topography and precipitation in these fields.

Finally, the effect of distance from the plant on C-14 concentration of each part of rice was investigated. **Fig. 6** shows such effect on stem. For stem, all of the 6-time samplings were made (note that a plot for the stem of 2nd sampling point at Field S2 is missing due to absence of the corresponding data in **Table 2**). Although it is not as expected, the effect of distance can be recognized as such: the shorter the distance the higher is the C-14 concentration. In addition, the effect of distance seems to work only within a 5km radius from the plant. The same result was observed in root that is not presented.

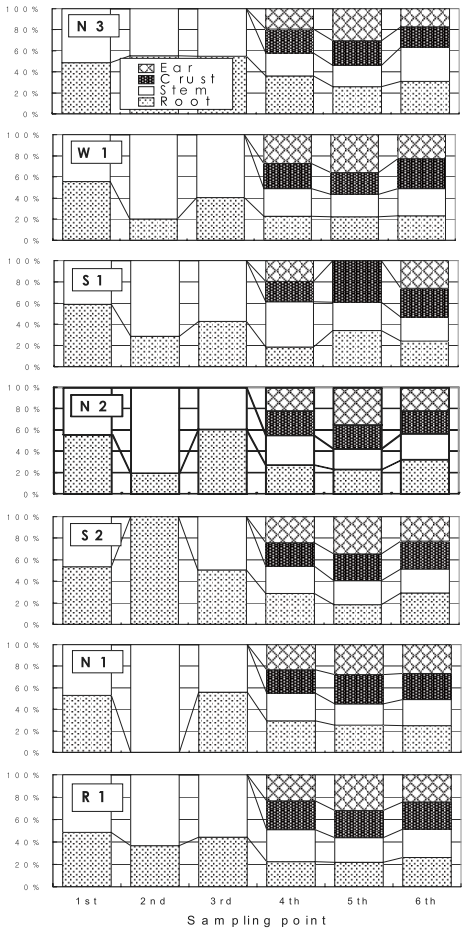

Fig. 4 Change of C-14 distribution among parts of rice with time

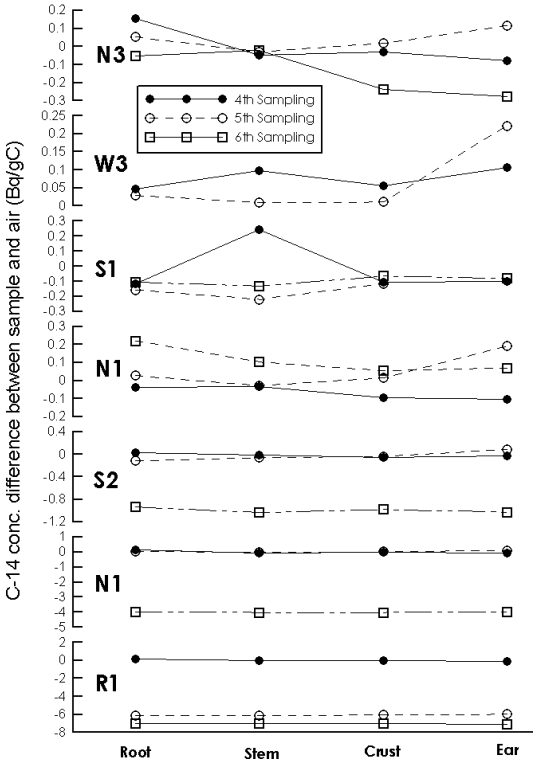

Fig. 5 The difference of C-14 concentration between each part of rice and air.

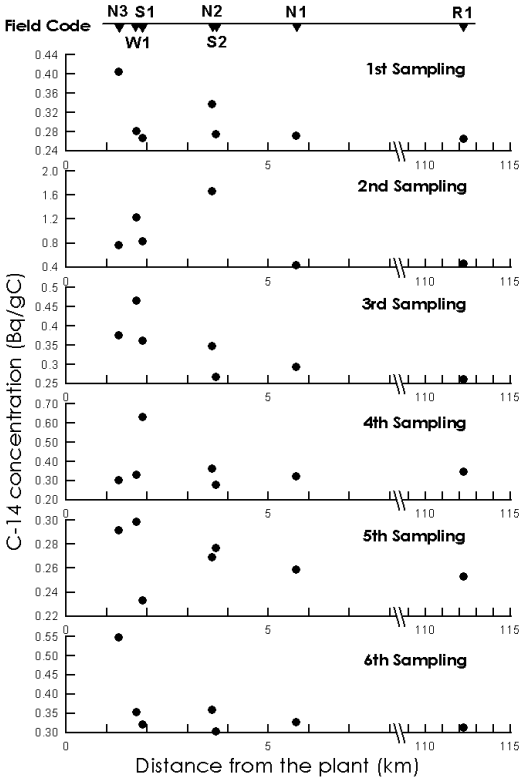

Fig. 6 Distance effect on C-14 concentration of stem.

IV. Concluding Remarks

To investigate the pattern of the C-14 distribution among parts of rice that was raised around Korean CANDU plant, six-time samplings of rice and air were made from rice planting to harvest in seven rice fields whose distances from the plant are different each other. The measurements of C-14 content were made by using a liquid scintillation counter on each of available parts of rice such as root, stem, crust and ear as well as on the sampled air.

The findings of this study are as follows. (i) the C-14 levels of all the rice fields studied were higher than the reported value of the global C-14 level. (ii) C-14 showed a relatively even distribution among the parts during the growth period. The reason for this was ascribed to the strong dependency of C-14 distribution on interactions among the parts such as transportation of nutrients rather than on photosynthesis occurring only in stem that has chlorophyll. (iii) the difference of C-14 concentration between each part of rice and the air decreased with time implying that the time is needed for establishment of equilibrium between both sides. Finally, the effect of the distance of rice field from the plant was recognized though it was not as clear as expected. The radius within which C-14 released from the Wolsong plant could have a significant effect on the C-14 concentrations of the parts of rice was observed to be about 5 km.

Since the C-14 distribution in rice can be subject to other factors such as wind direction, topography and precipitation and so on, a further study that will consider these factors as well is required for a better understanding of C-14 distribution pattern during the growth period.

References

1) S-R. Peterson, P. A. Davis, and R. R. Rao, Modeling doses from tritium and 14C in the environment, RC-1951, Atomic Energy of Canada Limited (1997).
2) W. Sohn, D.W. Kang and W.S. Kim, “An estimate of Carbon-14 inventory at Wolsong nuclear power plant in the Republic of Korea”, *J. Nucl. Sci. Technol*., 40[8], 604 (2003).
3) W. Sohn, D.W. Kang and J.H. Chi, “Approaches for reducing carbon-14 stack emissions from Korean CNADU nuclear power plant”, *J. Nucl. Sci. Technol*., 41[2], 235 (2004).
4) W. Sohn, D.W. Kang H.K. Ahn and I.H. Rhee, “Prediction model for exhausted point of ion exchange resin column of moderator purification circuit at Korean CANDU plant”, *J. Nucl. Sci. Technol*., 42[9], 833 (2005).
5) G.M. Milton, T.G. Kotzer and W.L. Watson, *Measurements of atmospheric levels of ^{14}C in vegetation growing in the vicinity of the CANDU-6 reactor site, Wolsong, South Korea*, RC-2142, Atomic Energy of Canada Limited (1999).

Journal of NUCLEAR SCIENCE and TECHNOLOGY, Supplement 5, p. 647–649 (June 2008)

Inter-Comparison Study of the ENSEMBLE Project

Kyung-Suk SUH[1*], Moon-Hee HAN[1], Sung-Hee JUNG[2], and Chang-Woo LEE[1]

[1]*Nuclear Environment Safety Research Center, Korea Atomic Energy Research Institute, P.O. Box 105, Yuseong, Daejeon, Korea*
[2]*Radioisotope Research and Development Center, Korea Atomic Energy Research Institute, P.O. Box 105, Yuseong, Daejeon, Korea*

During the days of the Chernobyl accident, the European national long-range dispersion forecasts would differ because of differences in national models, and differences in weather prediction methods. ENSEMBLE project was launched for a reconciliation and harmonization of the disparate long-range dispersion forecasts. Responsible European emergency organizations in addition to Canadian, Japanese, Korean and US agencies have participated in ENSEMBLE. KAERI joined the inter-comparison study for the exercise on the 901-001 scenario in ENSEMBLE. KAERI was assigned KR1 as a national code and 53 as a model number. The model of KAERI was compared with the other models of the participants in ENSEMBLE. The comparative results are presented with the scatter plots and statistical methods in this paper..

KEYWORDS: long-range dispersion, reconciliation, harmonization, emergency

I. Introduction

ENSEMBLE is a web-based decision support system for real-time exchange and evaluation of national long-range forecasts of a nuclear accident. The idea of ENSEMBLE originated from the 1994 ETEX (European Tracer Experiment) project where about 50 long-range dispersion models were run at several institutes to simulate two real long-range tracer experiments[1)].

At the time of ETEX, the World Wide Web was not readily available to all the exercise participants, and the plume predictions of the models were submitted by fax and mail. However, it is possible to develop a new inter-comparison system of a web-based model according to a rapid development of the World Wide Web.

ENSEMBLE compares and analyzes the predicted concentration and deposition at the grid nodes. During exercises, a hypothetical release is notified to participating modelers on the web. Participants then access the ENSEMBLE web page for detailed information on the actual release, and immediately run their dispersion models. After that, they can upload the results of model to the ENSEMBLE server[2)].

Twenty-five numerical models developed by twenty-two nations that participate in EMSEMBLE, submit their calculated results to the ENSEMBLE server in a real-time. The submitted results among the models are compared by using statistical methods and graphical presentations. In 2006, KAERI joined the inter-comparison study for the exercise on the 901-001 scenario in ENSEMBLE. KAERI was assigned KR1 as a national code and 53 as a model number.

*Corresponding Author, Tel No: +82-42-868-4788, Fax No: +82-42-868-8943, E-Mail: kssuh@kaeri.re.kr

II. Structure of ENSEMBLE

The ENSEMBLE web interface was designed to make its simple and straightforward. Any user can in principal operate the system without specific training. The web site is the interface between a remote user and a system, through which model results can be uploaded and consulted[3)]. On the top of the web pages, the same information and functions are always displayed.

A typical real-time session consists a notification of the occurrence of a nuclear accident at a specific geographical location within an area ranging from 30° N to 75° N and from 15° w to 60° E. The information on the release, includes the starting time, duration and rate, and is sent to the modeling groups to provide a real-time model prediction of the dispersion and deposition of the radionuclides over the spatial domain with a 0.5° x 0.5° resolution, for a time horizon of 60 h from a release beginning. Variables estimated include: concentration at 5 different levels (i.e. 0, 200, 500, 1300 and 3000 m above ground level), integrated concentration, dry and wet deposition and precipitation.

Data are transmitted to the ENSEMBLE website through the http protocol, after a preliminary processing made to assure data integrity and to compress the data for shorter transmission times. There is generally a time-window after the release notification when predicted values can be arbitrarily updated by users. Each user can submit results produced with different modeling tools and for each of them several sets.

At the top of the web-page one can find an “exercise number” selector where the user can specify the exercise number of interest. This is an important part of the site since by using this selector the users can work on different exercises. At any time, users have the opportunity to upload some model output to test the system files. Datasets must be provided in coded format by using the enform software. Data sets relating to an exercise with a different form 00 can only be uploaded during the exercise time-window.

III. Results of Comparative Study

KAERI participated in ENSEMBLE for an inter-comparison study. A long-range atmospheric dispersion model named LADAS is used to join the ENSEMBLE. LADAS was designed to estimate the air concentrations and the dry deposition as well as the wet deposition at distances of up to some thousands of kilometers from the release point in a horizontal direction[4].

LADAS was applied the exercise on the 901-001 scenario (ETEX-1) in ENSEMBLE. In order to compare the model results with the measured concentrations, the first results were integrated over a period of 3 h to reproduce the sampling time used during the tracer experiment. The measured concentrations were interpolated to the ENSEMBLE grid resolution for a direct comparison with other model results.

The ENSEMBLE web page includes tools for a graphical representation of the results. This feature allows a graphical and statistical comparison of 2 data sets. The graphics can represent an inter-comparison between two subsets of model results, each of which contains an average or the maximum value of a subset. ENSEMBLE makes use some tools for the analyses (**Table 1**). Space analysis means that the values at a fixed time are considered all over a domain. This analysis is useful to reveal space shifting among datasets. While time analysis means that, the values at a fixed location are considered for the whole duration of the episode. Global analysis is that all the values at any time and location are considered. For this analysis the distribution of the values is important as well as the overall tendency to underestimate or overestimate of one dataset compared to another.

Table 1 Main analysis menu

	Space Analysis	Time Analysis	Global Analysis
Concentration	Grid plot Overlap in space Scatter diagram Agreement in threshold level Agreement in percentile threshold	Time overlap	Global scatter diagram Agreement in threshold maximum level
Time-integrated Concentration	Grid plot Overlap in space Scatter diagram Agreement in threshold level Agreement in percentile threshold	Time overlap	Global scatter diagram
Dry deposition	Grid plot Overlap in space Scatter diagram Agreement in threshold level Agreement in percentile threshold	Time overlap	Global scatter diagram
Wet deposition	Grid plot Overlap in space Scatter diagram Agreement in threshold level Agreement in percentile threshold	Time overlap	Global scatter diagram
Total deposition	Grid plot Overlap in space Scatter diagram Agreement in threshold level Agreement in percentile threshold	Time overlap	Global scatter diagram
Precipitation	Grid plot Overlap in space Scatter diagram Agreement in threshold level Agreement in percentile threshold	Time overlap	Global scatter diagram

Fig. 1 shows the comparative results of KR1 (LADAS) and JP1 (WSPEEDI)[5], and an agreement in the percentile level for a surface air concentration. The clouds are displayed together with an indication of the overlapping region. **Fig. 2** shows the results of a time series. The horizontal axis is the hours after a release and the vertical axis is the concentration. The red and blue colors of the bars in **Fig. 2** are the results of KR1 and JP1 respectively. The overall distributions of the concentrations show similar patterns. This analysis allows to treat model results for a fixed location as a function of time. Similarly to the space overlap, it is possible to analyze several model results simultaneously at a fixed location, to combine them into an ensemble treatment and to compare the ensembles.

The statistical method is used to compare the results of the participating models. Most of the statistics is based on an analysis of pairs of datasets. The statistical parameters used for a comparison are FA2, FA5, FOEX, FMS and Bias[6]. FA2 and FA5 give the percentage of model results within a factor of 2 and 5 respectively of the corresponding model's results. FOEX (Factor of Excess) gives in the percentage of the modeled concentration values that overestimate or underestimate the corresponding measurements. FMS (Figure of merit in Space) is a statistical coefficient for the space analysis.

The scatter diagram is a plot where two sets of data are plotted one (y values) against the other (x values). It means that the results between models can be plotted one against the other. On this diagram the y=x line represents a perfect agreement between the models. A value above (below) the y=x line indicates an over-prediction (under-prediction).

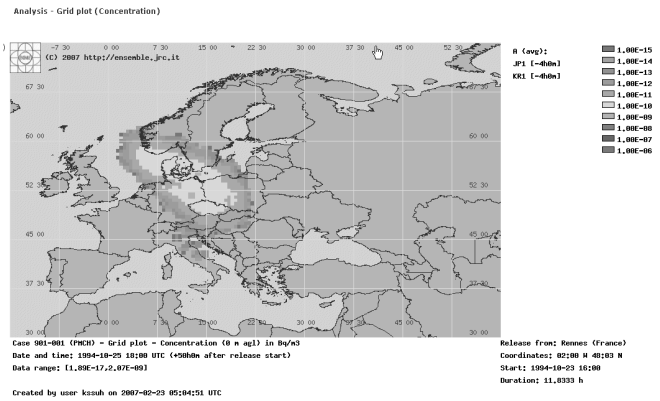

Fig. 1 Averaged concentrations on surface level at 50 h after release start

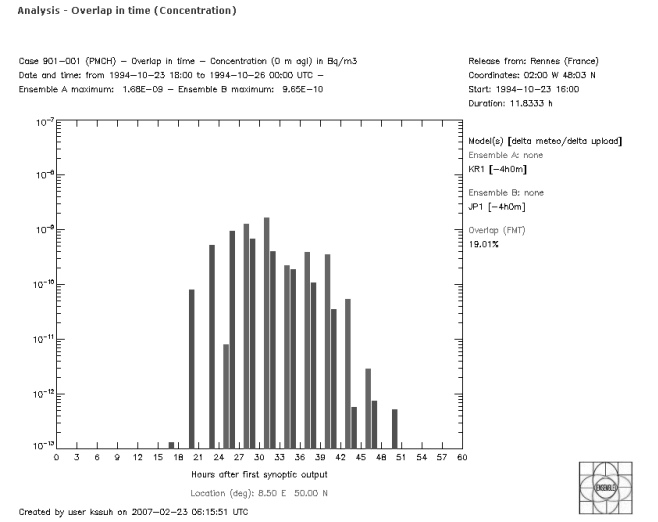

Fig. 2 Time series of the concentration for two models (LADAS and WSPEEDI)

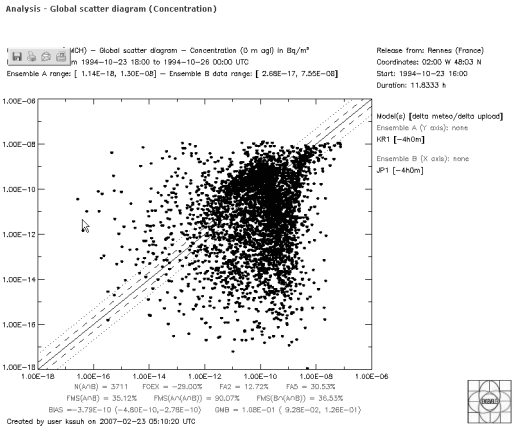

Fig. 3 Scatter plots of concentrations between LADAS and WSPEEDI

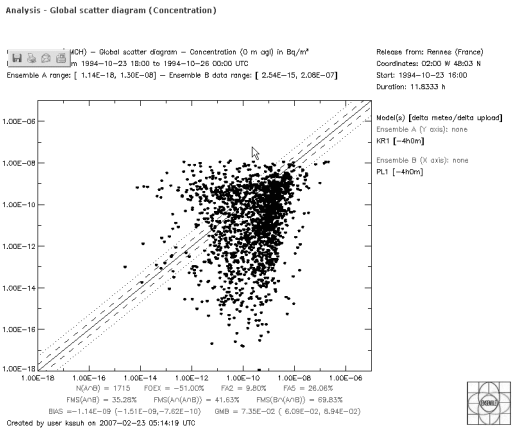

Fig. 4 Scatter plots of concentrations between LADAS and RODOS

Fig. 3 and **4** show the scatter diagrams of the concentrations. The horizontal and vertical axes in **Fig. 3** are the results of WSPEEDI[5] and LADAS respectively. The horizontal and vertical axes in **Fig. 4** are the results of RODOS[7] and LADAS respectively. Both the comparative results in **Fig. 3** and **4** show similar patterns.

IV. Conclusions

The ENSEMBLE system is introduced in its conceptual and technical aspects. Its conceptual and methodology consist of an analysis of the forecasts produced by several models used operationally by national meteorological services and environmental protection agencies worldwide.

During the exercises, a hypothetical release is notified to the participating forecasts on the web. Participants then access the ENSEMBLE web page for detailed information on the actual release and immediately run their national dispersion forecasts for up to +60 or to +72 hours ahead. Today, ENSEMBLE features a true real-time web based and user friendly decision support system for a long-range dispersion data exchange and a model evaluation. It has a build-in interactive evaluation package for immediately displaying results, inter-comparison and a decision-making support.

Acknowledgement

This work was supported by the MOST, Korea.

References

1) T. Mikkelsen, et al., ENSEMBLE Methods to Reconcile Disperate National Long Range Dispersion Forecasts, RISO-R-1435(EN), RISO, (2003).
2) S.Galmarini et al., “Ensemble dispersion forecasting – Part I: concept, approach and indicators,” Atmos. Environ. 28, 4607 (2004).
3) R. Bianconi, S. Galmarini, R. Bellasio, “Web-based system for decision support in case of emergency: ensemble modeling of long-range atmospheric dispersion of radionuclides,” Environ. Modelling & Soft. 19, 201 (2004).
4) K.S.Suh et al., “Verification of the Lagrangian particle model using the ETEX experiment,” Annals of Nuc. Ener. 33, 1159 (2006).
5) A. Furuno, et al., “Experimental verification for real-time environmental emergency response system;WSPEEDI by European tracer experiment,” Atmos. Environ. 38, 6989 (2004).
6) S. Mosca, et al., “A statistical methodology for the evaluation of long-range dispersion models: an application to the ETEX exrcise,” Atmos. Environ. 32, 4307 (1998).
7) K.N. Papamichail, S. French, “Design and evaluation of an intelligent decision support system of nuclear emergencies,” Decision Support Sys. 41, 84 (2005).

Journal of NUCLEAR SCIENCE and TECHNOLOGY, Supplement 5, p. 650–653 (June 2008)

Long-Term Predictions of the ^{90}Sr and ^{137}Cs Concentrations in Rice for Their Acute Deposition at Different Times of the Year

Yong-Ho CHOI*, Kwang-Muk LIM, In JUN, Dong-Kwon KEUM, and Chang-Woo LEE

Nuclear Environment Safety Research Center, Korea Atomic Energy Research Institute, P.O. Box 105, Yuseong, Daejeon, Korea

The concentrations of ^{90}Sr and ^{137}Cs in rice seeds for 50 years were predicted for a hypothetical acute deposition (1 Bq m^{-2} for each) at each of seven different times in 2007. This prediction was performed using several arithmetic equations and some empirical parameter values for the radionuclide transfer. The ^{90}Sr and ^{137}Cs concentrations (Bq kg^{-1}-brown rice) at the first harvest following each deposition were in the range of 4.2×10^{-4}–1.8×10^{-2} and 1.2×10^{-4}–1.8×10^{-1}, respectively, being higher for the growing-season depositions than for the non growing-season depositions. The highest concentrations came from the deposition on September 1 for both owing to their highest seed-translocation factors. At the second harvest, the ranges for ^{90}Sr and ^{137}Cs were 3.0×10^{-4}–4.2×10^{-4} and 7.9×10^{-5}–1.2×10^{-4}, respectively. Between the second and 50th harvests, the concentrations decreased by a factor of about 18 for ^{90}Sr and 17 for ^{137}Cs as a result of a reduced root uptake. The time-integrated concentrations (Bq·d kg^{-1}–white rice) of ^{90}Sr and ^{137}Cs for a 50 years' dietary consumption were in the range of 9.6×10^{-1}–4.1×10^{0} and 1.6×10^{-1}–3.2×10^{1}, respectively. The use of the empirical data might enhance the accuracy of the prediction considerably. The present results may be used for a quick prediction at the time of a real accident.

KEYWORDS: ^{90}Sr, ^{137}Cs, acute deposition, rice, concentration, prediction

I. Introduction

From a radiological point of view, ^{90}Sr and ^{137}Cs are two major radionuclides that remain in soils for a long time after a nuclear accident. Rice is a main source of human calories in most Asian countries including Korea and Japan. It is, therefore, necessary to predict the long-term concentrations of ^{90}Sr and ^{137}Cs in rice when a nuclear accident occurs in these countries.

Many dynamic models have been developed to predict the food concentrations of acutely-deposited radionuclides[1–3]. The accuracy of a model prediction largely depends on the suitability of the values chosen for the model parameters. Values of some parameters describing the environmental transfer of a radionuclide are markedly variable. Therefore, it is important to use as realistic values as possible for them.

Most dynamic food-chain models introduce simultaneous differential equations to calculate the radionuclide transfer during the time from deposition to harvest[1,3]. These equations need transfer rate constants, which are often derived from steady-state parameter values without considering their dependence on the time of deposition.

In this study, the concentrations of ^{90}Sr and ^{137}Cs in rice for 50 years were predicted for a hypothetical acute deposition at different times of the year. Several arithmetic equations instead of simultaneous differential equations were established and the deposition time-dependent values of major transfer parameters measured for rice were used[2,4,5]. It was expected that this use of the empirical data would help enhance the accuracy of the prediction.

*Corresponding Author, Tel No: +82–42–868–2392, Fax No: +82–42–861–1761, E–mail: yhchoi1@kaeri.re.kr

II. Calculation Procedure

1. Deposition Scenarios

It was assumed that ^{90}Sr and ^{137}Cs were deposited onto a paddy field at their respective levels of 1 Bq m^{-2} at each of seven different times in the year of 2007. The chosen times of deposition were April 1, June 1, July 1, August 1, September 1, October 1 and December 1. Rice plants were considered to be transplanted on May 25 and harvested on October 15.

2. Plant Contamination Pathways

In the case of a non-growing-season deposition (NGSD), rice plants are contaminated only via an indirect pathway involving root uptake of radionuclides from contaminated soils. In the case of a growing season deposition (GSD), not only an indirect pathway but also a direct pathway is effective.

The direct pathway involves a plant interception of radionuclides and a subsequent translocation to the seeds. A considerable fraction of the intercepted radionuclides can be lost from the plants by a weathering process. All of the activity lost in such a way was assumed to be deposited onto the soil surface and to become available for root uptake[1,3].

3. Concentrations at the First Harvest

The ^{90}Sr and ^{137}Cs concentrations in rice seeds at the first harvest after an NGSD (R1) were calculated as follows;

$$R1_i = S1_i \times TF_i \times EXP(-\lambda_i t_g) \quad (1)$$

$R1_i$: R1 concentration of radionuclide i (Bq kg^{-1})

$S1_i$: soil concentration at transplanting (Bq kg^{-1})

TF_i : soil–to–plant transfer factor (See Section 6.)

λ_i: decay constant (d^{-1}) (See Section 6.)

t_g: time from transplanting to harvest (143 d)

In equation (1), $S1_i$ was determined as follows;

$$S1_i = \frac{D_i \times EXP(-\lambda_i t_p)}{E} \quad (1\text{–}1)$$

D_i: deposition density (1 Bq m^{-2})

t_p: time from deposition to transplanting (d)

E: effective soil (0–15 cm) density (165 kg m^{-2})[6,7]

For the rice seeds harvested firstly after a GSD (R2), the following equation was applied.

$$R2_i = Cd_i + Cr_i + Cw_i \quad (2)$$

$R2_i$: R2 concentration of radionuclide i (Bq kg^{-1})

Cd_i: contribution by a direct pathway

Cr_i: contribution by root uptake due to an initial ground deposition

Cw_i: contribution by root uptake due to weathering

In equation (2), Cd_i and Cr_i were determined as follows;

$$Cd_i = \frac{Pd_i \times TL_{i,d}}{Y} \quad (2\text{–}1)$$

Pd_i: plant–deposition density decay–corrected to the time of the first harvest (Bq m^{-2})

$$Pd_i = D_i \times IC_d \times EXP(\lambda_i t_f) \quad (2\text{–}1.1)$$

IC_d: plant–interception fraction at d days after transplanting (See Section 6.)

t_f: time from deposition to the first harvest (d)

$TL_{i,d}$: seed–translocation factor for a deposition at d days after transplanting (See Section 6.)

Y: yield of rice seeds (0.5 kg m^{-2})[6]

$$Cr_i = A_i \times ATF_{i,d} \quad (2\text{–}2)$$

A_i: initial ground–deposition density decay–corrected to the time of the first harvest (Bq m^{-2})

$$A_i = D_i \times (1 - IC_d) \times EXP(-\lambda_i t_f) \quad (2\text{–}2.1)$$

$ATF_{i,d}$: areal transfer factor for a deposition at d days after transplanting (m^2 kg^{-1}) (See Section 6.)

In Equation (2), Cw_i was roughly estimated as follow;

$$Cw_i = \sum_{j=1}^{n} Dw_{i,j} \times mATF_{i,j} \quad (2\text{–}3)$$

$Dw_{i,j}$: ground–deposition density due to weathering for the j th period (Bq m^{-2}). Each period was each month after the initial deposition except for the n th period which ended on the harvest day.

If $j = 1$,

$$Dw_{i,j} = Pd_i \times (1 - EXP(-\lambda_w t_j)) \quad (2\text{–}3.1)$$

λ_w: weathering rate constant (0.0277 d^{-1})[2,4]

t_j: duration of the j th period (15–31 d)

If $j \geq 2$,

$$Dw_{i,j} = \left\{ Pd_i - \sum_{k=1}^{j-1} Dw_{i,k} \right\} \times (1 - EXP(-\lambda_w t_j)) \quad (2\text{–}3.2)$$

$mATF_{i,j}$: mean of two ATF_i values for depositions at the first and last days of the j th period.

4. Concentrations at the Subsequent Harvests

Rice seeds at the second and following harvests (R3) were considered to be contaminated only via root uptake from a ploughed soil. Therefore, the R3 concentrations were determined as follows;

$$R3_{i,n} = S3_{i,n} \times LTF_i \times EXP(-\lambda_i t_g) \quad (3)$$

$R3_{i,n}$: R3 concentration of radionuclide i at the n th harvest (Bq kg^{-1})

$S3_{i,n}$: soil concentration at transplanting for the n th harvest (Bq kg^{-1})

LTF_i: long-term transfer factor (See Section 6.)

In equation (3), $S3_{i,n}$ was estimated as follows;

- for the second harvest after a GSD ($n = 2$),

$$S3_{i,n} = \frac{(A_i + Q_i) \times EXP(-\lambda_i t_r)}{E} \quad (3\text{–}1)$$

Q_i: activity input due to weathering and recycling of plant litters (Bq m^{-2}). Assuming that half the plant activity at harvest return to soil by such a recycling,

$$Q_i = Pd_i \times (1 - 0.5EXP(-\lambda_w t_f)) \quad (3\text{–}1.1)$$

t_r: time from the first harvest to transplanting for the second harvest (d)

- for the second harvest after an NGSD ($n = 2$),

$$S3_{i,n} = S1_i \times EXP(-(\lambda_i + \lambda_{l,i}) t_n) \quad (3\text{–}2)$$

$\lambda_{l,i}$: leaching rate constant (d^{-1}) (See Section 6.)

t_n: time between transplanting for the $(n-1)$th harvest and transplanting for the n th harvest (d)

- for the third to 50th harvest after both depositions ($n \geq 3$),

$$S3_{i,n} = S3_{i,n-1} \times EXP(-(\lambda_i + \lambda_{l,i}) t_n) \quad (3\text{–}3)$$

5. Concentrations at the Time of Dietary Consumption

It was assumed that it would take at least 10 d to process harvested rice seeds for a dietary consumption. Via this processing, brown rice is polished to be white rice. The ^{90}Sr and ^{137}Cs concentrations in white rice on a consumption day (Rw) were calculated as follows;

$$Rw_{i,d} = Rh_i \times PF \times EXP(-\lambda_i t_{up}) \quad (4)$$

$Rw_{i,d}$: Rw concentration of radionuclide i at d (10–376) days after harvest (Bq kg^{-1})

Rh_i: concentration at harvest ($R1$, $R2$ or $R3$)

PF: brown–to–white rice processing factor (0.5)[2,6]

t_{up}: hold–up time (d d)

The time-integrated concentrations for 50 years' consumption were calculated as follows;

$$G_i = \sum_{y=1}^{50} \sum_{d=10}^{375(376)} Rw_{i,d,y} \times t_c \quad (5)$$

G_i: time–integrated concentration of radionuclide i for 50 years' consumption (Bq d kg^{-1})

$Rw_{i,d,y}$: $Rw_{i,d}$ from the y th harvest (Bq kg^{-1})

t_c: time length for $Rw_{i,d,y}$ (1 d)

6. Values of Model Parameters

In **Table 1**, the values of TF_i are means of some reported values and those of $\lambda_{l,i}$ were determined as follows[5–9];

Table 1. Values of the transfer factor (TF_i), decay constant (λ_i) and leaching rate constant ($\lambda_{l,i}$)

Parameter	Parameter value	
	^{90}Sr	^{137}Cs
TF_i (dimensionless)	7.6×10^{-2}	2.8×10^{-2}
λ_i (d^{-1})	6.78×10^{-5}	6.33×10^{-5}
$\lambda_{l,i}$ (d^{-1})	2.45×10^{-4} [a]	7.42×10^{-6} [a]
	7.40×10^{-5} [b]	1.49×10^{-6} [b]

[a] for the first 5 years
[b] for the subsequent years.

$$\lambda_{l,i} = \frac{Pw}{\left\{Dp \times \left(1 + \frac{K_i \times B}{W}\right)\right\}} \quad (6)$$

Pw: percolation rate of soil water (0.35 cm d^{-1})
Dp: ploughing depth of paddy soil (15 cm)
K_i: solid / liquid phase distribution coefficient (ml g^{-1})
(30 for ^{90}Sr and 1,000 for ^{137}Cs for the first five years and, thereafter, 100 and 5,000, respectively)
B: bulk density of paddy soil (1.1 g cm^{-3})
W: water content in paddy soil (0.35 ml cm^{-3})

For the LTF_i in Equation (3), annual decreases of 5% for the ^{90}Sr TF and 30% for the ^{137}Cs TF were applied for the first four years as a result of considering a soil fixation[2,5,10]. An additional annual decrease of 10% was given to the ^{137}Cs TF for another six years

The values of the $TL_{i,d}$ (**Table 2**) and $ATF_{i,d}$ (**Table 3**) were obtained by interpolations and extrapolations of those from Choi et al's experiments[4,5]. In order to determine the IC_d values (**Table 2**), Choi et al's experimental data[4] were compared with a Chamberlain's equation[11]. This comparison indicated that it would be reasonable to use 8.3 m^2 kg^{-1}–dry for retention factor (μ) in the equation but, when the calculated IC_d value was larger than 0.9, to adjust it to 0.9.

Table 2. Deposition time-dependent values of the translocation factor ($TL_{i,d}$) and interception fraction (IC_d)

Deposition time (date)	(DAT)	$TL_{i,d}$ (dimensionless)		IC_d (dimensionless)
		^{90}Sr	^{137}Cs	
June 1	7	2.6×10^{-4}	5.4×10^{-3}	8.9×10^{-2}
July 1	37	2.3×10^{-4}	1.9×10^{-2}	6.7×10^{-1}
Aug. 1	68	2.0×10^{-4}	3.9×10^{-2}	9.0×10^{-1}
Sept. 1	99	9.8×10^{-3}	9.9×10^{-2}	9.0×10^{-1}
Oct. 1	129	8.6×10^{-3}	1.8×10^{-2}	9.0×10^{-1}

DAT: days after transplanting.

Table 3. Deposition time–dependent values of the areal transfer factor ($ATF_{i,d}$)

Deposition time (date)	(DAT)	$ATF_{i,d}$ (m^2 kg^{-1}–dry)	
		^{90}Sr	^{137}Cs
June 1	7	3.7×10^{-4}	2.8×10^{-4}
July 1	37	4.6×10^{-4}	1.2×10^{-3}
Aug. 1	68	5.5×10^{-4}	2.2×10^{-3}
Sept. 1	99	5.3×10^{-4}	1.2×10^{-3}
Oct. 1	129	6.8×10^{-5}	6.2×10^{-5}

DAT: days after transplanting.

III. Results and Discussions

1. Concentrations at Harvest

Fig. 1 shows the ^{90}Sr and ^{137}Cs concentrations in rice seeds (brown rice) at the first, second and 50th harvests. At the first harvest, the ^{90}Sr and ^{137}Cs concentrations were in the range of 4.2×10^{-4}–1.8×10^{-2} Bq kg^{-1} and 1.2×10^{-4}–1.8×10^{-1} Bq kg^{-1}, respectively, depending on the times of deposition.

The highest concentrations came from the deposition on September 1 for both nuclides owing to their highest seed-translocation factors. For the GSDs, ^{137}Cs had much higher concentrations than ^{90}Sr because of a considerable difference in their translocation factors. For the NGSDs, however, the opposite was true. It was because the soil-to-plant transfer factor was much higher for ^{90}Sr than for ^{137}Cs.

The first-harvest concentrations in this study are not much different from those estimated by Lee et al.[1] in the case of NGSD, but considrable differences can be found in the case of GSD. It is because they used a single value 0.1 as the seed-translocation factor for both ^{90}Sr and ^{137}Cs.

At the second harvests after the GSDs, the concentrations of ^{137}Cs and, to a lesser degree, ^{90}Sr decreased significantly, whereas it was not the case with the NGSDs. The reason for this is that only root uptake from a ploughed soil was effective. A similar thing was also predicted by Lee et al.[1]. From the second harvests, the deposition time–dependent variations were not so significant for the same reason.

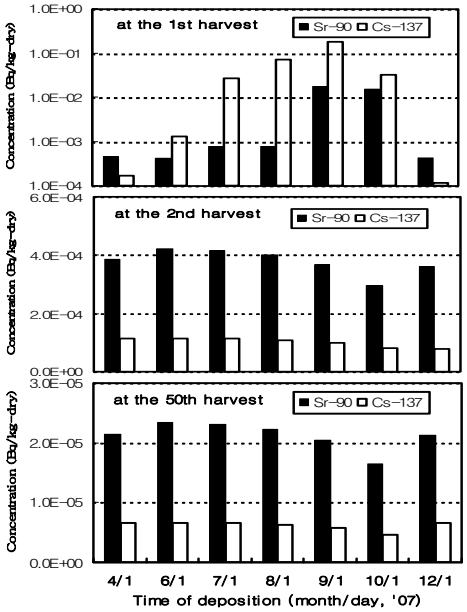

Fig. 1. Concentrations of ^{90}Sr and ^{137}Cs in brown rice at different harvest times after their depositions at different times of the year. A deposition of 1 Bq m^{-2} for each was assumed.

The concentrations of ^{90}Sr were about 4 times higher than those of ^{137}Cs at the second harvest, whereas the differences were slightly smaller at the 50th harvest in spite of a much greater decrease in the ^{137}Cs *TF* . This can be attributed to a more rapid decrease in the soil concentration of ^{90}Sr than of ^{137}Cs, which can be expected with their values of the leaching rate constant (**Table 1**).

Due to leaching, radioactive decay and annual *TF* decrease, the rice concentrations reduced by a factor of about 18 for ^{90}Sr and 17 for ^{137}Cs at the 50th harvest when compared with the second harvest.

2. Concentrations during 50 Years' Dietary Consumption

The ^{90}Sr and ^{137}Cs concentrations in white rice, which depended on the brown-rice concentrations, processing factors and radioactive decay during storage, decreased continuously for 50 years (**Fig. 2**). The decrease was more rapid in the earlier phase as was the case with the brown-rice concentrations.

Following the NGSDs, the time–integrated concentrations of white rice over 50 years were several times higher for ^{90}Sr than for ^{137}Cs, whereas the opposite was true for the GSDs in general (**Table 4**). The ^{137}Cs concentrations from the GSDs were up to two orders of a magnitude higher than those from the NGSDs. This suggests that a direct plant contamination in the first year would contribute to most part of the integrated concentration of ^{137}Cs in the case of the GSDs in general. Multiplication of the time-integrated concentrations by a daily rice consumption rate (kg d^{-1}) will produce a total intake of ^{90}Sr and ^{137}Cs for 50 years.

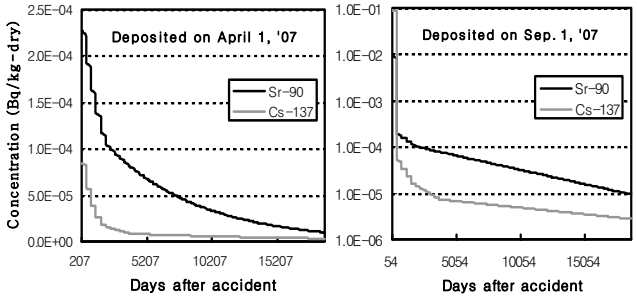

Fig. 2. Time courses of ^{90}Sr and ^{137}Cs concentrations in white rice for 50 years after their depositions at two different times.

Table 4. Time-integrated concentrations of ^{90}Sr and ^{137}Cs in white rice for 50 years' dietary consumption

Deposition time (date)	(DAT)	Time-integrated concentration (Bq d kg^{-1})	
		^{90}Sr	^{137}Cs
April 1	−54	9.8×10^{-1}	1.8×10^{-1}
June 1	7	1.1×10^{0}	3.9×10^{-1}
July 1	37	1.1×10^{0}	5.0×10^{0}
Aug. 1	68	1.1×10^{0}	1.3×10^{1}
Sept. 1	99	4.1×10^{0}	3.2×10^{1}
Oct. 1	129	3.5×10^{0}	6.0×10^{0}
Dec. 1	190	9.6×10^{-1}	1.6×10^{-1}

DAT: days after transplanting.

For an acute deposition of 1 Bq m^{-2}, Hwang et al.[3] estimated the 50–year–integrated rice concentrations to be 3.0×10^{-1}–6.0×10^{0} for ^{90}Sr and 6.0×10^{-3}–3.0×10^{1} for ^{137}Cs, depending on the times of deposition. The big difference between the present estimation and theirs for ^{137}Cs from NGSDs is attributable to a much higher value for the *TF* and a much smaller effect of soil fixation in this study.

IV. Conclusions

Using several arithmetic equations and empirical parameter values, the concentrations of ^{90}Sr and ^{137}Cs in rice for 50 years were predicted for a hypothetical acute deposition at different times of the year.

The results showed some differences from those of previous studies due to differences in the parameter values and equations. A more realistic estimation might be made in this study owing to a harmonization of established equations with the deposition time-dependent parameter values measured for rice.

Acknowledgement

This work was supported by the Ministry of Science and Technology, Korea, within the framework of a national long-term nuclear R&D program.

References

1) C. W. Lee et al., "Nuclides transport analysis and dose calculation using dynamic code for rice ingestion pathway," J. Kor. Associ. Radiat. Prot. 17, 15 (1992) (in Korean).
2) H. Mueller and G. Proehl, "ECOSYS-87: a dynamic model for assessing radiological consequences of nuclear accidents," Health Phys. 64, 232 (1993).
3) W. T. Hwang, et. al., "Development of a dynamic food chain model DYNACON and its application to Korean agricultural conditions," J. Nuc. Sci. Technol. 35, 454 (1998).
4) Y. H. Choi et al., "Transfer pathways of ^{54}Mn, ^{57}Co, ^{85}Sr, ^{103}Ru and ^{137}Cs in rice and radish plants directly contaminated at different growth stages," Ann. Nuc. Energy 29, 429 (2002).
5) Y. H. Choi et al., Parameters on the Radionuclide Transfer in Crop Plants for Korean Food Chain Dose Assessment, KAERI/TR-1993/2001, KAERI, (2001) (in Korean).
6) Y. H. Choi et al., "Improvement on the method of estimating radionuclide concentration in agricultural products," J. Kor. Associ. Radiat. Prot. 29, 73 (2004) (in Korean).
7) S. J. Cho et al., Soil Science, Hyangmon Press, Seoul (1997)
8) F. O. Hoffman and C. F. Baes III. (eds.), A Statistical Analysis of Selected Parameters for Predicting Food Chain Transport and Internal Dose of Radionuclides, NUREG/CR-1004, ORNL/NUREG/TM-282, ORNL, (1979)
9) Y. H. Choi et al., "Plant uptake and downward migration of ^{85}Sr and ^{137}Cs after their deposition on to flooded rice fields: lysimeter experiments," J. Environ. Radioac. 78, 35 (2005).
10) H. Noordijk et al., "Impact of ageing and weather conditions on soil-to-plant transfer of radiocesium and radiostrontium," J. Environ. Radioac. 15, 277 (1992).
11) A. C. Chamberlain, "Interception and retention of radioactive aerosol by vegetation," Atmos. Environ. 4, 57 (1970).

Journal of NUCLEAR SCIENCE and TECHNOLOGY, Supplement 5, p. 654–657 (June 2008)

Development of the DNAA System for Screening Environmental Samples to Measure fissile Material

Gil Hoon AHN[1*], Il-Jin PARK[1], J.G.KIM[1], Gyungsik MIN[2], Sunha KIM[3], and Yongsam CHUNG[3]

[1]*Korea Institute of Nuclear Nonproliferation and Control, Daejeon, Rep. of Korea*
[2]*Korea Meteorological Administration, Seoul, Rep. of Korea*
[3] *Korea Atomic Energy Research Institute, Daejeon, Rep. of Korea*

The DNAA system made up of pneumatic transport system, neutron detector assembly, and signal processing equipment was installed in the High-flux Advanced Neutron Application Reactor (HANARO). The optimized position of the detector in the delayed neutron counting (DNC) system was evaluated at a distance 15.1 cm from center of the DNC system with 18 He-3 detectors using MCNP simulation. The system shows excellent linearity from 0.67 ng to 713 ng U-235, and reproducibility of 1.26% standard deviation for the various mass groups of U-235 samples. The DNAA system shows detection efficiency of ~30 % and U-235 detection limit of 1ng. This system can be used on a screening method to assist the environmental sample analysis and to protect the clean room from elevated levels of fissile material that might be in routine samples.

KEYWORDS: neutron activation analysis, delayed neutron, environmental sample, screening, fissile material, DNAA

I. Introduction

The quantitative determination of fissile materials in environmental samples is becoming more and more important because of the increasing demand for nuclear nonproliferation. A number of methods have been proposed for screening environmental samples to measure fissile material content. Among them, neutron activation analysis coupled with delayed neutron counting (DNAA : Delayed Neutron Activation Analysis) without chemical preparation has numerous advantages over other screening techniques.[1)] Fissile materials such as ^{239}Pu and ^{235}U can be made to undergo fission in the intense neutron field. Some of the fission products emit neutrons referred to as "delayed neutrons" because they are emitted after a brief decay period following irradiation. Counting these delayed neutrons provides a simple method for determining the total fissile content in the sample. In delayed neutron counting, the chemical bonding environment of a fissile atom has no effect on the measurement process. Therefore, DNAA is virtually immune to the "matrix" effects that complicate other methods.[2)]

In this work, the DNAA system made up of pneumatic transport system, neutron detector assembly, and signal processing equipment was installed in HANARO under the DOE-MOST PCG (Permanent Coordinating Group) safeguards arrangement. This research reactor at KAERI has 30 MW maximum thermal power and sufficient neutron flux to detect less than one nanogram of the total fissile content. This system can be used on a screening method to assist the environmental sample analysis and to protect the clean room from elevated levels of fissile material that might be in routine samples.

*Corresponding Author, Tel No: +82-42-866-6933, Fax No: +82-42-861-8819, E-Mail: ahn@kinac.re.kr

II. DNAA System

1. Delayed Neutron Counting System

Several MCNP simulations were executed to optimize the delayed neutron counting system to achieve high detection efficiency changing the position and the number of He-3 detector in the polyethylene moderator with lead shield using the delayed neutron spectrum of precursors in the ENDF/B-VI data base as seen in **Fig.1**. Counts at the each detector position were calculated by the flux tally F4 times (n,p) cross section.

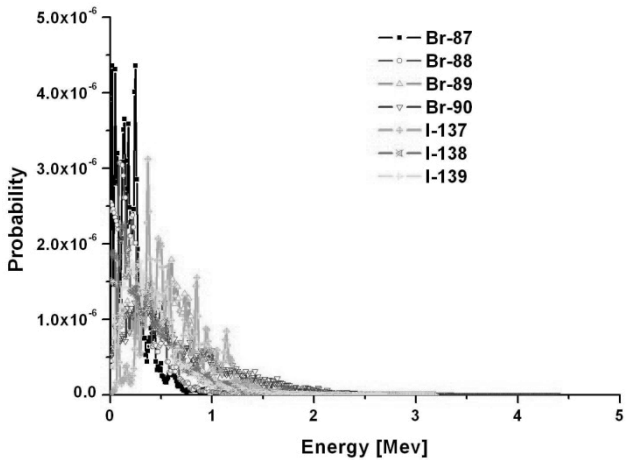

Fig. 1 Delayed neutron spectrum of precursors in the ENDF/B-VI

The result is shown in **Fig. 2**. The optimized position of the detector was evaluated at a distance 15.1 cm from center of the DNC system with 18 He-3 detectors after due consideration about the simulation result, maintenance of the

system, and assembling of the electronics. **Fig. 3** shows the optimized system design and **Fig. 4** shows a schematic diagram of the delayed neutron counting (DNAA) system. 18 He-3 proportional counters are spaced in one concentric rings around the flight tube. Each counter measures 2 inches in diameter and has an active length of 13 inches. Polyethylene moderator surrounds the detectors and flight tube and forms a cube approximately 20 inches in each dimension. Two inches of lead for shielding gamma radiation are molded around the flight tube and air exit line at the counting position. The polyethylene moderator is topped with a one-fifth inch aluminum plate and surrounded with four inches for neutron shield and one inches of lead.

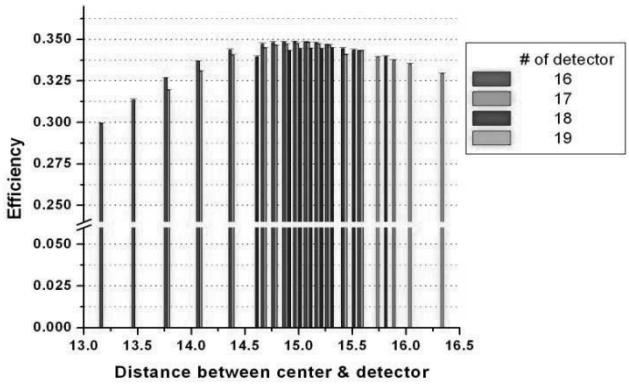

Fig. 2 Total efficiency of the detector assembly as a function of polyethylene thickness

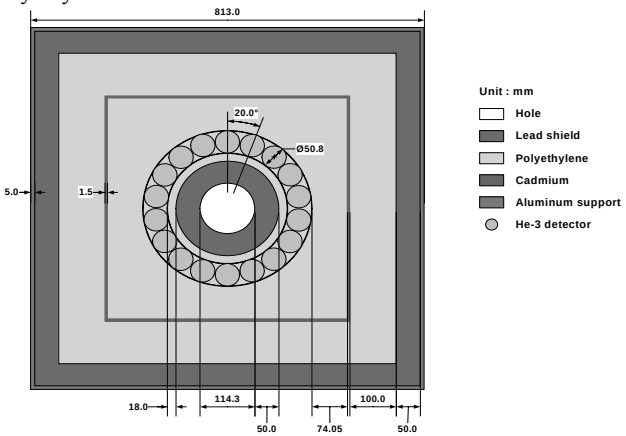

Fig. 3 Cross sectional view of the optimized DNC system

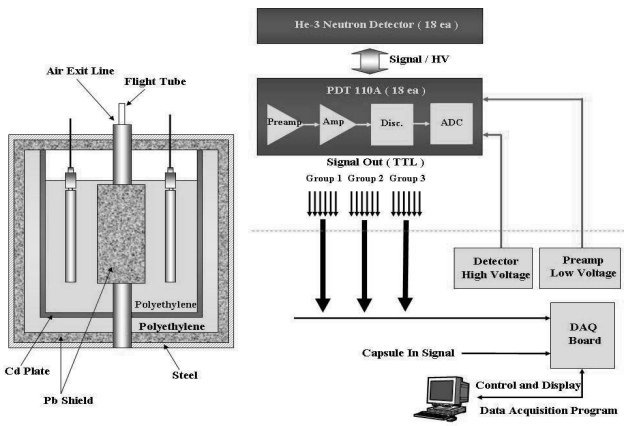

Fig. 4 A schematic diagram of the DNC system

The detectors are grouped in three groups of six, and the aggregate signal of each group is amplified and converted to digital signal. Bias is typically +1000 to +1600 V and is applied to all six detectors in a group through a multiplexer which contains a capacitor for smoothing. Ultimately, total counts for each detector group are obtained from a 3-channel scalar that also controls counting time.

2. Pneumatic Transport System

The polyethylene rabbit is used for sample irradiation. The rabbit diameter is 22.5mm and height is 57.9mm. The rabbits are loaded into the pneumatic tube in a loading station, irradiated for pre-selected time, and automatically moved to the DNC system. The loading station is designed to load 10 samples at a time and the samples can be analyzed one by one with pre-selected irradiation, decay and counting times. Rabbits are moved from the loading station to the reactor using nitrogen gas at a pressure of 0.75 bar. Transfer from the reactor to the counter takes about 7 seconds. The nitrogen exits the counter at midplane through an exit tube causing the rabbit to stop at midplane for counting. The PTS is controlled by programmable logic controller. **Fig. 5** shows the computer control program for PTS operation.

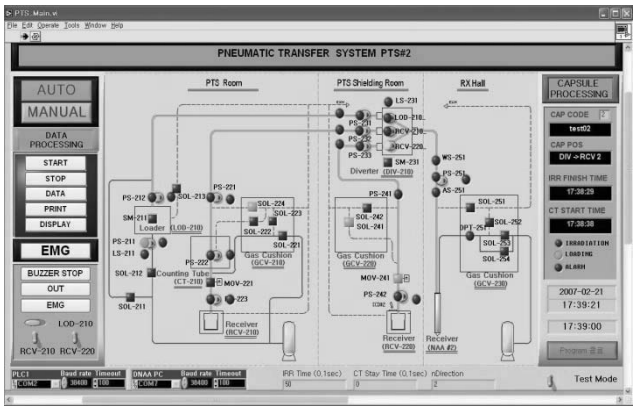

Fig. 5 PTS operation program

III. Performance Test

1. Neutron Flux Measurement at Irradiation Position

Flux measurement using dilute gold and manganese has been performed and the ratio of thermal to epithermal neutron flux was calculated using simultaneous activation equations. The 0.087 % Mn/Al foil and 0.1 % Au/Al foil were irradiated for 30 s for flux monitoring. As a result, thermal flux is 3.28×10^{13} n·cm^{-2}·s^{-1} and the ratio of thermal to epithermal flux is about 476. It is estimated that the interference threshold percentage from fast fission of ^{238}U is very small.

2. Linearity Test

A series of uranium standard samples, which have the range from 0.67 ng to 713 ng ^{235}U, were used to evaluate the DNAA system in HANARO. With increasing mass of prepared ^{235}U samples, linearity of the counter response was tested. The irradiation time, decay time and the measuring

time were 60 s, 20 s, and 60 s respectively. Measured counts showed excellent linearity with respect to ^{235}U contents as seen in **Fig. 6**.

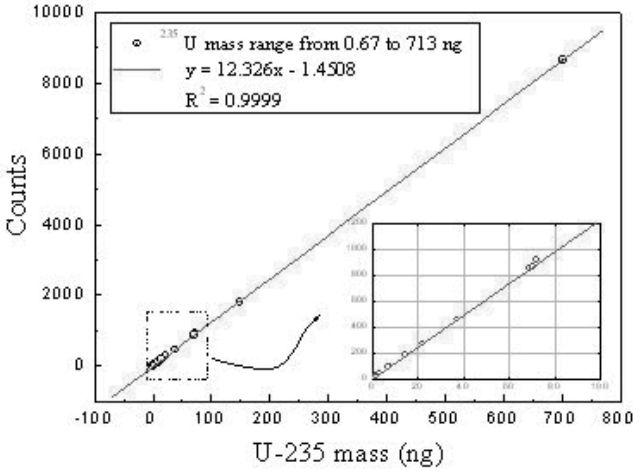

Fig. 6 Result of the linearity test

3. Reproducibility of Measurement

The reproducibility test was performed to measure the agreement between independent results obtained with the same method on identical test but under the different condition of ^{235}U mass. Three groups of ^{235}U samples, nominally 190 ng (sample ID : 1~3), 56 ng (sample ID : 4~6), and 8.9 ng (sample ID : 7~11), were analyzed to establish system reproducibility. **Fig. 7** shows the counts per nanogram ^{235}U for each sample. The standard deviation in the mean value was 1.26%. From the result, the reproducibility of the irradiation position, system timing, counting position, and sample preparation appear to be excellent.

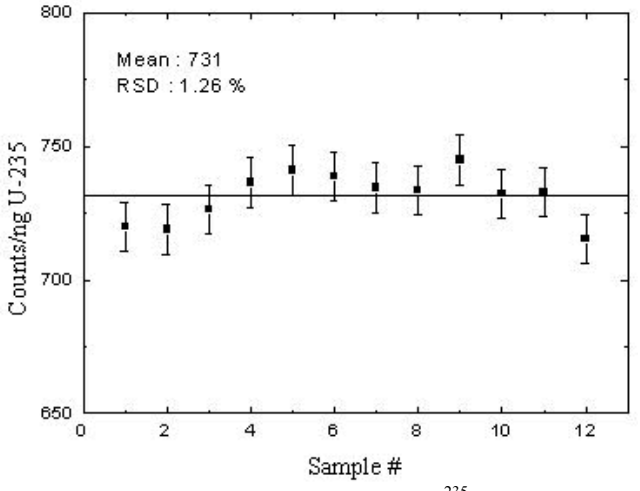

Fig. 7 Reproducibility tests of ^{235}U

4. Efficiency Calculation

The delayed neutron emitters can be categorized into six groups with half–lives ranging from approximately 0.2 to 55 s. The total delayed neutron count C_T of the system is a linear summation of these six groups and is given by the expression [3],

$$C_T = \left(\frac{\varepsilon \nu m N_A \sigma_f \Phi}{M}\right) \sum_{i=1}^{6} \beta_i \frac{1}{\lambda_i} \left(1 - e^{-\lambda_i t_b}\right)\left(e^{-\lambda_i t_c}\right) \times \left(1 - e^{-\lambda_i t}\right)$$

where ε = efficiency of the neutron counting system, ν = delayed neutron emission rate per fission , m = mass of fissionable nuclide (g), N_A = Avogadro's number, σ_f = fission cross-section (cm^2), Φ = neutron flux to which sample is exposed ($cm^{-2}\,s^{-1}$), M = atomic mass number of fissionable nuclide (g/mol), β_i =fraction of delayed neutrons emitted in group i, λ_i = decay constant of delayed neutron in group i, t_b = irradiation time (s), t_c = decay time (s), t = counting time (s).

Detection efficiency was estimated using the equation and measurement data. The sample which contains 70.263 ng ^{235}U was irradiated for 60 sec. After 20 sec decay time, total delayed neutron counts was measured for 60 sec. Delayed neutron data from three different literature sources was used for the efficiency calculation. The calculated efficiency were 26.97 %, 31.12 %, and 33.16 % for Keepin et al[4], England et al[5], and ENDF/B-IV respectively.

IV. Conclusions

DNAA system was installed in HANARO and evaluated through ORNL/KINAC collaboration effort. The system shows excellent linearity from 0.67 ng to 713 ng ^{235}U, and reproducibility of 1.26% standard deviation for the various mass groups of ^{235}U samples. These results are evidence of the accurate and consistent system control and sample preparation. The ratio of thermal to Epithermal flux is about 476 and thermal flux is 3.28×10^{13} $n \cdot cm^{-2} \cdot s^{-1}$ at the irradiation tube. As a result, interference threshold percentage from fast fission of ^{238}U is relatively small. The DNAA system shows detection efficiency of ~30 % and ^{235}U detection limit of 1ng. In the near future, inter-laboratory comparison of DNAA results will be conducted to provide independent verification and data validation. Also, determination of the concentration of different isotope mixtures, such as ^{235}U and ^{239}Pu, using DNAA system is one of the interesting future works for enlarging the DNAA application.

Acknowledgement

This work was performed under the PCG safeguards arrangement between the United States Department of Energy and the Ministry of Science and Technology of the Republic of Korea to strengthen environmental sampling analysis in ROK and sponsored by Ministry of Science and Technology of Korea.

References

1) D. Glasgow et al, "Fast, Sensitive, and Accurate Fissile Determination for Nuclear Nonproliferation Applications by Neutron Activation Analysis and Delayed Neutron Counting," INMM 45th Annuanl Meeting (2004)
2) F. F. Dyer et al., "A comprehensive study of the neutron activation analysis of uranium by delayed neutron counting," ORNL-3342 (1962).

3) X. Li et al., “Rapid determination of uranium and plutonium content in mixture through measurement of the intensity-time curve of delayed neutrons” Nuclear Instrument . Instr. and Meth. in Phys. Res. B 215, 246–251,(2004)
4) G.R.Keepin, T.F.Wimett and R.K.Zeigler.”Delyaed neutrons from fissionable isotopes of Uranium, Plutonium and Thorium”, J. Nuclear Energy, 6, 1-21 (1957)
5) M.C.Brady and T.R.England,”Delayed neutron dara and group parameters for 43 fissioning systems” Nucl. Sci. and Eng., 103, 129-149 (1989)

Journal of NUCLEAR SCIENCE and TECHNOLOGY, Supplement 5, p. 658–661 (June 2008)

A Correlation of the ^{60}Co and Beta-emitting Radionuclides in the Activated Concrete of KRR-2

Mun Ja KANG*, Sang Bum HONG, Un Soo CHUNG, Jin Ho PARK,
Kun Ho CHUNG, Geun Sik CHOI, and Chang Woo LEE

Korea Atomic Energy Research Institute,
150-1 Dukjin-dong, Yuseong-gu, Daejeon, 305-353 Korea

Dismantling work of the Korean Research Reactor-2 (KRR-2), including its shielding concrete, was completed in 2006. Some parts of the shielding concrete of the KRR-2 were activated by a thermal neutron reaction during operation of the reactor. The levels of gamma and beta-emitting radionuclides in the dismantled concrete are required to be measured and evaluated. The samples were collected from the inner surface to 90 cm horizontal depth on one side of the shielding concrete. The gamma-emitting radionuclides in the activated concrete were analyzed by using HPGe spectrometer. The radioactivities of ^{3}H and ^{14}C were determined by a commercially available tube furnace and liquid scintillation counter and ^{55}Fe and ^{63}Ni by a combined method of an extraction chromatography and a liquid scintillation analysis. A correlation of the measurement results based on the ^{60}Co radioactivity was investigated to estimate the radioactivity level of the activated concrete. The radioactivities of ^{3}H and ^{55}Fe in the dismantled concrete revealed a good correlation with that of ^{60}Co. The correlation formulas are y = 0.77x + 1.68 (r=0.984) and y = 0.96x +1.26 (r=0.995), respectively. In the case of ^{14}C, the correlation is represented as y = 0.60x -1.82 (r=0.998) in the higher range of activity.

KEYWORDS: activated concrete, correlation, cobalt-60, tritium, carbon-14, iron-55, nickel-63

I. Introduction

In the decommissioning of nuclear facilities, the radioactivity inventory of various materials needs to be assessed for the classification and disposal of the nuclear waste. Actually, the dismantling work of the Korean Research Reactor-2 (KRR-2) was completed in 2006.[1] Therefore, various radioactive wastes such as shielding concrete, graphite, metal and the others were generated from its dismantling. The main radioactivity came from the graphite and the shielding concrete. Some parts of the shielding concrete are radioactive due to a neutron activation reaction. The levels of gamma and beta-emitting radionuclides in the activated concrete are required to be measured and evaluated.

Especially in the concrete shield, a variety of radionuclides such as ^{3}H, ^{14}C, ^{55}Fe, ^{60}Co, ^{63}Ni, ^{134}Cs, ^{152}Eu, and ^{154}Eu were included. Of these radionuclides, the gamma emitters such as ^{60}Co, ^{152}Eu, and ^{154}Eu can be determined easily by gamma spectrometry. However, the determination of various beta emitters requires a complete separation of the individual radionuclide from the matrix and from other radionuclides due to a poor energy resolution of the beta spectroscopy.

The main contribution to an accumulation of ^{3}H in the concrete results from the neutron activation reaction ^{6}Li(n,α)^{3}H. A very small amount of ^{3}H probably comes from the reactions ^{2}H(n,γ)^{3}H and ^{3}He(n,p)^{3}H. Tritiated vapor can be exposed and adsorbed into the concrete. The adsorbed HTO is one of source of ^{3}H.

^{14}C is produced in the reactor core due to three neutron reactions: ^{13}C(n,γ)^{14}C, ^{14}N(n,p)^{14}C, and ^{17}O(n,α)^{14}C. In the concrete shielding around the reactor core, the reaction ^{14}N(n,p)^{14}C is the main contributor to ^{14}C due to the high neutron reaction cross section and isotopic abundance of ^{14}N. ^{17}O(n,α)^{14}C may have a slightly higher contribution due to the higher concentration of oxygen in the concrete.

Because ^{3}H and ^{14}C are pure beta emitters, and the energies of their beta particles are relatively low. The $E_{\beta max}$ of ^{3}H and ^{14}C are 18.6 keV and 156.5 keV, respectively. The samples need to be decomposed to separate ^{3}H and ^{14}C from that of the matrix and from other interfering nuclides before a measurement of their radioactivity by a liquid scintillation counting.[2, 3]

^{55}Fe is produced by neutron activation reactions of two major stable iron isotopes: ^{54}Fe(n,γ)^{55}Fe and ^{56}Fe(n,2n)^{55}Fe. Since iron is a component of steel or concrete, and ^{55}Fe is a main contributor to the radioactivity of nuclear waste in the first few years after a reactor operation has stopped. Measurement of ^{55}Fe can be carried out by a low energy gamma and an X-ray detector, but their counting efficiencies are normally very low. The most common and more sensitive technique is a liquid scintillation counting. Due to very low energy of ^{55}Fe, Fe has to be separated completely from other radionuclides before counting.[4]

^{63}Ni is also produced by two neutron reactions with Ni and Cu: ^{62}Ni(n,γ)^{63}Ni, ^{63}Cu(n,p)^{63}Ni, and ^{63}Ni mainly exists in steel materials. Other reactor materials such as graphite, concrete, lead, and Al alloy also contain trace amounts of

*Corresponding Author, Tel No: +82-42-868-2078, Fax No: +82-42-863-1289, E-Mail: munkang@kaeri.re.kr

^{63}Ni. ^{63}Ni is a pure beta emitting radionuclide with maximum beta energy of 66.95 keV and a half-life of 100 years. Liquid scintillation counting, especially for low energy beta emitters, is for the determination of ^{63}Ni. Since nuclear waste contains many different radionuclides, a chemical separation procedure of ^{63}Ni from other radionuclide is required.[4)]

II. Experimental

1. Measurement of Gamma Radionuclides

The samples were collected from the inner surface to a 90 cm horizontal depth on one side of the shielding concrete. The sampling part of shielding concrete of KRR-2 is described in **Fig. 1**. The collected samples were ground and put into a cylindrical vial. The gamma-emitting radionuclides were directly measured by using a well-type HPGe detector and associated electronics (Canberra). The FWHM resolution determined at 1.33 MeV of ^{60}Co was 1.8 keV and relative efficiency was 47.1%.

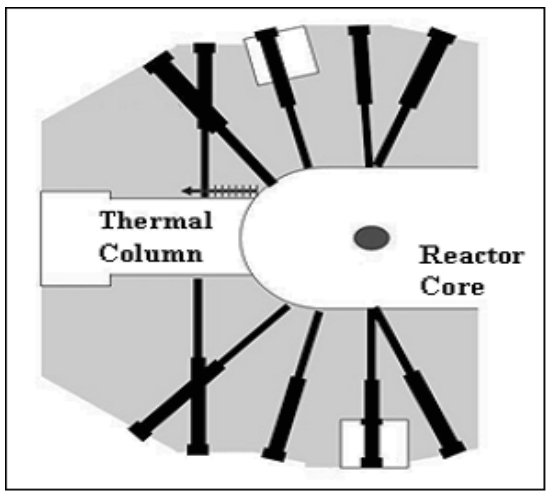

Fig. 1 The structure of shielding concrete of KRR-2 and the sampling part of the concrete

2. Measurement of ^{3}H and ^{14}C Radionuclides

Total tritium and ^{14}C were determined by combusting the concrete in a purpose-designed tube furnace.[5)] The schematic diagram for the combustion and trapping procedure is shown in **Fig. 2**. The solid sample was combusted to 500°C in a silica tube using air or O_2 carrier gas. The combustion products were passed over a Pt-alumina catalyst and heated to 800°C, to ensure a complete conversion of the tritiated species to tritiated water, and ^{14}C to $^{14}CO_2$. The tritiated water was then trapped in HNO_3 bubblers, and the $^{14}CO_2$ was trapped in Carbosorb bubblers. The ^{3}H and ^{14}C collected in the bubblers were then measured by using a liquid scintillation counter (Wallac 1220 Quantulus).

3. Measurement of ^{55}Fe and ^{63}Ni Radionuclides

^{55}Fe and ^{63}Ni were determined by a combined method of an extraction chromatography and a liquid scintillation counting.[6)] First, the concrete sample was digested by an aqua regia. Fe of the dissolved sample was separated by a precipitation with a pH adjustment. Ni was remained in the supernatant. The precipitate of $Fe(OH)_3$ was purified by extraction chromatography using diisobutyl ketone (DIBK) resin. The supernatant including Ni was also purified by an extraction chromatography using dimethyl glyoxime (DMG) resin. ^{55}Fe or ^{63}Ni in the elute was measured by using liquid scintillation counter (Wallac 1220 Quantulus). The chemical recovery was determined by the concentration difference of Fe and Ni in the initial and final solutions. Stable Fe and Ni were measured by using ICP-atomic emission spectroscopy (Jobin Yvon, Ultima 2C). The DIBK resin was prepared by adding technical grade DIBK to Eichrom pre-filter materials. The DMG resin was made by mixing DMG, pre-filter material, and acetone. The schematic diagram for the determination of ^{55}Fe and ^{63}Ni is shown in **Fig. 3**.

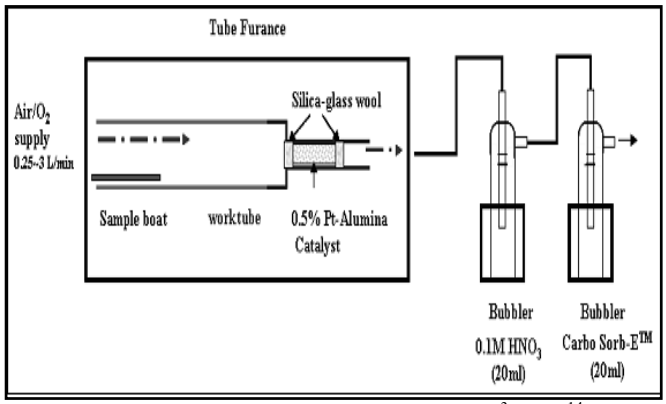

Fig. 2 Schematic diagram for the determination of ^{3}H and ^{14}C using oxidation combustion method

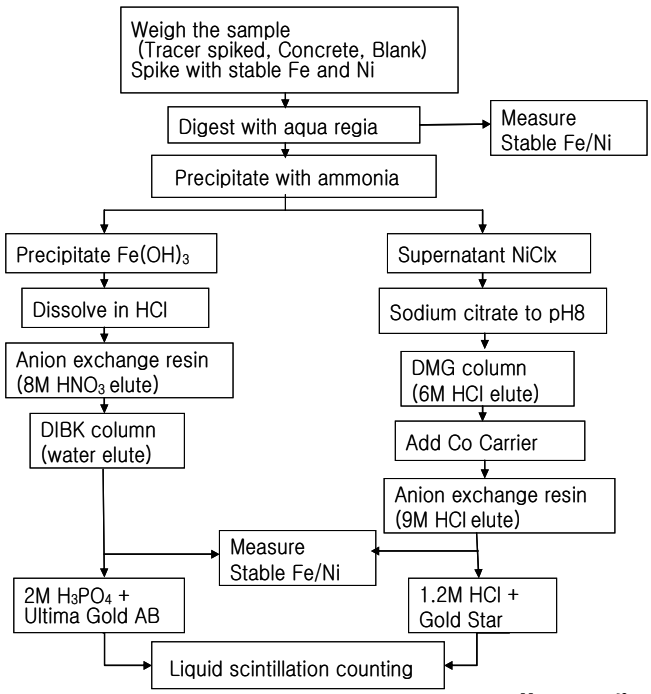

Fig. 3 Schematic diagram for the determination of ^{55}Fe and ^{63}Ni using extraction chromatography and LSC

Table 1 The radioactivity of the gamma-emitting and beta-emitting radionuclides in the dismantled concrete

Sampling depth (cm)	Radionuclides					
	^{60}Co	^{152}Eu	^{3}H	^{14}C	^{55}Fe	^{63}Ni
0-10	102	43.1	1690	0.25		
10-20	32.5	18.6	628	0.11		
20-30	19.4	7.72	286	0.09	362	<0.13
30-40	3.50	2.49	251	0.03	43.8	<0.22
40-50	1.09	0.38	47.6	0.03	22.5	<0.13
50-60	0.58	0.22	35.2	0.03	10.7	<0.15
60-70	0.24	0.18	18.9	0.03	5.25	<0.18
70-80	0.11	<0.01	10.4	0.03	2.03	<0.12
80-90	0.06	<0.01	3.21	0.03		

III. Results and Discussion

1. Gamma-Emitting Radionuclides in the Activated Concrete

The gamma-emitting radionuclides in the activated concrete were ^{60}Co, ^{134}Cs, ^{152}Eu, and ^{154}Eu. The dominant radionuclides are ^{60}Co and ^{152}Eu. The radioactivity of ^{60}Co and ^{152}Eu in the samples is summarized in **Table 1**. The radioactivity of ^{60}Co was measured from 0.06 Bq/g to 102 Bq/g. The minimum level of the radioactivity of ^{60}Co was obtained at the 80-90 cm depth from the surface and its maximum value was at the inner surface. ^{152}Eu was detected with a radioactivity of 43.1 Bq/g at the inner surface and below MDA at the 70-90 cm depth from the surface. ^{134}Cs and ^{154}Eu were only detected in the samples near to the surface.

2. ^{3}H and ^{14}C Radionuclides in the Activated Concrete

The radioactivity of ^{3}H and ^{14}C in the concrete samples is listed in **Table 1**. The radioactivity of ^{3}H or ^{14}C in a sample, *As*(Bq/g), was calculated by the following equation.

$$As = \frac{(Cs - C_B)}{60} \times \frac{100}{E} \times \frac{1}{M} \times \frac{(m_f - m_t)}{M_s} \times \frac{100}{R} \qquad (1)$$

Cs and C_B are the cpms of the concrete and background samples, respectively. *E* means the efficiency of LSC and *M* is the weight of the concrete sample. *Ms* is the mass of the bubbler solution for an analysis. m_f and m_t are the weights of the bubbler before and after the experiments, respectively. *R* is the recovery of the tube furnace using a tracer. The minimum level of the ^{3}H radioactivity in the dismantled concrete was obtained as 3.2 Bq/g at a depth of 80-90 cm from the surface and its maximum value of 1690 Bq/g was at the inner surface. In the case of ^{14}C, the radioactivity is a constant value of 0.03 Bq/g from 30 cm to 90 cm depth. At near the inner surface, the radioactivity of ^{14}C is distributed from 0.03 to 0.25 Bq/g. The specific activities of ^{3}H and ^{14}C tend to decrease exponentially to the investigated depth of the concrete from the surface. In this procedure, the counts of the background samples of ^{3}H and ^{14}C were obtained as 0.27 cpm and 1.24 cpm, respectively. The Minimum Detectable Activity (MDA) was calculated by Currie's equation.[7] The MDAs of ^{3}H and ^{14}C are 0.048 and 0.028 Bq/g in this experiment.

3. ^{55}Fe and ^{63}Ni Radionuclides in the Activated Concrete

The radioactivity of ^{55}Fe and ^{63}Ni in the concrete samples is also listed in **Table 1**. The radioactivity of ^{55}Fe and ^{63}Ni in the sample was calculated by the following equation

$$As = \frac{(Cs - C_B)}{60} \times \frac{100}{E} \times \frac{1}{M} \times \frac{100}{R} \times \exp(\ln 2 \frac{\Delta t}{t}) \qquad (2)$$

Cs and C_B are the cpms of the concrete and background samples, respectively. *E* means the efficiency of LSC and *M* is the mass of sample. *R* is the recovery of the separation procedure by stable Fe and Ni measurements. *t* is a half-life of the radionuclide and Δt is the time difference for a measurement and a sampling. The radioactivity level of ^{55}Fe in the concrete sample was measured from below MDA to a maximum of 362 Bq/g. In the case of ^{63}Ni, all the samples had a radioactivity level below MDA. The radioactivity of ^{55}Fe decreased with the increased depth of the concrete from the inner surface. The counts of the background sample were obtained as 1.07 cpm and 1.87 cpm in the ^{55}Fe and ^{63}Ni experiments, respectively. The MDAs of ^{55}Fe and ^{63}Ni are calculated as 0.015 and 0.017 Bq/g.

4. A Correlation of ^{60}Co and Beta-Emitting Radionuclides

The correlation between ^{60}Co and ^{3}H or ^{14}C in the activated concrete from KRR-2 is shown in **Fig. 4**. The radioactivity of ^{3}H revealed a good correlation with that of ^{60}Co. The correlation formula and correlation coefficient are y = 0.77x + 1.68 and r = 0.984, respectively. In the case of ^{14}C, the correlation is represented as y = 0.60x – 1.82 (r=0.998) in the higher range of radioactivity. In the lower range of ^{60}Co radioactivity, the radioactivity of ^{14}C is constant. The correlation between ^{60}Co and ^{55}Fe in the dismantled concrete is shown in **Fig. 5**. The radioactivity of ^{55}Fe is in good correlation with that of ^{60}Co. The correlation formula is y = 0.96x + 1.26 and the coefficient is r=0.995.

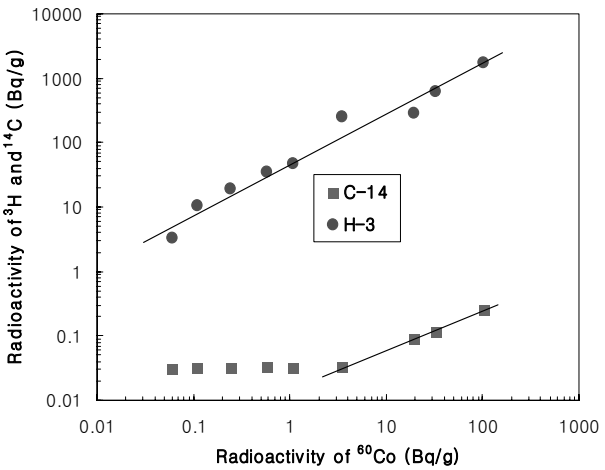

Fig. 4 The correlation of ^{60}Co and ^{3}H or ^{14}C in the activated concrete

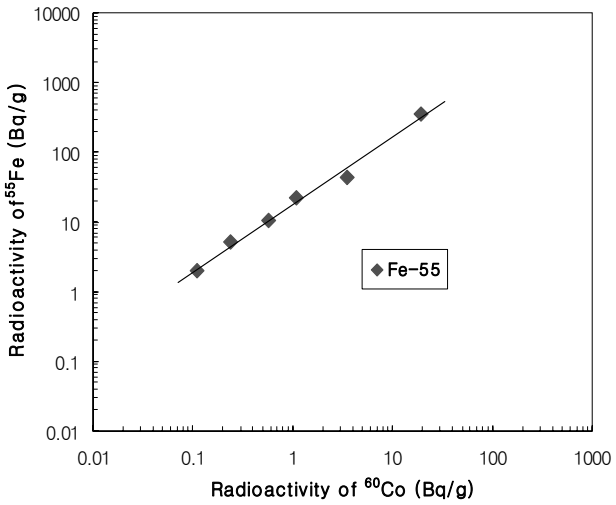

Fig. 5 The correlation of ^{60}Co and ^{55}Fe in the activated concrete

IV. Conclusions

The levels of gamma and beta-emitting radionuclides in the dismantled concrete of KRR-2 were measured. The specific activities of ^{60}Co, ^{3}H, and ^{55}Fe tended to decrease exponentially to a 90 cm depth from the inner surface of the concrete. In the case of ^{14}C, the radioactivity is a constant value of 0.03 Bq/g at a depth deeper than 30 cm. The radioactivities of ^{63}Ni in all the concrete samples were below MDA. A correlation of ^{60}Co and beta-emitting radionuclides was evaluated. The radioactivities of ^{3}H and ^{55}Fe in the dismantled concrete revealed a good correlation with that of ^{60}Co. The correlation formulas are y = 0.77x + 1.68 (r=0.984) and y = 0.96x +1.26 (r=0.995), respectively. In the case of ^{14}C, the correlation is represented as y = 0.60x -1.82 (r=0.998) in the higher of radioactivity. These correlations of the beta-emitting radionuclides with ^{60}Co could be useful to predict the radioactivity level of an activated concrete. This approach can also be applied for the other types of radioactive waste.

Acknowledgements

This work has been carried out under the Nuclear R&D program by MOST.

References

1) K. W. Lee, S. K. Park, S. B. Hong, U. S. Chung, and J. H. Park, "Experiences of the dismantling on non-activated and activated bio-shielding concrete of KRR-2," Proceedings of the 7th joint workshop between China and Korea, 271 (2006)
2) X. Hou, "Rapid analysis of ^{14}C and ^{3}H in graphite and concrete for decommissioning of nuclear reactor," Applied Radiation and Isotopes, 62, 871 (2005).
3) A. Endo, Y. Harada, K. Kawasaki, and M. Kikuchi, "Measurement of depth distributions of ^{3}H and ^{14}C induced in concrete shielding of an electron accelerator facility," Applied Radiation and Isotopes, 60, 955 (2004)
4) X. Hou, L. F. Østergaard, and S. P. Nielsen, "Determination of ^{63}Ni and ^{55}Fe in nuclear waste samples using radiochemical separation and liquid scintillation counting," Analytica Chimica Acta, 535, 297 (2005).
5) S. B. Hong, H. R. Kim, et al, "Spatial distribution of ^{3}H and ^{14}C in the shielding concrete of KRR-2," J. of the Korean Radioactive Waste Society, 4(4), 329 (2006)
6) P. E. Warwick and I. W. Croudace, "Isolation and quantification of ^{55}Fe and ^{63}Ni in reactor effluents using extraction chromatography and liquid scintillation analysis," Analytica Chimica Acta, 567, 277 (2006).
7) L. Currie, "Limits of qualitative determination and quantitative determination," Anal. Chem., 40(3), 586 (1968)

Journal of NUCLEAR SCIENCE and TECHNOLOGY, Supplement 5, p. 662–665 (June 2008)

The Establishment of an In-Situ Real Time Radiation Contour Mapping Technique

Hee Reyoung KIM*, Wanno LEE, Mun Ja KANG, Kun Ho CHUNG, Young Hyun CHO, Geun Sik CHOI, and Chang Woo LEE

Korea Atomic Energy Research Institute, Daejeon 305-353, Korea

The goal of this study is to present that an in-situ radiation dose distribution on an area measured by using a gamma radiation measuring instrument is grasped without a delay. Fundamentally, the test includes an area map as well as real numerical data from the measured area. The map is a computer file with a format of 'bmp' which is used in the gamma radiation measuring instrument, and the data is a text file which has numerical values of the latitude, longitude and radiation dose rates of the measured points. The radiation dose rates of the unmeasured points in the area are displayed through an interpolation with those of the measured ones. A 2D plot shows the contour lines with an overlapped map image and a 3D one gives contour lines on the z-axis for an immediate understanding of the radiation level. It is available to optionally display the numerical values of the radiation dose rates and to zoom up and down the image of a certain part for a detailed view. This contour mapping method programmed by using a commercial software requires only a mouse click to show in-situ in a real time the radiation distribution on the corresponding map in a laptop window screen.

KEYWORDS: gamma radiation distribution, in-situ real time contour mapping, transmission of the radiation dose information

I. Introduction

The goal of an environmental radiation monitoring (ERM) is to keep the public safe from radiation from nuclear installations or a nuclear emergency. In general, an ERM is carried out because of social, political and technical reasons such as a compliance with statutory legislation, an assessment of the radiation exposure of the public, public reassurance and information, research, the establishment of preoperational radiation levels, and assistance in an emergency situation.[1)] An ERM process has been accomplished for nuclear safety by tracing the environmental changes due to the operations of a nuclear installation all over the world.[2-4)] In Korea, a regular or routine environmental radiation monitoring is being carried out around nuclear installations such as research reactors and nuclear power plants based on a statutory obligation by the Atomic Energy Act.[5)] In fact, a continuous monitoring result at a specific spot, where the environmental radiation monitor is installed, is in-situ displayed and transferred to the main station in a real time.[6)] Also many portable commercial gamma radiation detecting systems provide the function of a radiation level measurement and file storage. However, few radiation monitoring systems are available for understanding in a real time an overall distribution of a radiation level over an arbitrary region surveyed in spite of these environmental radiation monitoring activities at fixed points. So, to overcome this limit and to observe the dose distribution without a delay right after a survey, a fundamental technique for an in-situ real time contour mapping of the radiation level over a region is established by using commercialized software in this paper. At present, a commercialized mobile monitoring system with a GPS (Geographical Positioning System) is used as an environmental gamma radiation measurement hardware. The gamma radiation dose rates are actually measured around the research reactor installations of Seoul and Daejeon in Korea. The contour of the radiation dose rate is displayed on the corresponding map according to the latitude and longitude in a real time with a mouse click action in the developed program.

II. Materials and Methods

1. Description of a Mobile Gamma Radiation Monitoring System

The equipment employed for measuring the radiation level is a commercialized mobile detection system, FHT1376. The hardware consists of a high sensitive 5 liter plastic scintillation detector (~ 3 MeV), electronics called a NBR (Natural Background Reduction) detector and a GPS (Geographical Positioning System) as seen in **Fig. 1**. The embedded program represents the radiation dose level numerically and graphically in the notebook computer according to time while the vehicle with the device moves over the corresponding area. Finally it generates a text file with the radiation level data and geographical information which can be commonly accessed and managed.[7)] The file has more than 10 information points including the stored file path, data entry, date, time, dose rate, latitude and longitude. But it can not display in-situ the radiation contour in a real time on the map of the measured region.

2. The Radiation Contour Mapping Program

MATLAB, which is a commercial software with a function of a mathematical calculation and graphical

*Corresponding Author, Tel No: +82-42-868-2048, Fax No: +82-42-863-1289, E-mail: kimhr@kaeri.re.kr

visualization, is used for a real time contour mapping. First of all, the text file generated after the measurement of a region is brought to the MATLAB space. The text file with an extension of "txt" has various information as represented in **Fig. 2** where the fourth, eighth and ninth column are the total dose rate, longitude and latitude, respectively. Then, three columns corresponding to information on the longitude, latitude and dose rate are needed and extracted by file I/O commands.

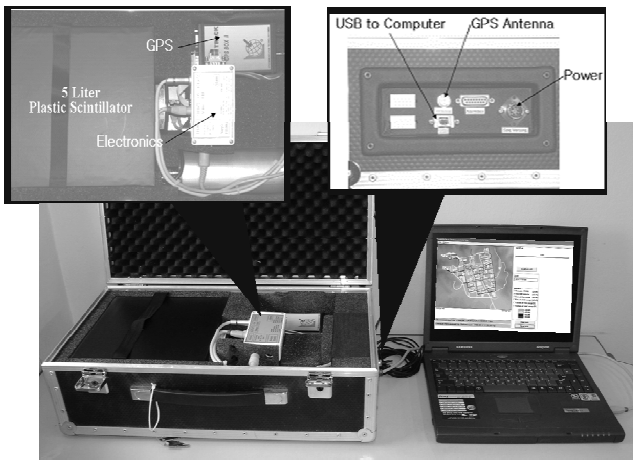

Fig. 1 The mobile environmental radiation monitoring system (FHT 1376) connected to a notebook

File ::c:\progra~1\mobisys\daten\kimhr1~1.bin
Route :;Unkown route - 2007-03-10 9:28:26
Data entry:;985
Date;Time;FH40G-dosrate;total dosrate;dosrate artif. low;dosrate artif. mid;Status;Longitude;Latitude;
Altitude;Speed;Direction;GPS-Status; GPS-Source;GPS-Time
[dd.mm.yyyy];[hh:mm:ss];[nSv/h];[nSv/h];[nSv/h];[nSv/h];;[?;[?;[m];[km/h];[?;;;[s]UTC
10.03.05;09:28:46;0000000.000;**00064.950**;00000.474;00001.257;0;**127.08500**;**036.63350**;067;000;000;2;1;030527
10.03.05;09:28:47;0000000.000;**00061.500**;00001.435;00001.384;0;**127.08550**;**036.63355**;067;000;000;2;1;030529
10.03.05;09:28:48;0000000.000;**00067.700**;00000.617;00001.310;0;**127.08560**;**036.63360**;067;000;000;2;1;030529
10.03.05;09:28:49;0000000.000;**00064.650**;00000.589;00000.423;0;**127.08570**;**036.63400**;067;000;000;2;1;030531
10.03.05;09:28:50;0000000.000;**00067.000**;00001.209;00000.220;0;**127.08565**;**036.63450**;067;000;000;2;1;030531
.
.
.

64.950 127.08500 36.63350
61.500 127.08550 36.63355
67.700 127.08560 36.63360
64.650 127.08570 36.63400
67.000 127.08565 36.63450
.
.
.

Fig. 2 The Example Extraction of dose rate, latitude and longitude from the original text file of FHT 1376

The program is composed by using such commands as "mesh" and "contour" which were provided by MATLAB for displaying the contour. Next, the map file with the extension of "bmp" is also brought to the MATLAB space and programmed by using corresponding commands to display the map and contour at a plotting area.[8-11] Then, the program which is composed of a series of the corresponding commands and syntaxes is stored in an appropriate file name. It is finally converted to an execution file, for example, "contouring.exe" so that it is available by a mouse click in the window OS without MATLAB software as seen in **Fig. 3**.

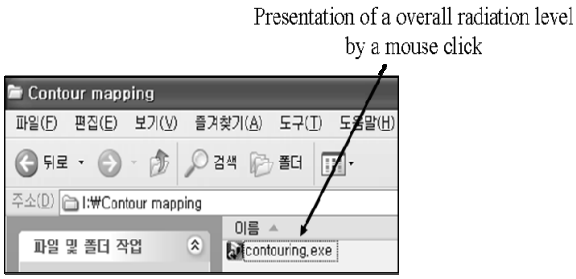

Fig. 3 The radiation contour mapping by a mouse click of an execution file

On the other hand, the radiation level values of the unmeasured points are interpolated by using the measured data points. The default method provided by a MATLAB contour and grid function is adopted for this program. That is, the interpolation is carried out by using the piecewise cubic spline method where the numerical values of the secondary derivative at the first and last ends is zero as a boundary condition. In the same way, the image, which is the map corresponding to the measured area, has the interpolation procedure between pixels where the coordinate values of the longitude and the latitude have not been assigned. The bicubic interpolation provided basically by MATLAB is employed for the purpose of a better accuracy in spite of taking a longer computation time than the other methods. The zoomed image with a numerical presentation of the radiation level is available by this interpolation on the pixel of an image.

III. Actual Application to Environmental Monitoring around Nuclear Installation Sites

To verify the developed in-situ contour mapping program, the measurement of a radiation level was carried out by moving the vehicle with the mobile detection system in the Seoul and Daejeon sites which had research reactor installations as represented in **Fig 4**.

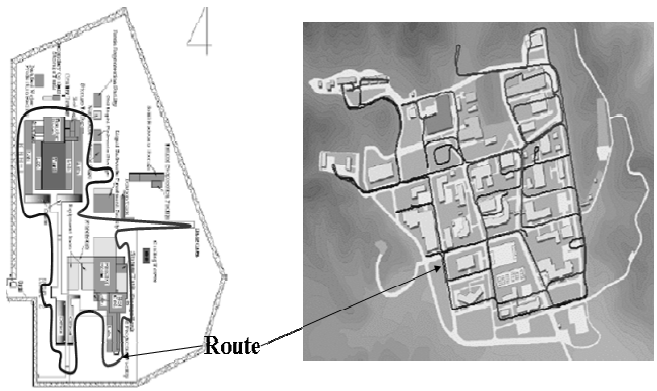

(a) Seoul site (b) Daejeon site

Fig. 4 The measurement for verifying the developed program

Right after surveying the corresponding area of **Fig. 4 (a)** and **(b)**, a mouse click graphically displayed in-situ a radiation distribution by a real time contour mapping in the form of two and three dimensions, as represented in **Fig. 5 (a)** and **(b)**. First of all, the comprehensive distribution of the radiation level is displayed with the labeled figures over the corresponding map. Especially, the relative difference of the radiation level is directly understood by the help of a 3D surfacing and the color bar representing its intensity. In the Seoul sites, the research reactor has been dismantled and the radioactive wastes, which were low or extremely low level radioactive wastes, were stored in the temporary waste storage when all the dismantled wastes were taken out from the research reactor hall. Accordingly, the radiation level is expected to be relatively high at the temporary waste storage and as such the in-situ real time contour mapping program also displayed that the radiation level was high around the temporary waste storage as seen in **Fig. 5 (a)**. In the Daejeon sites, HANARO with a thermal output of 30 MW, which is a facility that produces radioisotopes and that performs various nuclear experiments, has been operated since 1995. Therefore, the radiation level is expected to be relatively high at the radioisotope product facility and it was actually higher than the other points as seen in **Fig. 5 (b)**.

On the other hand, the specific part that a user wants to see in detail is zoomed in and out by a mouse dragging as represented in **Fig. 6**. Also, the numerical figure of the radiation level is labeled in the contour lines of the zoomed area.

IV. Results and Discussion

By the contour mapping tool, the time requested from the start of the measurement to display the radiation distribution was tremendously reduced. It has taken more than five hours to obtain the complete contours after surveying the regions when the measurement and file editing and contour mapping were carried out separately. First of all, in **Fig. 5 (a)** and **(b)**, the horizontal and vertical axes of the overlapped map with the contour represent the same values of the longitude and latitude as the measured area. The numbers of measured data points were 1,428 and 3,320, respectively from the measurement experiments at the Seoul and Daejeon sites which have an area of a few ten thousand square meter and a few square kilometer,. In **Fig. 5 (a)** and **(b)**, the values of the radiation level at most points in the Seoul and Daejeon sites were approximately 80 nSv/h. Those of the surroundings of the temporary waste storage in the Seoul site were between 150 nSv/h and 300 nSv/h in **Fig 5. (a)**. And those of the radioisotope product facility in the Daejeon site were between 150 nSv/h and 800 nSv/h in **Fig 5. (b)** as already predicted.

On the other hand, comparing these values by using the present contour mapping program with the actual measurement values, the maximum values of the radiation level at the Seoul and Daejeon sites, 300 nSv/h and 800 nSv/h, were more or less higher than those of the actual measurement, 270 nSv/h and 750 nSv/h. The relative errors are 11.1 % and 6.7 % each. In fact, the points corresponding to the value of 300 nSv/h and 800 nSv/h were the ones where a measurement of the activity by the vehicle could not be conducted because they were inside the buildings. It was thought that these discrepancies were caused by the interpolation between the unmeasured points during the contour mapping procedure of this program.

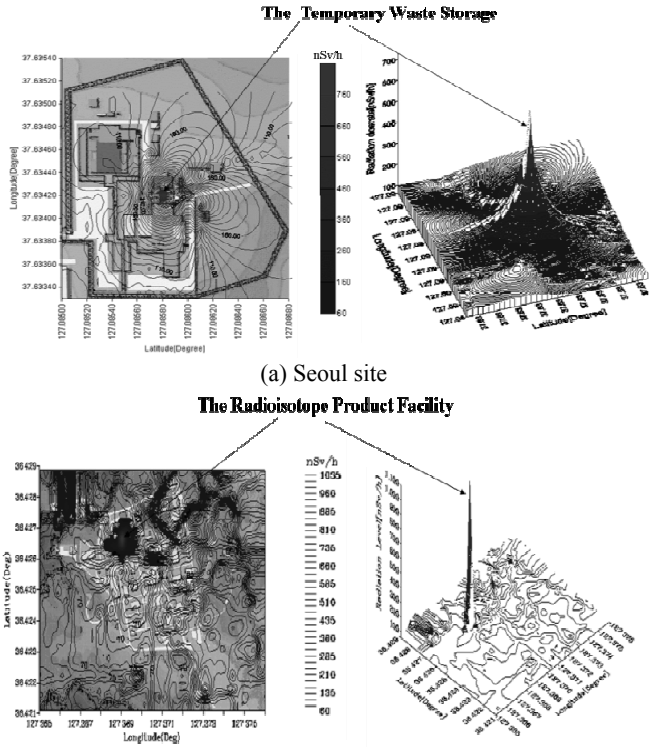

(a) Seoul site

(b) Daejeon site

Fig. 5 2D and 3D contour mapping image by the developed program

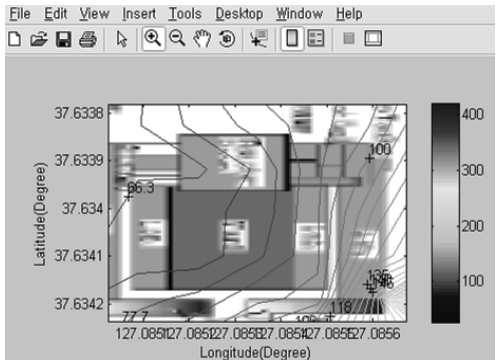

Fig. 6 The zoomed and labeled image for a specific part of the measurement area

Especially, it was grasped that the wider the variation of the values of the measured ones was according to the longitude and latitude, the larger the fluctuation of the interpolated values was. But it was understood that the errors due to the interpolation in these experiments did not distort the actual situation so much, by considering that the present study aimed to represent a comprehensive and general distribution of a radiation level over a measured area. In **Fig.**

6, the numerical values of the radiation level were between 78 nSv/h and 135 nSv/h and the interval between the contour lines has some difference at the upper left part and lower right part. Therefore, it is predicted that the lower right part has a more rapid change than the upper left one. Actually, the lower right part is nearer to the temporary waste storage than the upper left part is. So the value of the radiation level was increased rapidly near the lower right part while the upper left part had a little change of the radiation level. As a result, the developed contour mapping program managed to immediately display the general information such as the overall radiation distribution and the changing rate at a specific part.

V. Conclusions

The hardware of the gamma radiation detector and software of the radiation contour mapping program were integrated so that the comprehensive distribution of the radiation level could be in-situ displayed without a delay as soon as the survey was finished. This study showed that an immediate in-situ radiation contour mapping was possible by only one mouse click of the corresponding execution file. The comprehensive distribution of the radiation level on the measured area could be understood by the help of a simple contour mapping program. The developed contour mapping program showed the possibility that it could be practically used to grasp the radiation information on the relevant regions due to the abnormal operation of a nuclear facility or a nuclear accident, qualitatively and promptly. It is understood that the fundamental approach of the present specific detector model could be extended to a general measurement system.

Acknowledgement

This work has been carried out under the Nuclear R&D program by Korea Ministry Of Science and Technology.

References

1) A. R. Ware, C. W. Fern, "The need and requirements for environmental monitoring", Nuclear Europe **3**[4], 20 (1988).
2) Wendy Peters, "Radiation monitoring and local authorities", ATOM **378**, (1988).
3) D. van Lith, "Duch environmental monitoring for nuclear emergencies", Nuclear Europe **5**[6], 20 (1989).
4) A. Buhling, et al., "Integrated measurement & information system for surveillance of environmental radioactivity in F.R.G. ", Nuclear Europe **3**[4], 22 (1988).
5) C. W. Lee, et al., *Environmental Radiation Monitoring Around the Nuclear Facilities*, KAERI/RR-2723/2006, Korea Atomic Energy Research Institute, (2006).
6) H. R. Kim, et al., "The development of an on-line ERM system for the research reactors in Korea", Nuclear Instruments and Methods in Physics Research A, in press, (2007).
7) Thermo Electron Corporation, *FHT 1376 Mobile Radioactivity and GPS Detection System*, Operation Manual, (2004).
8) The MathWorks, *Image Processing Toolbox*, User's Guide, Natick, (2005).
9) P. C. Hansen, et al., *Deblurring Images*, 19 Siam, (2006).
10) R. C. Gonzalez, et al., *Digital Image Processing*, Prentice-Hall, 16 (2004).
11) H. R. Yu, et al., Data Analysis in Oceanography using MATLAB, Ajin, 181 (2006).

Journal of NUCLEAR SCIENCE and TECHNOLOGY, Supplement 5, p. 666–669 (June 2008)

Radiological Dose Assessment and Survey of a Radioactive Contamination in Foodstuffs

Wanno LEE[1*], Kun-Ho CHUNG[1], Hee Reyoung KIM[1], Young Hyun CHO[1], Mun Ja KANG[1], Geun Sik CHOI[1], Ji Yeon KWAK[1], Chang Woo LEE[1], Sung-Kug PARK[2], Soojung Hu[2], and Dongmi CHOI[2]

[1]*Korea Atomic Energy Research Institute, Daedeok-daero, Yuseong-Gu, Daejeon, Korea*
[2]*Korea Food & Drug Administration, Jinheung-Ro, Eunpyung-Gu Seoul, Korea*

Radiological dose assessments and surveys of a radioactive contamination have been performed for domestic and imported foodstuffs since 2003. The following samples among the imported foodstuffs were selected from open markets; one group is imported foodstuffs and the other group is domestic foodstuffs produced from around nuclear facilities. These included imported samples from a country associated with the Chernobyl nuclear accident, samples produced around nuclear power plants or nuclear tests, and foodstuffs reported as radioactively contaminated materials in a foreign country. After pretreatments such as a drying and homogenization, the samples were analyzed. Only the ^{137}Cs radionuclide was measured from among the regulation radionuclides(^{137}Cs, ^{134}Cs, ^{131}I) of the Korea food code. All foodstuffs except Inonotus Obliquus (Chaga mushooms) were less than 25.24 Bq/kg or below the minimum detectable activity (MDA). The average activity concentrations of 203 mushroom samples was 38.60 Bq/kg but the effective dose was also far less than 1 mSv/yr. Based on the radiological dose assessments and surveys of a radioactive contamination, the radioactivity of the domestic and imported foodstuffs has not shown any significant levels during recent years in Korea.

KEYWORDS: radioactive contamination, radioactivity of foodstuffs, ^{137}Cs radionuclide

I. Introduction

After the Chernobyl nuclear accident in 1986, radiological dose assessment and survey of a radioactive contamination for foodstuffs has been investigated. Especially, a lot of countries including EU, Japan, USA has strengthened the radioactive contamination survey of imported foodstuffs[1-5]. Based on surveys of a radioactive contamination for foodstuffs in Korean open markets since 2003, radiological dose assessment via the food chain was studied for the regulation radionuclides (^{137}Cs, ^{134}Cs, ^{131}I) of Korean food code[6] from among the gamma-emitting radionuclides.

II. Sampling and Analysis Methods

1. Sampling Methods

Sampled foodstuffs are collected from the open markets; one group is imported foodstuffs and the other group is domestic foodstuffs produced around nuclear facilities and northeast of Sokcho city concerning recent situations.

The import foodstuffs were as follows; the imported samples from a country associated with the Chernobyl nuclear accident, samples produced around nuclear power plants or nuclear tests, and foodstuffs reported as radioactively contaminated materials in foreign countries. Samples are usually bought from traditional markets, marts, department stores or the internet. After pretreatments such as a drying, ashing, and homogenization, all the samples were analyzed by a gamma spectrometer system for a survey and assessment of radioactive contamination. In **Fig. 1**, the sampling area and quantitative sampling number are shown.

2. Analysis Methods

A nondestructive gamma spectrometry system is used to identify and measure the radioactive concentration of gamma-ray emitting radionuclides in foodstuffs by the high-purity germanium (HPGe) detector. It is applicable to nuclide emitting gamma rays with energies from 50 keV to 3 MeV. This method includes procedures for an energy and efficiency calibration, an analysis of spectra, the determination of an activity concentration of various radionuclides in a studied sample, and a combined uncertainty calculation. It is only applicable to homogeneous samples.

3. Calculation of Activity and Uncertainty

The specific activity, A, of a gamma emitting radionuclide in a sample, is calculated as follows;

$$A=\frac{N}{m\times\varepsilon\times\gamma\times t\times K_i}, \qquad (1)$$

where N, is the corrected net counts of the corresponding photopeak; m, is the mass of a measured sample; ε, is the efficiency factor; γ, is the emission probability of a gamma ray corresponding to a peak energy; t, is the measurement time; K_i, is the correction factors.

*Corresponding Author, Tel No: . +82-42-868-2324, Fax No: +82-42-863-1289, E-mail: petor@kaeri.re.kr

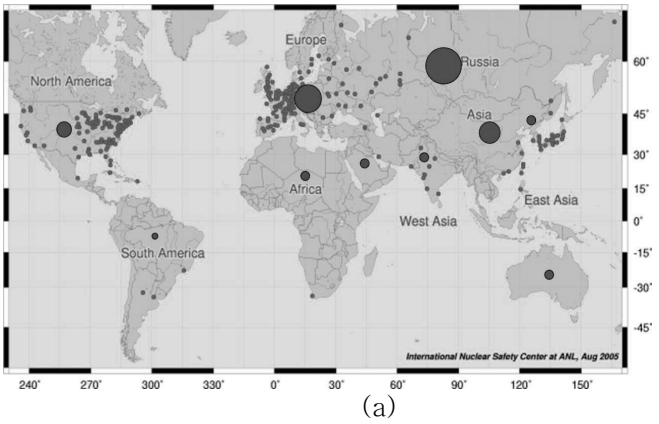

(a)

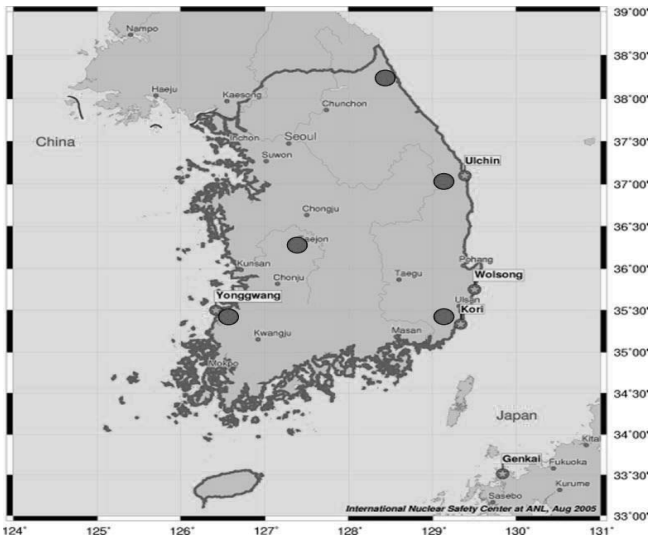

(b)

Fig. 1 Sampling area, (a) the producer countries of the imported foodstuffs: the circles are a sampling area, the size of circles means the sampling number of foodstuffs, the circles are the locations of nuclear power plants, (b) national producing area of foodstuffs are selected in this study.

If the measured value is above a background at a level of confidence of 95%, then the concentration of the radionuclide is reported. The reported uncertainty is based on a combined standard uncertainty (u_c) multiplied by a coverage factor (k) = 2 (providing a level of confidence of 95 %). The relative uncertainty is described as follows;

$$r(u_c)=\sqrt{(\frac{u(N)}{N})^2+(\frac{u(\varepsilon)}{\varepsilon})^2+(\frac{u(m)}{m})^2+(\frac{u(\gamma)}{\gamma})^2+(\frac{u(K_i)}{K_i})^2} \qquad (2)$$

4. Radiation Dose Assessment

The releaseed radiation source determines the crtical pathways in the environment between the point of discharge and human[7]. **Fig. 2** illustrates the pathways of radinuclides to human. In this paper, the activity concentration was surveyed in foodstuffs and the radiation dose was also eveluated. The equation for the effective dose by an ingestion of a food is expressed by (3)

$$H_r = \Sigma D_r C_{rf} U_f \,(\mathrm{mSv/y}) \qquad (3)$$

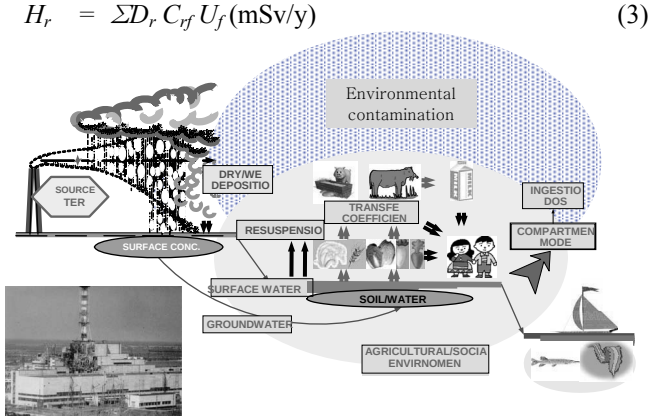

Fig. 2 Pathway of a dose to human from a radiation accident or release

where H_r is the effective dose by an ingestion of nuclide r, D_r, is the effective dose conversion factor by an ingestion of nuclide r, in mSv/Bq (^{137}Cs : 1.3×10^{-5}), C_{rf} is the activity concentration of nuclide r in the ingested food, in Bq/kg or Bq/L, and U_f is the consumption rate of the foodstuffs, in kg/y or L/y.

III. Results and Discussions

The 528 imported foodstuffs and 72 domestic samples were analyzed. The ^{131}I radionuclide wasn't detected among all the foodstuffs. The ^{137}Cs radionuclide among the regulation radionuclides (^{137}Cs, ^{134}Cs, ^{131}I) of the food code was only detected for the imported foodstuffs. All foodstuffs except for Inonotus Obliquus (Chaga mushooms) were less than 25.24 Bq/kg or below the minimum detectable activity (MDA). **Table 1** shows the activity concentration of Inonotus Obliquus (Chaga mushrooms) surveyed in 2003 year and it showed the highest valve among all imported foodstuffs. The average activity concentration of 203 mushroom samples were 38.60 Bq/kg but the effective dose was far less than 1 mSv/yr. The reported average activity concentrations since 2003 are shown in **Fig. 4**. The results of the radiological dose assessment show that the annual effective dose rate of all the foodstuffs is far less than 1mSv/yr which is dose limit to the public. Although the activity of Inonotus Obliquus is some what higher than that of other foodstuffs, the annual effective dose is not a significant level when the consumption rate is considered. As shown in **Table 2**, the annual effective dose by the mushrooms which had the highest radioactivity level, is about 8.44E-02 % of the dose limit for the public. In the case of the domestic foodstuffs, the average radioactivity shown in **Table 3**, is overestimated because the MDA(minimum detective activity) is set from 1 Bq/kg to 3.7 Bq/kg which is 1 % of the maximum permitted level of the Korean Code written by KFDA(Korea Food Drug and Administration). Therefore, if the radioactivity of a foodstuff is not detected, its activity is determined by MDA value for a conservative dose assessment. The average radioactivity of grains shown in **Table 3** is lower than the level of MDA. These results

mean that the effective dose by the imported and domestic foodstuffs could be negligible.

Table 1 The 137Cs radioactivity of Inonotus Obliquus foodstuffs (chaga Mushrooms) surveyed in 2003 year: "<" means less than MDA (Minimum Detectable Activity).

Food type	Foodstuffs	Country	^{137}Cs (m ± σ) Bq/kg
Mushrooms	Inonotus Obliquus (Chaga)	Russia	83.48±5.31
		Russia	131.25±1.32
		Russia	34.85±3.21
		Russia	22.97±2.71
		Russia	22.27±2.93
		Russia	20.34±2.78
		Russia	32.38±3.33
		Russia	35.23±3.40
		Russia	31.80±3.11
		Russia	24.37±2.80
		Russia	21.88±3.68
		Russia	12.58±2.35
		Russia	22.30±2.84
		Russia	24.35±3.46
		Russia	11.88±2.11
		Russia	13.20±2.42
		Russia	40.65±3.96
		China	29.43±3.28
		China	13.27±2.10
		N.Korea	22.92±3.16
		Russia	25.65±3.00
		Russia	12.83±2.20
		Russia	31.29±3.64
		Russia	12.86±2.21
		Russia	13.2±1.08
		N.Korea	< 3.06
		N.Korea	3.19±1.01

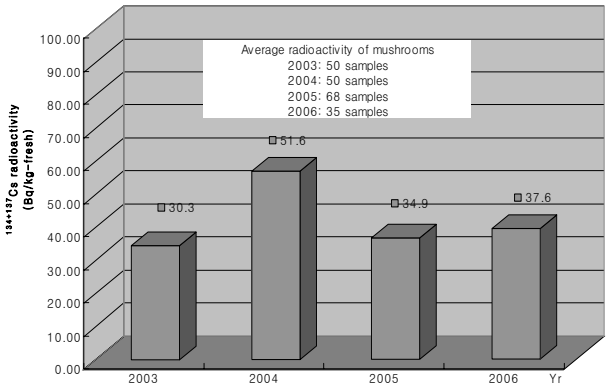

Fig. 4 Radioactivity distribution for mushrooms among the imported foodstuffs since 2003.

Table 2 Effective Dose rate of the imported foodstuffs since 2003.

Foodstuffs	Sample number	Average ^{137}Cs activity(Bq/kg)	Effectvie dose (mSv/yr)
Grains	34	2.01	3.06E-03
Vegetable	5	2.19	3.40E-03
Mushrooms	203	38.6	8.33E-04
Fruits	61	10.12	4.20E-03
Beverage	28	1.75	1.21E-03
Spices	73	2.96	5.27E-04
Fish	20	3.39	1.09E-03
Dairy products	23	2.48	1.06E-03
others	81	2.53	2.91E-04

Table 3 Effective dose rate of the domestic foodstuffs since 2003.

Foodstuffs	Sample number	Average ^{137}Cs activity(Bq/kg)	Effective dose (mSv/yr)
Grains	13	1.38	2.10E-03
Vegetable	10	1.76	2.73E-03
Mushrooms	10	6.22	1.30E-04
Fruits	3	2.02	3.77E-04
Beverage	5	3.45	2.39E-03
Spices	5	2.48	1.00E-04
Fish	6	2.54	8.16E-04
Dairy products	7	1.50	4.25E-04
others	13	2.04	1.49E-04

IV. Conclusions

The radioactivity of all foodstuffs is below the regulation level. Based on the survey results of the radioactivity contamination of foodstuffs since 2003, a radiological dose assessment was performed. The annual effective dose was far less than 1 mSv/yr and these results have not shown any significant change during recent years in Korea. However, a survey of a radioactive contamination needs to be continuously carried out because contaminated foodstuffs have occasionally been founded in some counties.

References

1) Hille R., P. Hill, K. Heinemann, V. Ramzaev, A. Barkovski, V. Konoplia and R. Neth, "Current development of the human and environmental contamination in the Bryansk-Gomel Spot after the Chernobyl accident", *Radiat. Environ. Biophys*, 39, 99-109, (2000).
2) Scottish environmental protection agency, "*Radioactivity in Food and the Environment, 2000*", RIFE-6, Scottish Environment Protection Agency, (2001).
3) William C. Cunningham and William B. Stroube, "Radionuclides in Domestic and Imported Foods in the United States, 1983- 1986", *J. Assoc. OFF. Anal. Chem*. Vol.72, No.1, 15-18, (1989).
4) Gaso, M.I., N. Segovia, O. Morton, M.L. Cervantes, L. Godinez, P. Pena and E. Acosta , "^{137}Cs and relationships with major and trace elements in edible mushrooms from Mexico", *Sci. Total Environ*., 262, 73-89, (2000).
5) Charmasson, S., E. Barker, D. Calmet, A.S. Pruchon and H. Thebault, "Long-term variations of man-made radionuclide concentrations in a bio-indicator *Mytilus galloprovincialis* from the French Mediterranean coast", *Sci. Total Environ*., 237/238, 93-103, (1999).
6) KFDA, "Food Code", Chapter 7, Appendix 351-354, (2002).
7) IAEA technical reports series No. 295, “Measurement of radionuclides in food and the environment", (1989).

Journal of NUCLEAR SCIENCE and TECHNOLOGY, Supplement 5, p. 670–673 (June 2008)

Attempt at Neutrino Detection by Resonance-Type Electrochemical Detector with a Small Size

Norichika Terao*, Kenji Ishibashi, Shunsuke Ishimoto, Takeshi Nishimura, Yasushi Takayama, and Hidehiko Arima

Department of Nuclear Engineering, Kyushu University, Fukuoka, Japan

Neutrinos make only the weak interaction, and have quite a small reaction cross-section. A huge detector system was usually required to detect neutrinos in such experiments as Homestake and Kamiokande. We consider that the neutrinos have an elaborated mass-generation mechanism on the basis of axial-vector (AV) type neutral scalar field. A resonance perturbation on this mechanism may exert influence on the neutrino structure, and make neutrinos to be very reactive in a similar degree to the electromagnetic interaction. According to this idea, we attempt to detect neutrinos by using a resonance-type electrochemical detector with a small size.

A nuclear reactor produces an intense neutrino flux. The detector experiment was initiated in a location close to a nuclear reactor. The voltage of our detector increased with time, and showed a periodical saw-teeth waveform. After the initial experiment, the detector was moved back to our laboratory. The saw-teeth waveform was seen again for long-distant reactor and environmental neutrinos. We consider that the detector acquired the AV type neutral scalar field in the initial experiment.

KEYWORDS: neutrino, weak interaction, mass-generation mechanism, V-A interaction, neutral scalar field, electromagnetic interaction

Ⅰ. Introduction

Neutrinos are one of leptons, own the spin 1/2, and a quite small rest mass[1]. Nuclear reactors generate anti-neutrinos through the beta decay of fission products. In 1956, Frederick Reines and Clyde Cowan measured the anti-neutrinos from the nuclear rector of Savannah River, South Carolina[2]. Since neutrinos have no electric charge, they make only the weak interaction, which works in the potentials of vector-axial-vector (V-A) type. As a result, neutrinos rarely interact with other substances. This property makes neutrinos extremely hard to be detected, and detection of neutrinos needs large-sized measurement system like Homestake and Kamiokande experiments[3), 4)].

The potential type of V-A and the coupling constant characterize the weak interaction. The coupling constant of the weak interaction is quite small, compared with that of other interactions such as electromagnetic and strong ones. Since the magnitude of weak charge is the same as the conventional electric charge e[5], the reason for the small coupling constant is thought to be originated from internal self-shielding effect. This effect works to make the mass of weak bosons much heavier, and then the interaction range to be shorter. If the self-shielding function of the weak charge system is made imperfect under a specific situation, it may readily interact with other substances[6].

We consider that neutrinos have an elaborated mass-generation mechanism on the basis of axial-vector (AV) type neutral scalar field[7]. A resonance perturbation on this mechanism may influence the neutrino structure, and make neutrinos to be very reactive in a similar degree to the electromagnetic interaction. According to this idea, we attempt to detect neutrinos by using an electrochemical detector with a resonance-type operation. The electrochemical system makes use of weak-interaction electrons like that in our previous approach[8]. The use of the resonance property may lead to utilization of the weak interaction to the engineering purposes in future.

* Corresponding Author, Tel No:.+81-92-802-3484, Fax No: +81+92+802+3484, Email: kenshin@meteor.nucl.kyushu-u-ac.jp

Ⅱ. Experiment Apparatus

Fig. 1 shows the cross section of experiment apparatus. The main part was fabricated in an aluminum container with a size of 9-cm in diameter and 17.7-cm long and was separated into two zones by a titanium plate.

In the front zone, incident neutrinos pass through layers of calcium fluoride, indium, soda glass, barium iodide, Permalloy, and ferrite. These materials supply a pretreatment to neutrinos to make them in a collective like exited state. A supersonic oscillator vibrates air molecules and the structure material of the detector, and gives a resonance perturbation[6] to neutrino internal orbits. One of orbital angular momentums of neutrino constituents is expected to be excited and then reactive to other materials. The supersonic oscillator was operated at varying frequency of 55-65 kHz. Aluminum foil covers the inside of the front zone container. Eight permanent magnets of 420 G form an 8-pole configuration, and supply magnetic-field gradient in the front zone container. Neutrinos being made in the excited state reach the titanium plate covered by coal tar and potassium carbonate.

In the second zone, the reactive neutrinos are decomposed into fragments, and finally make a voltage generation through a weak-electrochemical process with semiconductors. Solution of sodium sulfate (12 % in weight) and methylene blue (2.5 % in weight) is filled in the second zone container. The volume of this container is 80 cc. Semiconductors of titanium oxide plate and n-type diamond device constitute a pair of electrodes. The titanium oxide plate works as anode and is wired by silver line, while the n-type diamond device is connected through

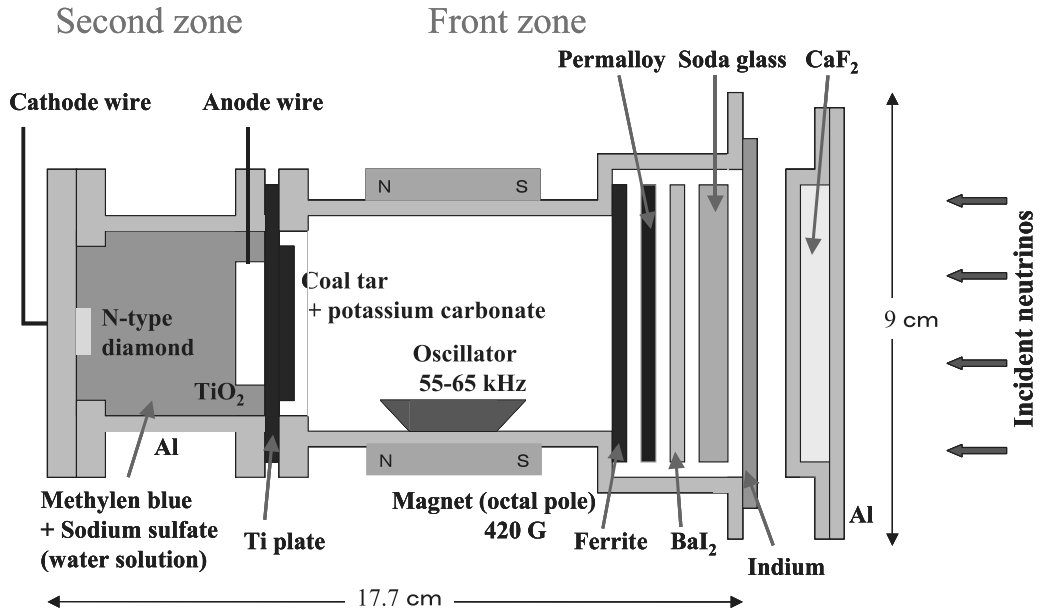

Fig. 1 Main part of experiment apparatus. Neutrinos enter from the right side.

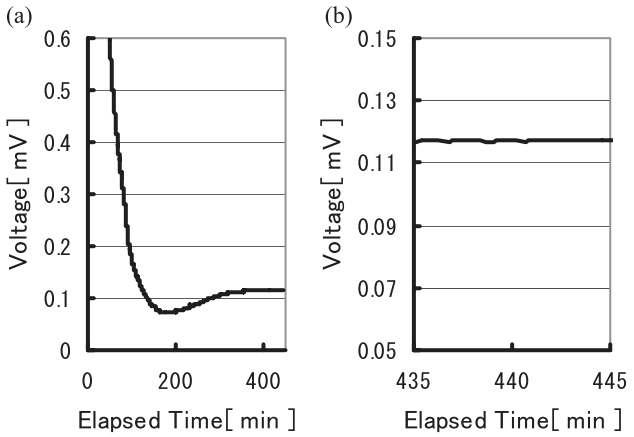

Fig. 2 Voltage evolution of the detector with supersonic oscillation at Kyushu University. (a) voltage-time curve in initial state (b) voltage-time curve in stable state

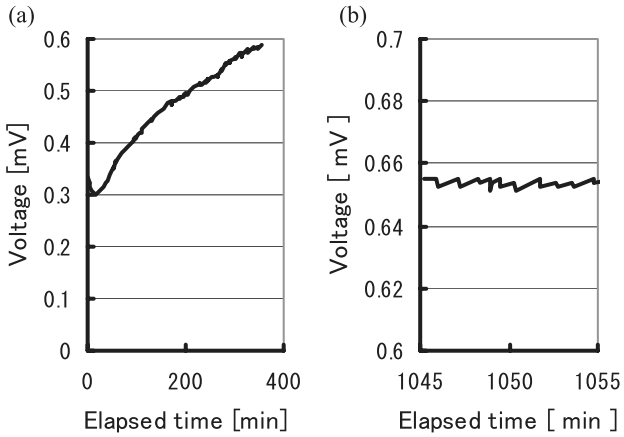

Fig. 3 Voltage evolution of the detector with the supersonic oscillation under irradiation of reactor neutrinos. (a) voltage-time curve in initial state (b) voltage-time curve in stable state

aluminum by copper wire and functions as cathode. The two wires produce output voltage across a resistor of 50 ohms connected in series.

The apparatus of Fig. 1 is covered by a cylindrical electrically-conductive polyvinyl chloride container, except the neutrino entrance region. The container keeps the weak-interaction working potential field, and is constituted by three layers: water solution of copper acetate and epicatechin gallate, packed marble, and packed polyurethane. The best performance was achieved by try-and-error-base experimental efforts.

Ⅲ. Experiment

The initial experiment was carried out as a background measurement at our laboratory (Kyushu University), which is about 60 km far from the nearest nuclear power stations. A small amount of anti-neutrinos come from the power station to Kyushu University. **Fig. 2 (a)** shows the experimental signal voltage across the resister (50 ohms) with 55-65 kHz supersonic wave. The voltage quickly decreased to a level of 0.1 mV, even under application of the supersonic oscillation. The slight increase in voltage around 300 sec is supposed to be ascribed to the temperature rise of the solution due to heat dissipation from the ultrasonic oscillator. **Fig. 2 (b)** shows the signal voltage in a stable state in expanded time and voltage scales. Since no clear phenomena were soon, a larger amount of neutrinos are required to observe an appreciable neutrino effects in our measurement system.

The antineutrino irradiation experiment was carried out at Kyoto University Reactor (KUR, 5MWth) of Kyoto University Research Reactor Institute (KURRI). The detector

was set in a location close to the nuclear reactor core. **Fig. 3 (a)** shows the measurement signal voltage across the resister (50 ohms).

The voltage from the detector increased with time, with application of the supersonic oscillation. The voltage from the detector stably made a periodical saw-teeth voltage waveform, as shown in **Fig. 3 (b)** with a magnified scale. The appearance of saw-teeth waveform is considered to indicate that a certain field is accumulated and then released suddenly, in a repetitive way. We consider that the field corresponds to the AV-type neutral scalar field B_0, which is something like magnetic field in the time direction and exerts influence on neutrino stability[6]. The n-type diamond in the detector is commercially unavailable. Use of the n-type diamond readily made the voltage evolution through a smooth transfer of weak interaction electrons to the cathode wire. In contrast, it was quite difficult to generate the detector signal with use of n-type silicon probably due to the lattice constant different from that of diamond.

After the reactor-neutrino irradiation, the detector was moved back to Kyushu University, and the experiment was continued for attempting to detect natural neutrinos. At first the voltage decreased to a level of 0.4 mV without the supersonic oscillation. When the supersonic oscillator was operated, the signal began to increase with time. The saw-teeth voltage waveform appeared again particularly in the detector direction of nuclear power station plants. Good performance was obtained under the supersonic oscillation with in a repetitive frequency sweep of 55 kHz to 65 kHz typically in 2000 s. The measurement was carried out for more than three months.

During the operation, the detector was set in directions to nuclear power stations, and the detector signal was recorded. The directions are drawn in **Fig. 4** with nuclear power stations and a distance scale, and the voltage signals are presented in **Fig. 5**. The antineutrino flux is largest in the direction to Genkai, while it is basically none in that to Miyazaki. The signal level is

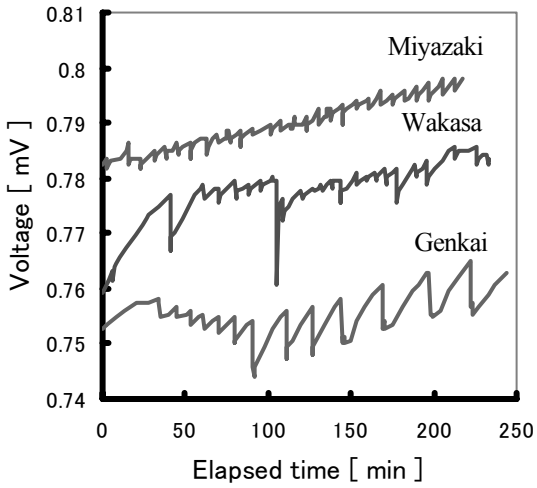

Fig. 5 Signal wave form obtained in different directions. The lower, middle and upper curves show the Genkai (4 reactors), Wakasa (13 ones), and Miyazaki directions (no reactor), respectively.

the highest in the direction to Miyazaki, and the lowest in that to Genkai. This suggests that the detector is sensitive to both environmental (presumably normal neutrinos) and reactor neutrinos, once the antineutrinos from the power stations reduce the signal level. The shape of saw-teeth lines are different each other. The result in the Genkai direction shows

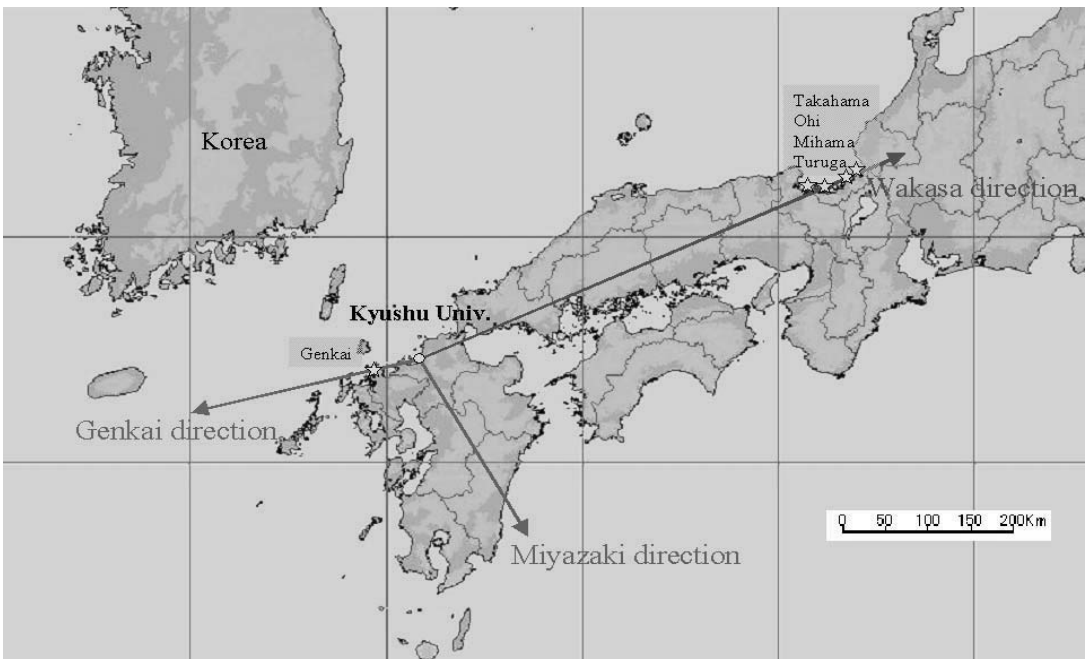

Fig. 4 Detector direction in the measurement at Kyushu University. There are 4 nuclear reactors in the direction of Genkai,13 in that of Wakasa and non in that of Miyazaki.

that the saw-teeth form tends to have a longer interval and show bolder behavior than in Miyazaki and Wakasa directions. Although antineutrino flux is quite low, the detector with the AV-type neutral scalar field is sensitive to antineutrinos with the enhanced saw teeth form.

A further experiment was performed with series connection a silicon diode device to the 50-ohm resistors. The results are presented in **Fig. 6**, again in the different detector directions.

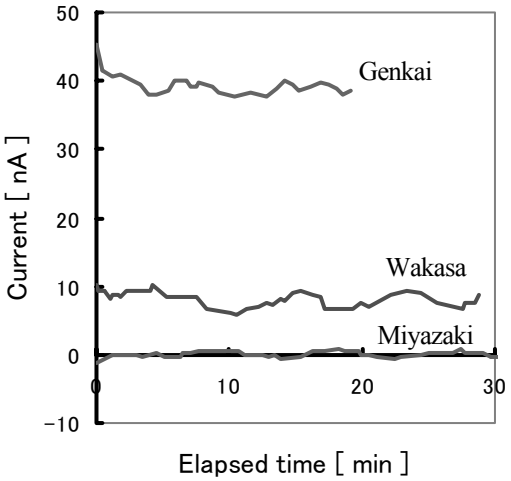

Fig. 6 Signal obtained in the use of diode in series to the resistor. The upper, middle and lower curves show the Genkai (4 reactors), Wakasa (13 ones), and Miyazaki directions (no reactor), respectively.

The use of the diode with a reversed-direction connection almost suppressed the output signal. Although the signal level is low, the detector responded to antineutrinos in directions of Genkai and Wakasa. This suggests that the diode filtered some peak-charge flow that is ascribed to environmental neutrinos.

Ⅳ. Conclusion

We detected reactor neutrinos by using a small-size detector. The detector utilized the supersonic oscillator to give resonance-perturbation to neutrinos. Among the materials and devices in the detector, n-type diamond played a significant role for generation of detector signal. Once the detector acquired the AV-type neutral scalar field in the initial experiment, it responded in the later measurement to environmental neutrinos and antineutrinos in location far from the nuclear reactors.

The experimental results may propose an alternative new detector system and new physical and engineering aspect for neutrinos.

Acknowledgement

Authors express our gratitude to Dr. Satoshi Koizumi of Research Center for the Advanced Materials, National Institute for Research in Inorganic Materials, for supplying the newly fabricated n-type diamond, and to Prof. Youichi Kawase of Kyoto University Research Reactor for initiation of the experiment at the reactor.

Reference

1) S.M. Bilenky, C. Giunti, J.A. Grifols, E. Masso, Absolute Values of Neutrino Masses: Status and Prospects, Phys. Rept. 379, 69-148 (2003), hep-ph/0211462
2) F. Reines, The neutrino: from poltergeist to particle, Rev. Mod. Phys. 68, 317 - 327 (1996)
3) Raymond Davis, A review of the Homestake solar neutrino experiment, Prog.Part.Nucl.Phys. 32, 13-32 (1994)
4) K. S. Hirata et. al, Results from One Thousand Days of Real-Time, Directional Solar-Neutrino Data, Phys. Rev. Lett. 65, 1297-1300 (1990)
5) S.Weinberg, Phys. Rev .Lett. 19, 1264 (1967); A. Salam, Elementary Particle Theory (ed. By N. Svartholom, Almquist and Forlag, 1968), 367.
6) K. Ishibashi et al. to be published elsewhere.
7) Shigeaki Nagamachi and Noburnichi Mugibayashi, Neutral Scalar Field Theory with a Point Source, Prog. Theor. Phys. Vol. 49 No. 1, pp. 329-340 (1973)
8) Liu Wei et. al, Possible Detection of Natural Neutrinos by Use of Small Apparatus , *J. Nucl. Sci. and Techonol.* **4,** 487-490 (March 2004)

Journal of NUCLEAR SCIENCE and TECHNOLOGY, Supplement 5, p. 674–676 (June 2008)

Radiological Dose Assessment for a Regulatory Clearance of the Soil and Concrete Wastes at KAERI

Dae Seok HONG*, Young-Yong JI, Il Sik KANG and Jong-Sik SHON

Korea Atomic Energy Research Institute, 1045 Daedeokdaero, Yuseong, Daejeon, Korea

At the KAERI, about 4,800 drums of radioactive contaminated soils and concretes wastes have been stored since their generation in 1988. As these wastes have been stored for more than 18 years, some of them can be regulatory cleared. Before such a regulatory clearance, the radiological characteristics of these wastes should be analyzed first. And based on the analysis result, radiological dose should be estimated to confirm the safety of a disposal of these cleared wastes. In this study, a working procedure for a representative sampling and analysis of the wastes was developed. According to the analysis result, Co-60 and Cs-137 were major radionuclides while some wastes were contaminated with Mn-54, Fe-59, I-131, Cs-134 or Eu-152 of an extremely low concentration. The analysis results show that about 75% of wastes have a radioactivity concentration below 0.1Bq/g and were considered for a clearance. It was assumed that radiation workers are exposed by the inhalation dose and the external dose. The radiological dose was estimated using the RESRAD code for the disposal workers and the management workers as 5.32μSv/yr and 3.13μSv/yr for an individual dose and 1.60E-4 man·Sv/yr and 3.13E-5 man·Sv/yr for a public dose, respectively.

KEYWORDS: dose assessment, regulatory clearance, soil waste, concrete waste

I. Introduction

In the radioactive waste storage facility at the Korea Atomic Energy Research Institute (KAERI), about 4,800 drums of radioactive contaminated soil and concrete wastes have been stored since their generation in 1988. These wastes were generated during the decommissioning process of a research reactor and its attached facilities in Seoul[1]. The radiological characteristics of these wastes were not analyzed but their surface dose rates measured at their generation time are known and used for their management.

As the wastes have been stored for more than 18 years, some of them with a very low level radioactivity can be regulatory cleared. For such a clearance, the radiological characteristics of these wastes should be analyzed first and then, the radiological dose should be analyzed to confirm their safety for disposal.

In this study, a working procedure for a representative sampling and an analysis of the wastes was developed and described. Also, the methodology and the result of the radiological dose assessment were discussed.

II. Equipment and Working Procedure

1. Equipment Development

Unsealing a waste drum in the storage facility is not allowed because the radioactive material in the drum can spread to contaminate the working area. However, to transfer the drums from the storage facility to another place for a sampling, a considerable amount of time, cost and labor is required. Also, as a drum weighs over 250kg, it can cause a problem during a transfer. So, for an effective sampling process, some equipment and tools for restricting a contamination during a unsealing of a drum in a storage facility were developed and applied to a sampling and an analysis.

First, for limiting a contamination, an airtight working booth with dimensions of 3,500mm × 2,500mm × 2,500mm was made and installed within the storage building. At the exterior of the booth, a ventilation system, a water line and a power line can be connected. For a convenience, an air inlet with a filter is installed on one side of the booth. While on the other side of the booth, a ventilation system is attached and operated during the sampling process. For lighting, there are windows at the front side and at the rearside of the booth. The top of the booth can be separated from the body for an easy transfer of the booth and an easy insertion of a material with a large volume into the booth. **Fig 1** shows the working booth with a ventilation system.

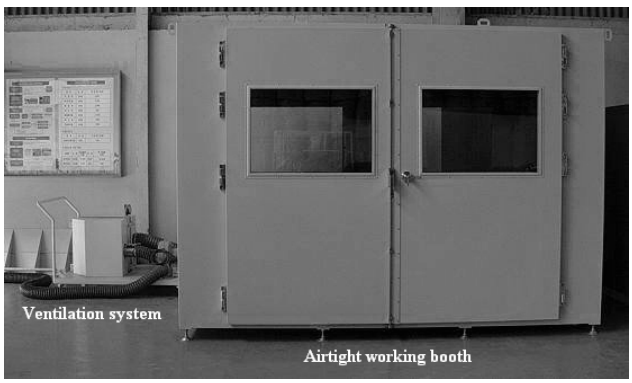

Fig. 1 Airtight Working Booth with a Ventilation System

Second, a stainless steel tray with the dimensions of 1,400mm × 1,400mm × 320mm was manufactured. It was used for holding the soils and concretes poured out of the

* Corresponding Author, Tel. No: +82-42-868-4724, Fax. No: +82-42-868-8221, E-Mail:dshong@kaeri.re.kr

package drum. As a hole with a cover is located in the center of the tray, after a sampling, the remaining soils can be discharged into the packaging drum easily. During the discharge, radioactive dust can be scattered and it will be exhausted by a ventilation system.

Finally, a 10 × 10 grid was used to create 100 even sections in the homogenized waste. A number is assigned to each section. Soil and concrete samples are taken as a total of 30 sections according to the randomly pre-generated numbers. The 30 samples are mixed to make a 2 liter representative sample out of a 200 liter drum.

2. Working Procedure

For an identification of the radioactivity of the soils and concretes, a systematic working process was developed. First, a drum with a written surface dose rate below 0.3μSv/hr was selected for a sampling. Then, by unsealing it, the contents of the drum were identified. After recording the current surface dose rate of the drum, concrete wastes were crushed and these wastes were poured onto the tray. Following a homogenization of the soil and the concrete, a sampling was performed. By the analysis result of the sample, the waste with a radioactivity concentration of more than 0.4Bq/g was categorized as a radioactive waste or an objective for a regulatory clearance2). The diagram for the working process is shown in Fig 2.

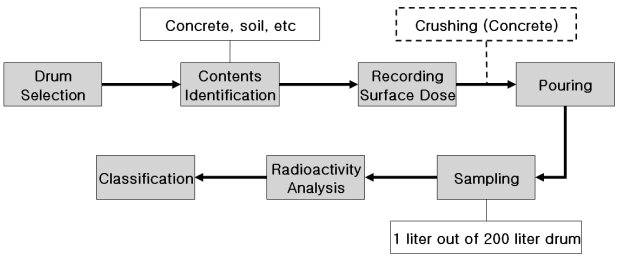

Fig. 2 Working Procedure for Sampling and Classification

III. Analysis Result

According to the analysis result, Co-60 and Cs-137 were the major radionuclides in the soil and concrete. Also, as minor nuclides, Mn-54, Fe-59, I-131, Cs-134 or Eu-152 were detected in soils and concretes with a relatively high radioactivity concentration. Distribution of the γ-radioactivity concentration of the soils and concretes are described in **Fig 3**. As shown, about 90% of the wastes could be classified as an 'Objective for a regulatory clearance'. Among them, most of the soils and concretes (about 2,900 drums) have a radioactivity concentration less than 0.1Bq/g.

Based on a historical review, it is expected that there were no α or β emitters in the soils and concretes. This was verified by analyzing some samples with a relatively high radioactivity concentration. The analysis result is shown in **Table 1**. As shown, except the γ-emitters, α or β emitters are unlikely to exist in the soils or concretes.

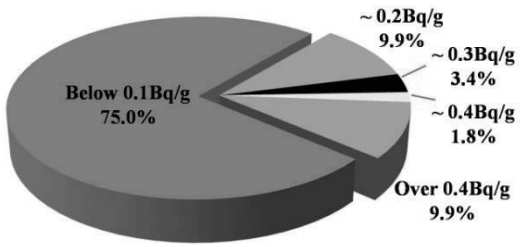

Fig. 3 Distribution of γ-radioactivity concentration

Table 1 Analysis Result of Samples with Relatively High Radioactivity Concentration (S1: soil, C1: concrete) [unit : Bq/g]

	tot. γ	tot. α	Fe-55	Ni-63	H-3	C-14
S1	26.06	MDA	<0.06	<0.08	<1,0E-2	5.1E-3
C1	15.20	MDA	<0.06	<0.08	<9.6E-3	5.4E-3

IV. Radiological Dose Assessment

1. Clearance Scenario and Criteria

For a clearance scenario, the cleared wastes were assumed to be land-filled before the storage facility at the KAERI site. So, only the radiation workers were considered for the exposure dose estimation during a working hour by the disposed wastes.

Two criteria of **Table 2** were applied for a determination of the range of wastes for a regulatory clearance. One was the radioactivity concentration criteria recommended by the IAEA. Another is the dose criteria regulated by Korean nuclear law.

Table 2 Criteria for Regulatory Clearance

	Criteria
IAEA[3]	$(C_{Co-60}+C_{Cs-137})/0.1 < 1$
Korean regulation[4]	Individual dose <10μSv/yr Collective dose <1man·Sv/yr

where, CCo-60 : activity concentration of Co-60,
CCs-137 : activity concentration of Cs-137

2. Parameters for the Assessment

The radiological dose for the persons working in the disposal area was estimated based on about 1,900 drums of soil and about 1,000 drums of concrete with a radioactivity concentration of less than 0.1Bq/g. In the estimation, no dose due to ingestion was considered but an inhalation pathway and an external dose were considered. Also, it is assumed that all the cleared wastes will be disposed of homogeneously in a facility. Some parameters important for the assessment were assumed. Those parameters are listed in Table 3.

Table 3 Parameters for the Assessment

Parameter	Value
Thickness of cover soil	15cm/day, 60cm(final)
Inhalation rate	7,400m3/yr
No. of workers	10 (40hrs work/week)
Avg. concentration	
Co-60	0.0171Bq/g (soil)
	0.0182Bq/g (concrete)
Cs-137	0.0232Bq/g (soil)
	0.0182Bq/g (concrete)

V. Assessment Result

Using the data and the scenario discussed above, radiological dose due to the cleared waste was estimated for the disposal workers and the management workers after the disposal. For the estimation, the RESRAD code was used.

According to the result, total annual individual radiological dose due the cleared wastes were estimated as 5.32 μSv/yr for the disposal workers and 3.13 μSv/yr for the management workers. Additionally, total annual collective radiological dose were estimated as 1.60E-4 man·Sv/yr for the disposal workers and 3.13E-5 man·Sv/yr for the management workers. The assessment results are shown in **Table 4**.

Table 4 Radiological dose due to cleared wastes

Disposal workers						
Wastes	Individual dose(μSv/yr)			Collective dose(man·Sv/yr)		
	Co-60	Cs-137	Tot.	Co-60	Cs-137	Tot.
Soil	2.19	0.45	2.64	6.56E-5	1.36E-5	7.91E-5
Concrete	2.33	0.35	2.68	6.98E-5	1.06E-6	8.04E-5
Total	5.32 μSv/yr			1.60 E-4 man·Sv/yr		
Management workers						
Wastes	Individual dose(μSv/yr)			Collective dose(man·Sv/yr)		
	Co-60	Cs-137	Tot.	Co-60	Cs-137	Tot.
Soil	0.41	1.29	1.70	4.13E-6	1.29E-5	1.70E-5
Concrete	0.44	0.99	1.43	4.39E-6	9.87E-6	1.43E-5
Total	3.13 μSv/yr			3.13E-5 man·Sv/yr		

VI. Conclusion

Before the disposal of wastes, their safety should be analyzed first. In this study, the radiological characteristics of about 2,900 drums of wastes was analyzed and based on the analysis result, their radiological dose was estimated. Also, a working procedure and equipment were developed and applied. Based on the dose assessment results, it can be concluded that the disposal of the cleared wastes meets not only the radioactivity concentration criteria recommended by the IAEA but also the dose criteria regulated by the Korean government. The individual dose due to the cleared wastes were estimated to be 53.2% of dose criteria for the disposal workers and 31.3% of dose criteria for the management workers. Additionally, the collective dose were estimated to be 1.60E-2 of dose criteria for the disposal workers and 3.13E-3% of dose criteria for the management workers.

Finally, it can be concluded that the cleared radioactive wastes can be disposed of safely according to the clearance scenario and the procedure, equipment and results of this study can be applied to the estimation of other regulatory clearance activities.

References

1) T. K. Kim, K. J. Kim, S. J. Ahn et al., "Re-evaluation of the Radionuclides and Activity Concentration of Radioactive Contaminated Soils Stored in the Storage Facility", KAERI/RR-2650/2005, Korea Atomic Energy Research Institute (KAERI), (2006), [in Korean]
2) D. S. Hong, J. S. Shon, T. K. Kim, et al., "A Study on the Radioactive Characteristics of Soils in the Storage Facility of KAERI", Transactions of the Korean Nuclear Society Autumn Meeting, Busan, Korea, Oct. 27-28, (2005)
3) International Atomic Energy Agency, "Derivation of Activity Concentration Values for Exclusion, Exemption and Clearance", Safety Reports Series No. 44, International Atomic Energy Agency (IAEA), (2005).
4) Korean regulation, notification No. 2001-30 [in Korean]

Journal of NUCLEAR SCIENCE and TECHNOLOGY, Supplement 5, p. 677–680 (June 2008)

Radiation Dose Assessment of the Uranium Rich Regions in Korea

Geun Sik CHOI, Hee Reyoung KIM*, Wanno LEE, Kun Ho CHUNG, Mun Ja KANG, Young Hyun CHO, and Chang Woo LEE

Korea Atomic Energy Research Institute, Daejeon 305-353, Korea

The radiation dose was assessed for the inhabitants living in the Kumsan, Geosan and Miwon regions which belong to an Okchun metamorphic belt with plenty of uranium resources. The grain, vegetable, milk, and water, which the inhabitants generally ate or drunk, were sampled to reflect the dose effects. And TLD (Thermoluminescence dosimeter) was used for measuring the external dose in the sampled area. An external exposure includes the accumulated gamma dose measured by TLD and an internal exposure includes an ingestion of the food, and an inhalation of the air and radon gas. The radionuclides such as ^{137}Cs, ^{7}Be, ^{40}K as well as ^{238}U were included for measuring the radioactivity concentrations of the samples. Radioactivity concentrations for the samples were calculated as averaged annual values. The effective dose by TLD analysis was similar to the domestic average when considering that it was between 0.63 mSv/y and 0.71 mSv/y. The ^{222}Rn concentration of indoor air significantly contributed to the total effective dose where the concentration of these uranium belt regions was more or less higher than the average domestic one. This study revealed that the dose level for the inhabitants of the uranium rich regions in Korea was similar to that of the other regions except for the effect by radon.

KEYWORDS: ^{238}U, ^{222}Rn, radioactivity, dose assessment, concentration in air, external and internal exposure

I. Introduction

A natural radioactivity is originated from primordial radionuclides and their daughter products. These natural radionuclides spread over all environments and cause a radiation effect to a human body through internal and external pathways. In the same manner, the uranium which is a natural radioactive material is widely distributed in the earth's crust. In some cases, it exists densely in the soil or a rock layer. There is a mineral vein of a black argillite region including uranium and vanadium called the Okchun metamorphic belt in the central part of South Korea. This is formed over 120 km from northeast to southwest of the Korean Peninsula and has seven uranium rich regions. Among these, most of the uranium lies under the ground in three regions called Goesan, Miwon and Kumsan. The content of uranium of this black argillite ranges from 250 ppm to 400 ppm. The estimated amount of the deposit is about 12 million tons in Goesan, 10 million tons in Miwon and 9 million tons in Kumsan.[1)] These figures are much higher than those of any other regions of the Okchun metamorphic belt where the reserves are less than 500 thousand tons respectively. Therefore, the health condition of the inhabitants exposed to this natural radiation is usually of concern in view of a radiation protection when a radiation monitoring is carried out on the artificial radionuclides around a nuclear installation like nuclear power plants for the radiation safety of the public.[2)] In fact, the natural radioactive chains from ^{238}U or ^{232}Th produce a group of radionuclides with a wide range of half-lives. So, their alpha radiation causes an internal exposure when they are inhaled by respiration or ingested by a food intake. Also the gamma radiation contributes to the dose that the human body receives by an external exposure. Especially radon gas accumulates in indoor air and can be one of the factors inducing a health risk such as lung cancer, depending not only on its concentration but also on a people's smoking habit and the time they spend in an indoor room. In the present study, the accumulated radiation dose by TLD is measured for an external dose and a radioactivity analysis for ^{238}U is performed to find its own contribution to the internal dose in the uranium rich regions. Then, the effective dose on the inhabitants from the natural radiation sources is estimated using the analyzed data and discussed in terms of a comparison with the average values of Korea.

II. Sampling and Analysis Methods

The environmental monitoring program covered 144 sampling points within a radius of 10 km from the closed coal mine in the Okchun metamorphic belt, where 45 sampling points are in the region of Goesan, 51 sampling points in Miwon, and 48 sampling points in Kumsan, respectively as represented in **Fig. 1**. The monitoring sites are mountainous area composed of small forest hills and valleys. The sampling points were set up by considering the geomorphology and population distribution of the residential area where the number of people was about 2,500, 11,000 and 15,000 in the regions of Goesan, Miwon and Kumsan, respectively. Air, soil, surface water and underground water were sampled every three months for a year. Food samples were also taken during their harvest season to analyze their concentration. The accumulated dose in the environment was analyzed by using the TLD where it was deciphered every ninety days. The gamma emitting nuclides were analyzed by using an HPGe gamma-spectrometer. An alpha-ray spectrometer was used for an analysis of the uranium isotopes after a chemical separation of the samples. The detector used for a measurement of the radon activity of the indoor and outdoor air was Terradex

* Corresponding Author, Tel No: +82-42-868-2048, Fax No: +82-42-863-1289, E-mail: kimhr@kaeri.re.kr,

Radtrack (Landauer, Inc U.S.A) and the analysis was carried out every ninety days.

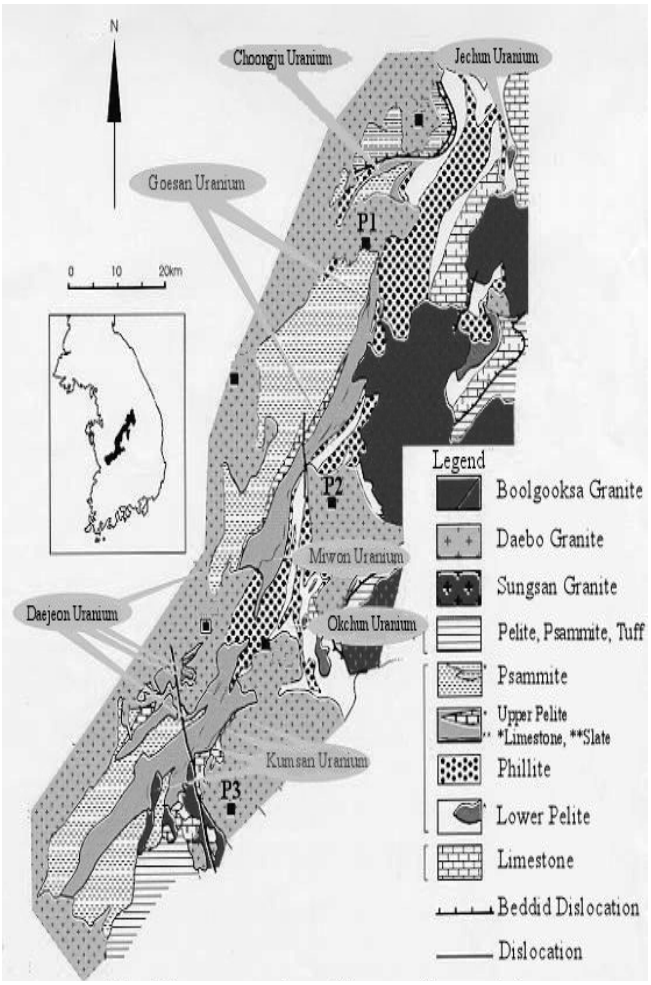

P1: Goesan region, 45 sampling points, P2 : Miwon region, 51 sampling points, P3 : Kumsan region, 48 sampling points

Fig. 1 The geomorphologic and geological distribution of Okchun metamorphic belt and the sampling points

III. Dose Assessment

Considering the exposure pathways, the annual effective dose is calculated by the following equation,

$$H_E = \Sigma\Sigma H_{pr}\,(Sv/y) \quad (1)$$

where H_E is the effective dose and H_{pr} is the effective dose of a nuclide r through pathway p. The exposure pathways to a human body are considered as external and internal ways. The dose estimation in this study was carried out on the basis of the annual effective dose per capita for adults.

1. The Calculation of the Dose Rate from an External Exposure

The external exposure is caused by several sources including cosmic ray, beta/gamma radiation from surrounding air, ^{238}U, ^{137}Cs, ^{7}Be and ^{40}K in the soil. In this study, it was assumed that the accumulated gamma dose measured by TLD represents a total external dose rate. The dose rate is calculated by the equation,[3)]

$$H_{ex} = 0.0087\, G_g\, C_T\,(Sv/y) \quad (2)$$

where H_{ex} is the effective dose rate, G_g is the dose conversion factor from the absorbed dose (= 0.7 Sv/Gy) [3)] and C_T is the accumulated dose in TLD, in mR/y.

2. Internal Dose by an Ingestion of Contaminated Foodstuffs

Four groups of food were taken into account. The equation for the effective dose by an ingestion of the food is expressed by[4)]

$$H_{gr} = \Sigma\Sigma G_{gr}\, C_{rf}\, U_f\,(Sv/y) \quad (3)$$

where H_{gr} is the effective dose by an ingestion of nuclide r, $G_{gr,}$ is the effective dose conversion factor by ingestion of nuclide r, in Sv/Bq (^{238}U: 4.5×10^{-8}, ^{7}Be: 2.8×10^{-11}, ^{40}K : 6.2×10^{-9}, ^{137}Cs : 1.3×10^{-8}), C_{rf} is the activity concentration of nuclide r in the ingested food, in Bq/kg or Bq/L, and U_f is the consumption rate of the food f, in kg/y or L/y.

3. Internal Dose by an Inhalation of Radionuclides in Air

The inhalation dose of nuclide r depends on the nuclide concentration of the air at the place under consideration. The dose calculation equation is represented by[4)]

$$H_{hr} = \Sigma G_{hr}\, C_{ar}\, V\,(Sv/y) \quad (4)$$

where H_{hr} is the effective dose by inhalation of nuclide r, G_{hr} is the effective dose conversion factor by inhalation of nuclide r, in Sv/Bq (^{238}U: 8.0×10^{-6}, ^{7}Be: 5.5×10^{-11}), C_{ar} is the activity concentration of nuclide r in air, in Bq/m^3, and V is the respiratory rate of air, in m^3/s

4. Internal Dose by an Inhalation of Radon

The effective dose is calculated according to the following equation,[5,6)]

$$H_{Rn} = G_{Rn}\, C_{Rn}\, T\, F\, T_R\,(Sv/y) \quad (5)$$

where H_{Rn} is the effective dose by inhalation of Radon, G_{Rn} is the effective dose conversion factor (9×10^{-9}), in Sv/(Bq h m^{-3}), C_{Rn} is the concentration of radon, in Bq/m^3, F is the equilibrium constant (indoor : 0.4 and outdoor : 0.6), T is the ratio of residence time (indoor : 0.9 and outdoor : 0.1), and T_R is the residence time (8,760), in hr/y.

IV. Results and Discussions

Table 1 represents the accumulated dose by TLD and effective dose by the external exposure including cosmic rays of 0.4 mSv/y.[7)]

Table 1 Annual effective dose by an external exposure in the Okchun metamorphic uranium belt

Region	Accumulated dose by TLD (mR/y)	Effective dose rate (mSv/y)
P1	116	0.71
P2	114	0.69
P3	104	0.63

Considering that the effective dose by TLD of the other regions in Korea ranges from 0.58 mSv/y to 1.32 mSv/y and the worldwide average annual effective dose from an external exposure is 0.9 mSv/y, the effective dose of P1, P2 and P3 was not thought to be higher than those of the other regions because these regions belong to the uranium deposit belt. Actually, the portion of the effective dose from cosmic rays is between 56 % and 63 %.

Table 2 Nuclide concentration of the food samples and the effective dose from their ingestion

Region	Nuclides	Grain (Bq/kg)	Vegetable (Bq/kg)	Milk (Bq/L)	Drinking water (Bq/L)	Effective dose (mSv/y)
P1	238U	1.9E-03	1.1E-01	<MDA	1.8E-03	1.0E-03
	137Cs	<MDA	5.2E-01	<MDA	<MDA	1.3E-03
	7Be	<MDA	5.0E-01	<MDA	<MDA	2.7E-06
	40K	3.0E+01	8.9E+01	5.4E+01	<MDA	1.4E-01
P2	238U	2.5E-02	8.3E-03	<MDA	8.5E-01	1.3E-02
	137Cs	<MDA	<MDA	<MDA	<MDA	-
	7Be	<MDA	<MDA	<MDA	<MDA	-
	40K	1.3E+02	8.3E+01	<MDA	<MDA	2.0E-01
P3	238U	1.1E-03	1.0E-01	<MDA	1.6E-02	1.1E-03
	137Cs	2.0E-02	2.0E-02	<MDA	<MDA	8.4E-05
	7Be	<MDA	5.0E-01	<MDA	<MDA	2.7E-06
	40K	2.7E+01	9.8E+01	5.4E+01	5.0E-01	1.5E-01

The effective dose by an ingestion of the foodstuffs was calculated in **Table 2** in consideration of the consumption of foodstuffs such as grain, vegetable, milk, and water as seen in **Table 3**. The artificial nuclide, ^{137}Cs, was detected in P1 and P3. It is thought that this results from the atmospheric nuclear tests since 1960. The food consumption rates used for the calculation of an ingestion dose assumed that the inhabitants consumed the food harvested in the sampled area and used the underground water as drinking water. The effective dose by an ingestion of the foodstuffs was estimated to range from 142 μSv/y to 213 μSv/y where the contribution of ^{238}U was negligible. It is understood that most effective dose was caused by ^{40}K. These values are slightly higher than the average domestic value.[8)]

Table 3 The annual rates of the food consumption and air respiration for the Korean adult

Food9)	Consumption rate
Grain	128 kg/y
Vegetable*	196 kg-fresh/y
Milk	19 L/y
Drinking water	323 L/y
Respiratory rate10)	7,313 m3/y

* leafy, root and fruit vegetable

The ^{238}U and ^{7}Be were measured in air, and their concentrations were the same in P1, P2 and P3, respectively as represented in **Table 4**. The effective dose by an inhalation of the dust in air was calculated to be 0.7 μSv/y. The concentration of radon in the indoor and outdoor air is given in **Table 5**. The concentration of radon was more or less high when compared with the domestic average as a recent study has reported that the averages of a radon concentration were 53 Bq/m^3 and 23 Bq/m^3 for indoor and outdoor air, respectively.[11)] The effective dose by a radon inhalation, which was the main contributor to the dose by an inhalation, was between 1.7 mSv/y and 2.5 mSv/y. In **Table 4 and 5,** the portion of ^{238}U was seen to be negligible for the internal dose. On the other hand, the total effective dose including an internal and external exposure ranges from 2.6 mSv/y to 3.3 mSv/y. It is more or less higher than the world wide average of 2.4 mSv/y.

Table 4 Effective dose from the inhaled air with 238U and 7Be

Region	Nuclides	Concentration in air (Bq/m3)	Effective dose (mSv/y)
P1	238U	1.2E-06	7.0E-05
	7Be	1.6E-03	6.4E-07
P2	238U	1.2E-06	7.0E-05
	7Be	1.6E-03	6.4E-07
P3	238U	1.2E-06	7.0E-05
	7Be	1.6E-03	6.4E-07

Table 5 Effective dose from the inhalation of ^{222}Rn

Region	Concentration in air (Bq/m3)		Effective dose (mSv/y)
	Indoor	Outdoor	
P1	8.4E+01	3.8E+01	2.5E+00
P2	5.7E+01	2.8E+01	1.7E+00
P3	8.4E+01	3.5E+01	2.5E+00

The portion that radon contributes to the effective dose is between 65 % and 76 % as represented in **Fig. 2**. In addition, in considering natural radiation, which gives human body 2.4 mSv/y in average[7], most of the effective dose from nature seems to be due to radon.

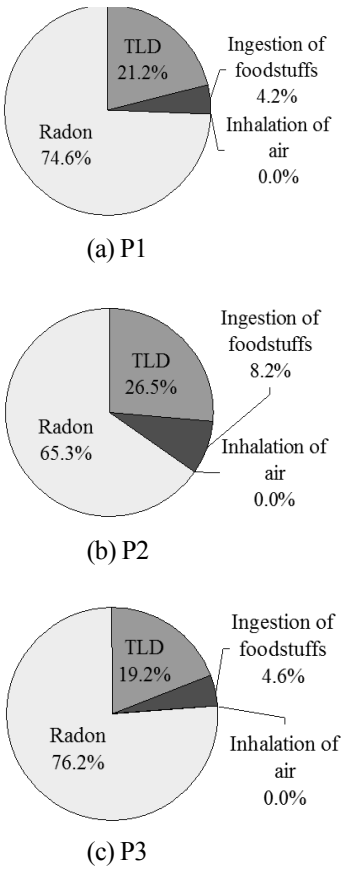

Fig. 2 The distribution of the effective dose from the various exposure pathways

V. Conclusions

This study showed that the annual effective dose of the inhabitants in the uranium rich regions was not so different from the average level of Korea if the dose from radon is excluded. The contribution of ^{238}U to the total internal dose was found to be much smaller from the analysis. The radon inhalation was largely responsible for the total effective dose. The internal dose by an inhalation of air dust was negligible. Also the internal dose by an ingestion of foodstuffs was relatively small although the natural radioisotope, ^{40}K, in foods was a major radiation source to the human body. It was thought that less than half of an external dose was probably attributed to ^{238}U, ^{7}Be and ^{40}K in the soil since the portion of cosmic rays was more than half.

References

1) H. Lee, et al., "Concentration and activity ratio of uranium isotopes in the groundwater of the Okchun belt in Korea", J. of Environmental Radioactivity, 57, 105 (2001).
2) L. Colmenero, et al., "Uranium-238 and thorium-232 series concentrations in soil, radon-222 indoor and drinking water concentrations and dose assessment in the city of Aldama, Chihuahua, Mexico", J. of Environmental Radioactivity, 77, 205 (2004).
3) UNSCEAR, Ionizing Radiation : Source and Biological Effects, UNSCEAR 1982, United Nations Scientific Committee on the Effect of Atomic Radiation, (1982).
4) IAEA, International Basic Safety Standards for Protection against Ionizing Radiation and for the Safety of Radiation Sources, IAEA Safety Series No. 115, (1996).
5) UNSCEAR, Sources and Effects of Ionizing Radiation, UNSCAER 1993, United Nations Scientific Committee on the Effect of Atomic Radiation, (1993).
6) UNSCEAR, Sources and Effects of Ionizing Radiation, Annex B: Exposures from Natural Radiation Sources, UNSCAER 2000, United Nation Scientific Committee on the Effect of Atomic Radiation, (2000).
7) UNSCEAR, Sources and Effects of Ionizing Radiation, Annex A: Dose Assessment Methodologies, UNSCAER 2000, United Nation Scientific Committee on the Effect of Atomic Radiation, (2000).
8) C. W. Lee, et al., "Dose assessment from monitoring data around the nuclear facilities", 10th International Congress of the ICRP, Hiroshima, Japan, (2000).
9) KHNP, A Study on the Food Consumption Rates for the Radiological Dose Assessment around Nuclear Power Plant Sites, KHNP-25, Korea Hydro & Nuclear Power Co. Ltd., (2006), [in Korean].
10) KAERI, A Development of Computer Code for Evaluating Internal Radiation Dose through Ingestion and Inhalation Pathways, KAERI/RR-998/90, Korea Atomic Energy Research Institute, (1991), [in Korean].
11) KINS, Nationwide Survey of Indoor Radon in Korea, KINS/GR-246, Korea Institute of Nuclear Safety, (2002), [in Korean].